Modelling of Pervaporation Separation of Butanol from Aqueous Solutions Using Polydimethylsiloxane (PDMS) Mixed Matrix Membranes

by

Arian Ebneyamini

Thesis submitted to the Faculty of Graduate and

Postdoctoral Studies in partial fulfillment of the

requirements for the

Master of Applied Science

Department of Chemical and Biological Engineering

Faculty of Engineering

University of Ottawa

Abstract

In this thesis, a theoretical description of mass transport through membranes used in pervaporation separation processes has been investigated for both dense polymeric membranes and mixed matrix membranes (MMMs). Regarding the dense polymeric membranes, the Maxwell-Stefan model was extended to consider the effect of the operating temperature and membrane swelling on the mass transport of species within the membrane. The model was applied semi-empirically to predict the membrane properties and separation performance of a commercial Polydimethylsiloxane (PDMS) membrane used in the pervaporation separation of butanol from binary aqueous solutions. It was observed that the extended Maxwell-Stefan model has an average error of 10.5 % for the prediction of partial permeate fluxes of species compared to roughly 22% for the average prediction error of the Maxwell-Stefan model. Moreover, the parameters of the model were used to estimate the sorption properties and diffusion coefficients of components through the PDMS membrane at different butanol feed concentrations and operating temperatures. The estimated values of the sorption properties were observed to be in agreement with the literature experimental data for transport properties of butanol and water in silicone membranes while an exact comparison for the diffusion coefficient was not possible due to large fluctuations in literature values.

With respect to the MMMs, a new model was developed by combining a one-directional transport Resistance-Based (RB) model with the Finite Difference (FD) method to derive an analytical model for the prediction of three-directional (3D) effective permeability of species within ideal mixed matrix membranes. The main novelty of the proposed model is to avoid the long convergence time of the FD method while the three-directional (3D) mass transport is still considered for the simulation. The model was validated using experimental pervaporation data for the separation of butanol from aqueous solutions using Polydimethylsiloxane (PDMS)/activated carbon nanoparticles membranes and using data from the literature for gas separation application with MMMs. Accurate predictions were obtained with high coefficient of regression (R^2) between the calculated and experimental values for both applications.

Résumé

Dans cette thèse, une description théorique du transfert de matière à travers des membranes de séparation par pervaporation a été étudiée pour deux types de membranes : membranes polymériques denses et des membranes à matrice mixte (MMM). Pour les membranes polymériques denses, le modèle de Maxwell-Stefan a été modifié pour tenir compte de l'effet de la température d'opération et du gonflement de la membrane sur le transfert de matière des molécules pervaporées à travers la membrane. Un modèle semi-empirique a été utilisé pour prédire les performances de la membrane et pour caractériser une membrane commerciale de polydiméthylsiloxane (PDMS) pour la séparation par pervaporation des solutions butanol-eau. Il a été observé que l'extension du modèle de Maxwell-Stefan peut prédire avec une erreur moyenne de 10.5 % les flux partiels des espèces chimiques dans le perméat comparée avec une erreur de prédiction d'environ 22% pour le modèle de Maxwell-Stefan. De plus, les paramètres du modèle ont été utilisés pour estimer les propriétés de sorption et les coefficients de diffusion des espèces chimiques de la membrane PDMS à différentes concentrations d'alimentation de butanol et différentes températures de fonctionnement. Les valeurs estimées concordent assez bien avec les données expérimentales publiées dans la littérature pour les propriétés de transport du butanol et de l'eau dans les membranes de PDMS.

Pour les MMMs, un modèle simple basé sur l'analogie d'un circuit de résistances électriques, corrigé à l'aide de simulations obtenues par la méthode de différences finies (DF), pour obtenir un modèle analytique pouvant prédire la perméabilité effective des espèces chimiques à l'intérieur de la MMM. La principale nouveauté de la méthode proposée est de contourner les temps de calcul importants de la méthode DF tout en considérant le transfert de matière de façon tridimensionnelle. Le modèle a été validé à l'aide de données expérimentales pour la séparation par pervaporation du butanol à partir de solutions aqueuses en utilisant des membranes PDMS/nanoparticules de charbon activé ainsi que pour la séparation de gaz. Des prédictions relativement précises ont été observées avec un bon coefficient de régression (R^2) entre les valeurs calculées et expérimentales pour les deux applications.

Statement of Contributions

Chapter 2:

The idea of extending the Maxwell-Stefan model was proposed by Arian Ebneyamini. Hoda Azimi carried out the experimental pervaporation tests and measured the pervaporation performance. Arian Ebneyamini thoroughly performed the derivation of the model and used the extended model to analyze the experimental results of pervaporation tests. The numerous versions of the paper were written by Arian Ebneyamini with editorial comments from PhD candidate Hoda Azimi, Dr. Jules Thibault and Dr. Handan Tezel. The latter three are co-authors of the paper.

Chapter 3:

The resistance-based model was proposed by Arian Ebneyamini. The idea of coupling the model with the finite difference method was suggested by Dr. Jules Thibault who also contributed in the VBA coding for the finite difference method. Arian Ebneyamini performed the adsorption experiments and analysis of the results. Arian Ebneyamini conducted all numerical experiments and modeled independently the correction factors for the extended resistance-based model and applied the model for both pervaporation and gas separation applications. The numerous versions of the paper were written by Arian Ebneyamini with editorial comments from PhD candidate Hoda Azimi, Dr. Jules Thibault and Dr. Handan Tezel.

Acknowledgments

First and foremost, I would like to express my deepest appreciation to my beloved parents Jalil Ebneyamini and Shahnaz Etminan for their endless love, support and motivation throughout my life. I also want to express my sincere gratitude to my dear brother, Armin, for his constant support and kindness. I would not be the person I am today without their presence and encouragement.

I am sincerely grateful to my supervisors, Dr. J. Thibault and Dr. F. H. Tezel, for giving me the opportunity of working in their research groups and for all the skills and knowledge I have gained throughout my M.A.Sc program. It would absolutely not be possible to complete this thesis without their continuous support, insights and help.

I also want to specially thank my colleagues and friends Hoda Azimi and Mohammadali Baghbanzadeh for their sincere friendship, constant presence and help which was truly valuable to make this research journey a very enjoyable experience.

Table of Contents

Abstract ii

Résumé iii

Statement of Contributions iv

Acknowledgments v

Table of Contents vi

List of Figures viii

List of Tables xi

Chapter 1: Introduction and structure of the thesis 1

1.1. Introduction 1

1.2. Research Objectives 4

1.3. Thesis structure 6

1.4. References 7

Chapter 2: Mass transport in dense polymeric membranes 13

Description of Butanol Aqueous Solution Transport through Commercial PDMS Membrane via Pervaporation Process Using Extended Maxwell–Stefan Model 13

Abstract 13

2.1. Introduction 14

2.2. Materials and methods 15

2.2.1. Membrane and materials 15

2.2.2. Three-membrane Pervaporation Experimental System 16

2.3. Pervaporation modeling method 19

2.3.1. Maxwell-Stefan model 19

2.3.2. Extended Maxwell-Stefan model based on the concentration and temperature effect 22

2.4. Results and discussion 26

2.4.1. Feed partial pressure calculation 26

2.4.2. Modeling of membrane performance 28

2.4.3. Simulation of membrane properties 34

2.5. Conclusions 42

Acknowledgements 43

2.6. References 45

Chapter 3: Mass transfer in mixed matrix membranes (MMM's) 50
Mixed Matrix Membranes for pervaporation and gas separation applications: A Resistance-Based Model 50
Abstract 50
3.1. Introduction 51
3.2. Modelling of the Mass Transport through MMMs 53
3.2.1. Resistance-Based (RB) Model 53
3.2.2. Finite difference method 56
3.2.3. Correction factor of the resistance-based model 62
3.3. Applications 69
3.3.1. MMM for the Pervaporation Separation 69
3.3.2. Mixed Matrix Membranes for Gas Separation 82
3.4. Conclusions 85
Acknowledgment 86
3.5. References 89
Chapter 4: Conclusions and recommendations 94
A. Appendix 97

List of Figures

Figure 2.1.SEM picture of the cross section of the Pervatech commercial PDMS..... 16
Figure 2.2. Schematic diagram of the three-module pervaporation experimental set up..... 17
Figure 2.3. Experimental (▲) and calculated (—) values of infinite dilution activity coefficient of butanol in water as a function of temperature [33]. 27
Figure 2.4. Estimated (MS Model — —, Extended MS Model —) and experimental (▲) butanol ((a) 310 K, (b) 320 K, (c) 330 K) and water fluxes ((d) 310 K, (e) 320 K, (f) 330 K) vs butanol feed concentration at different temperatures. 32
Figure 2.5. Effect of temperature on butanol (a) and water (b) permeation fluxes at a feed butanol concentration of 20 g.L^{-1} (MS Model — —, Extended MS Model —, Experimental ▲)..... 33
Figure 2.6. Simulated Henry's law constant (H^*) and solubility factor (H) of butanol ((a) for H^* and (b) for H) and water ((c) for H^* and (d) for H)) in a commercial PDMS membrane vs butanol feed concentration at different temperatures (310 K —, 320 K — ●, 330 K — —)..... 35
Figure 2.7. Simulated diffusion coefficients of butanol (a) and water (b) vs butanol feed concentration at different temperatures (310 K —, 320 K — ●, 330 K — —)..... 37
Figure 2.8. Simulated coupling effect vs butanol feed concentration at different temperatures (310 K —, 320 K — ●, 330 K — —)..... 38
Figure 2.9. Simulated butanol (a) and water (b) permeability vs butanol feed concentration at different temperatures (310 K —, 320 K — ●, 330 K — —). 40
Figure 2.10. Simulated selectivity vs butanol feed concentration at different temperatures (310 K —, 320 K — ●, 330 K — —)..... 41
Figure 2.11. Simulated PSI vs butanol feed concentration at different temperatures (310 K —, 320 K — ● , 330 K — —). 42
Figure 3.1. Schematic diagram for (a) the mixed matrix membrane with uniformly dispersed cubical filler particles, and (b) a basic repeatable unit consisting of a cubical filler particle centered in a cubical polymeric matrix unit element. 54
Figure 3.2. Equivalent electrical resistance circuit in a repeatable basic element. 54
Figure 3.3. Discretized RB element (a) and the (i, j, k) interior mesh point within the element (b)..... 57
Figure 3.4. Predictions of RB and FD models for different ratios of permeability and for a fixed filler volume fraction (ϕ=0.42). 63
Figure 3.5. Experimental and estimated correction factor for mixed matrix membranes containing a HPF. 65

Figure 3.6. Comparison between the predictions of the extended RB model (— .), Maxwell model (— —) and Hennepe model (——) for HPF. 66
Figure 3.7. Experimental and estimated correction factors for a mixed matrix membrane containing LPF. 67
Figure 3.8. Comparison between the predictions of the extended RB model (— .), Maxwell model (— —) and Hennepe model (——) for LPF. 68
Figure 3.9. Experimental and calculated partial permeate fluxes of the butanol and water for the separation of a 5 $g.L^{-1}$ butanol binary aqueous solution by pervaporation using neat PDMS membranes. 72
Figure 3.10. Experimental and calculated permeabilities of butanol and water in PDMS as a function of temperature at a fixed feed concentration of 5 $g.L^{-1}$. 73
Figure 3.11. Experimental and modelled adsorption isotherms of butanol on AC nanoparticles at different temperatures. 75
Figure 3.12. Variation of the intrinsic diffusion coefficient for butanol and water in the activated carbon powder. 78
Figure 3.13. Comparison of the experimental and estimated values of the thickness of MMMs as a function of the activated carbon nanoparticle content. 79
Figure 3.14. Comparison between the experimental (310 K (■), 320 K (▲) and 330 K (●)) and predicted permeate fluxes (310 K (——), 320 K (— —) and 330 K (— .)) of butanol (a) and water (b) as a function of the nanoparticle mass fraction at different temperatures. 81
Figure 3.15. Parity plot between experimental and estimated partial fluxes for the separation of butanol using a pervaporation MMM 82
Figure 3.16. Comparison between the experimental (He (▲), CO_2 (●), O_2 (■) and N_2 (◆)) [30] and predicted permeabilities in PVDF/MCM-41 (a) and PVDF/Zeolite 4A (b) as a function of the volume fraction of the filler in polymer matrix 84
Figure 3.17. Parity plot between the experimental and estimated permeabilities of gases in mixed matrix membranes. 84
Figure 3.18. Comparison between the error of predictive models for pervaporation (a) and gas separation (b) processes and the total comparison between predictive models (c). 85
Figure A.1. Overall concentration profile within a RB element for a permeability ratio $P_d.P_c^{-1}$ = 1000, solubility ratio $S_d.S_c^{-1}$ = 1 and a filler volume fraction of 0.166 for a butanol feed concentration of C_f = 5 $g.L^{-1}$) 97
Figure A.2. Contour plot of the concentration profile in two directions of x and y at central position of z direction for a permeability ratio $P_d.P_c^{-1}$ = 1000, solubility ratio $S_d.S_c^{-1}$ = 1 and a filler volume fraction of 0.166 for a butanol feed concentration of C_f = 5 $g.L^{-1}$). 98

Figure A.3. Surface plot of the concentration profile in the central position of z direction for a permeability ratio $P_d.P_c^{-1}$ = 1000, solubility ratio $S_d.S_c^{-1}$ = 1 and a filler volume fraction of 0.166 for a butanol feed concentration of C_f = 5 $g.L^{-1}$). 98

List of Tables

Table 2.1. List of the parameters determined in the Extended Maxwell-Stefan model 25
Table 2.2. Antoine coefficients for vapour pressure of butanol and water [36] 28
Table 2.3. Henry's law constants of butanol and water in PDMS at different temperatures from literature. 29
Table 2.4. Initial guesses for the coefficients of Arrhenius equation for the solubility of butanol and water in PDMS. 29
Table 2.5. Values of the parameters for the Maxwell-Stefan model. 30
Table 2.6. Values of parameters determined from the extended Maxwell-Stefan model. 30
Table 2.7. Comparison between the estimated degree of swelling of Pervatech PDMS and extracted from a graph for silicone membranes [4]. 36
Table 2.8. Comparison between literature and simulated diffusion coefficients of butanol and water in PDMS 38
Table 3.1.Parameters of Equation (4) for each of the resistances required to calculate R_{eff}. 55
Table 3.2. Initial and boundary conditions of the FD model 58
Table 3.3. Effect of ratio of the diffusion coefficient and solubility factor of the two phases of a mixed matrix membrane on the estimation of the relative permeability for a percentage volume fraction of 16.6%. 61
Table 3.4. Antoine coefficients for calculating the vapour pressure of butanol and water [33] 70
Table 3.5. Estimated values for the parameters of Arrhenius equation for the partial permeate fluxes. 71
Table 3.6. Estimated values of the permeability of butanol and water in neat PDMS membranes expressed in two different sets of units. 74
Table 3.7. Fitted Sips parameters for the prediction of butanol sorption isotherm at different temperatures 75
Table 3.8. Parameters of Arrhenius equation for the sorption of water in neat PDMS membranes [24] 76
Table 3.9. Some parameters for the calculation of Knudsen and molecular diffusion coefficients [41] 77
Table 3.10. Permeabilities of gases through the continuous and dispersed phases of MMMs [30]. 83

Chapter 1: Introduction and structure of the thesis

1.1. Introduction

This study is conducted in the field of renewable energy, and particularly focused on the modeling of pervaporation separation of biobutanol from aqueous solutions. Fluctuations in the price of fossil fuels over the last decades and their impact on the environment have drastically increased the global awareness and the motivation to develop renewable energy and sustainable fuel technologies [1]. Among the various types of biofuels, biobutanol has been considered to be a potential alternative for the partial replacement of the traditional petroleum-based fuels [2–4]. The biological production of biobutanol is mainly performed via Acetone-Butanol-Ethanol (ABE) fermentation which uses *Clostridia* bacteria as the associated microorganism [5]. However, there are some important challenges, such as the toxic effect of butanol on microorganisms and the low final butanol concentration in the fermentation broth, which need to be resolved in order to make this fermentation process economically viable [6,7]. Various types of integrated recovery methods such as vacuum fermentation, adsorption separation, liquid-liquid extraction and pervaporation separation have been successfully applied to enhance the productivity of the fermentation process by reducing the toxicity effect of butanol on the microorganisms via the selective removal of a portion of the ABE solvent from the fermentation broth [8–12].

Pervaporation is one of the most promising solvent recovery methods which is essentially based on the selective permeation of species through a dense polymeric membranes [13,14]. In this process, a liquid feed solution to be separated is contacted with the membrane while the permeate side of the membrane is kept under vacuum or a sweeping gas is used to maintain a very low concentration of the migrating components [14]. High selectivity, low energy consumption and ease of design are the key advantages of pervaporation in comparison to the traditional separation methods such as distillation. Moreover, the pervaporation process have no or minimal impact on the viability of microorganisms [15–18].

Membranes made of a variety of polymeric materials have been widely used for butanol separation by pervaporation process. Among them, Polydimethylsiloxane (PDMS) membranes are the most often used membranes for butanol separation due to their high level of hydrophobicity, high flux and selectivity, in addition to their good thermal, chemical and mechanical stability [13,19].

However, similar to the majority of the polymeric materials, PDMS membranes are suffering from the trade-off between selectivity and permeate flux [20]. It has been reported that embedding some organic or inorganic fillers within the polymer matrix can enhance the separation performance as well as the thermal and mechanical stability of the membranes. Various types of filler materials such as zeolites, metal organic frameworks (MOFs) and activated carbons have been successfully used in the polymeric membranes to improve the separation performance (flux and selectivity) in the pervaporation process [13,21,22].

A theoretical description of the mass transfer through mixed matrix membranes is essential to enhance the material selection and to select operating conditions in addition of increasing the scientific knowledge about the permeation properties through these types of membranes. A mixed matrix membrane (MMM), as used in this study, consists of at least two phases: a polymeric matrix and an embedded filler [23]. To investigate the molecular permeation through MMMs, it is important to initially study the mass transport of migrating species in the two phases individually.

Polymeric materials have been widely used as the continuous phase in mixed matrix membranes [13,21,24–27]. Therefore, investigating the mass transport through these membranes is paramount to predict the overall permeation properties of mixed matrix membranes. Species penetration through dense polymeric materials has been studied widely over the last decades. Various models such as solution-diffusion [28], thermodynamic of irreversible process (TIP) [29], pore flow [30] and Maxwell-Stefan [31] have been studied to describe the mass transport through numerous types of membranes. The simplest model, based on the solution-diffusion theory, was proposed by Graham (1866) to describe the permeation properties of gases through rubber septa. The model was then applied by Binning et al. for pervaporation separation applications [28,32]. Based on the solution-diffusion theory, the molecular transport through dense membranes consists of the following three steps [14,32–34]:

1- Sorption of species on the feed side of the membrane
2- Diffusion through the membrane due to the chemical potential gradient
3- Desorption from the permeate side

All three steps of the solution-diffusion theory could be encapsulated into a single parameter: the permeability of a migrating component within the membrane. Permeability has been widely used by many authors as a factor to compare membrane performances in both pervaporation and gas

separation processes [1,13,21,35]. However, in many cases, the solution-diffusion theory is limited to the permeation of very dilute feed solutions when the effect of coupling fluxes is negligible in comparison with the individual permeation of the penetrants [32].

The Maxwell-Stefan theory is a more comprehensive model introduced by Stefan to describe the mass transport through membranes in the pervaporation separation process [32]. The model uses the combination of the solution-diffusion theory with the Maxwell-Stefan coupled diffusion to consider the effect of species coupling in the estimation of the permeate flux [32,36,37]. However, the lack of experimental method to measure the coupling diffusion limits the application of the Maxwell-Stefan model in different cases. Moreover, the temperature and concentration dependency of the diffusion coefficient and the solubility factor are other significant factors which have to be considered for estimating the species permeate fluxes at different operating temperatures and feed concentrations [1,32].

Permeability of a species in the filler is another significant parameter which affects the overall permeability of components through mixed matrix membranes. The presence of a high permeable solid filler within the polymeric matrix could result in a more permeable composite membrane while a solid filler with lower permeability than the permeability of the polymer decreases the overall permeability of MMMs. However, according to the structure of porous material (especially nano fillers), it is not possible yet to experimentally measure the permeability of a solid filler by performing pervaporation tests. A number of studies have used different predictive models for the effective permeability of MMMs to estimate semi-empirically the permeability of the dispersed phase within the polymer matrix [38–40]. However, a better approach could be achieved by combining the effective diffusivity and solubility of species to estimate the permeability of components through the filler phase in MMMs [35,41,42]. The diffusion coefficient of slow penetrating components could be achieved by several classical methods such as sorption rate, microscopic diffusion measurements, frequency response and time lag measurements [41,43,44] while the diffusivity of fast diffusing components has usually been estimated theoretically using different diffusion mechanism such as Knudsen diffusion, molecular diffusion and surface diffusion [41,42]. Furthermore, the solubility factor of components in the filler material could be estimated using adsorption isotherm of species in the filler particles [35,41].

Regarding the mixed matrix membranes, various types of models such as Maxwell [45], Bruggeman [46], Lewis-Nielson [47,48] and Pal [49] have been introduced to analytically estimate the effective dielectric or thermal conductivity of composite materials. These models were later applied to calculate the effective permeability of permeating species through ideal mixed matrix membranes [23]. The estimated effective permeability describes the steady-state transport of components through the MMMs with ideal interface morphology (no rigidification, interface void and pore blockage). Moreover, a number of investigations have recently been performed to accurately calculate the effective diffusivity of species through mixed matrix membranes by solving Fick's 1st and 2nd law equations numerically [50–52]. However, the transport behavior reported in these studies denotes significant discrepancies. Indeed, the effect of particle size and the ratios of solubility factors and diffusion coefficients on the mass transport of species in membrane have shown important differences.

For the purpose of this research, the main effort has been devoted to propose an extended resistance-based model by coupling an analytical simple model with a more accurate three-dimensional finite difference solution to obtain an accurate analytical solution for estimating the effective permeability through mixed matrix membranes. Moreover, it was also desired to describe the mass transport through neat polymeric membranes in pervaporation separation by Maxwell-Stefan model while the effect of coupling flux, operating temperature and membrane swelling has been taken into consideration.

1.2. Research Objectives

The objectives of this research project are twofold:

1- Proposing a model to study the mass transfer of the components through dense polymeric membranes in a pervaporation membrane process by including the operating temperature and membrane swelling effect.
2- Introducing an analytical model to estimate the three-directional mass transport of species through ideal mixed matrix membranes used in a pervaporation separation process.

To achieve these objectives, the research was divided into two main sections:

1) To introduce a new modeling approach to include the effect of the operating temperature and membrane swelling on the parameters of the Maxwell-Stefan model. The new model is then validated with experimental data obtained from pervaporation experiments.

2) To propose a simple analytical resistance-based (RB) model to estimate the effective permeability of migrating species through ideal MMMs. Correction factors, based on the comparison of the simple RB model and an accurate solution obtained by solving the problem with the finite difference method, were incorporated into the model to obtain an accurate extended RB model.

1.2.1. Modeling of pervaporation using polymeric dense membranes

A new approach of the Maxwell-Stefan (MS) theory was investigated to describe the mass transport of species for the pervaporation separation of binary solutions using neat polymeric membranes. The model was constructed using a linear sorption isotherm (Henry's law) to represent the solubility factor of the migrating species within the membrane. Moreover, the effects of operating temperature and membrane swelling were considered for both the solubility factor and the diffusion coefficient. The coupling diffusion coefficient was estimated using a linear weighted combination of the individual component diffusion coefficients. The semi-empirical model was used to analyze the pervaporation separation of butanol from binary aqueous solutions with a commercial-type PDMS membrane. Pervaporation experiments were conducted at different butanol feed concentrations and operating temperatures to study the effect of these parameters on the membrane performance. Moreover, the estimated values of the diffusion coefficients and the solubility factors using the new model were presented and discussed. They were also compared to the ones reported in the literature.

1.2.2. Modeling of pervaporation using polymeric Mixed Matrix membranes (MMMs)

Three-directional species mass transport through ideal MMMs was investigated using a combination of a Resistance-Based (RB) model and Finite Difference (FD) method. The mixed matrix membrane was described by the repetition of a cubical membrane element which was called a RB element. Resistances to mass transport were defined as a function of the diffusion pathway, the area of penetration and the membrane permeability while Kirchhoff's rules were applied to

estimate the effective resistance of a RB element of the mass transport of the migrating species. The effective resistance of a RB element was used to estimate the permeability of MMMs as a function of permeability in two phases (continuous and dispersed phases) as well as the volume fraction of the filler material within the polymer matrix.

The finite difference method was used to solve the Fick's second law and to calculate the three-dimensional concentration profile within the RB element. Zero stage cut condition on the feed side and perfect vacuum on the permeate side of the RB element were assumed for the boundary conditions for the two planes of the RB element that are parallel to the flat membrane surfaces. Moreover, symmetrical conditions were used as the boundary conditions in the other four planes of the RB element and a linear concentration profile was used for the initial condition of the numerical solution to shorten the time to reach steady state. The component flux was calculated using the Fick's first law at the top, middle and bottom planes of the pervaporation membrane. The numerical solution was performed iteratively as a function of time in Visual Basic for Applications (VBA) until steady state permeation was reached. The steady-state flux, the thickness of the RB element and the concentration driving force were used to calculate the effective permeability of species in the RB element.

A new analytical model was developed by defining a correction factor for the RB model based on the ratio of effective permeability obtained from the accurate FD solution and the simple RB model. The correction factor was investigated for different ratios of permeability for the dispersed and continuous phases (P_d/P_c) and the volume fraction of the filler within the polymeric matrix (ϕ). The correction factors for MMMs containing high and low permeable fillers were modeled using two different Langmuir-type equations where the Langmuir parameters in both cases were observed to be strictly a function of the volume fraction ϕ. Two sets of polynomial equations were used to estimate the Langmuir parameters and, consequently, to obtain the final analytical model. Various sets of experimental data were obtained from the literature and used to validate the model for both pervaporation and gas separation applications.

1.3. Thesis structure

The main body of this thesis is mainly comprised of 4 chapters: introduction, modeling the pervaporation process with neat polymeric membranes, modeling the pervaporation process where

MMMs are used, and the conclusions and recommendations. Chapters 2 and 3 are two journal papers covering the entire scope of the research. These chapters have been written using the format of the particular journals.

Chapter 1 presents some background information on the research considered in this thesis as well as the objectives and the structure of the thesis. **Chapter 2** presents a new approach of the Maxwell-Stefan model to describe theoretically the mass transport of migrating species through polymeric membranes. Pervaporation experiments were conducted for the separation of butanol from binary aqueous solutions using a commercial PDMS membrane and the semi-empirical Maxwell-Stefan model was used to describe the membrane characterization and pervaporation performance. **Chapter 3** presents a new analytical model to predict the effective permeability of permeating species through ideal mixed matrix membranes. **Chapter 4** provides some overall conclusions of the research undertaken in this thesis as well as some recommendations for future work.

1.4. References

[1] A. Ebneyamini, H. Azimi, J. Thibault, F.H. Tezel, Description of Butanol Aqueous Solution Transport through Commercial PDMS Membrane via Pervaporation Process Using Extended Maxwell–Stefan Model, To be Submitted.

[2] Y. Zhu, F. Xin, Y. Chang, Y. Zhao, W. Weichong, Feasibility of reed for biobutanol production hydrolyzed by crude cellulase, Biomass Bioenergy. 76 (2015) 24–30. doi:10.1016/j.biombioe.2015.02.013.

[3] S. Heitmann, V. Krüger, D. Welz, P. Lutze, Experimental Investigation of Pervaporation Membranes for Biobutanol Separation, J. Membr. Sep. Technol. 2 (2013) 245–262. doi:http://dx.doi.org/10.6000/1929-6037.2013.02.04.5.

[4] P. Dürre, Biobutanol: An attractive biofuel, Biotechnol. J. 2 (2007) 1525–1534. doi:10.1002/biot.200700168.

[5] N. Abdehagh, F.H. Tezel, J. Thibault, Separation techniques in butanol production: Challenges and developments, Biomass Bioenergy. 60 (2014) 222–246. doi:10.1016/j.biombioe.2013.10.003.

[6] M. Kumar, K. Gayen, Developments in biobutanol production: New insights, Appl. Energy. 88 (2011) 1999–2012. doi:10.1016/j.apenergy.2010.12.055.

[7] X. Liu, Q. Gu, C. Liao, X. Yu, Enhancing butanol tolerance and preventing degeneration in Clostridium acetobutylicum by 1-butanol–glycerol storage during long-term preservation, Biomass Bioenergy. 69 (2014) 192–197. doi:10.1016/j.biombioe.2014.07.019.

[8] H. Dong, W. Tao, Z. Dai, L. Yang, F. Gong, Y. Zhang, Y. Li, Biobutanol, Adv. Biochem. Eng. Biotechnol. 128 (2012) 85–100. doi:10.1007/10_2011_128.

[9] W.J. Groot', C.E. van den Qever, N.W.F. Kossen, Pervaporation for simultaneous product recovery in the butanol/isopropanol batch fermentation, Biotechnol. Lett. 6 (1984) 709–714. doi:10.1007/BF00133061.

[10] A.P. Mariano, M.J. Keshtkar, D.I.P. Atala, F. Maugeri Filho, M.R. Wolf Maciel, R. Maciel Filho, P. Stuart, Energy Requirements for Butanol Recovery Using the Flash Fermentation Technology, Energy Fuels. 25 (2011) 2347–2355. doi:10.1021/ef200279v.

[11] A.P. Mariano, N. Qureshi, R.M. Filho, T.C. Ezeji, Bioproduction of butanol in bioreactors: new insights from simultaneous in situ butanol recovery to eliminate product toxicity, Biotechnol. Bioeng. 108 (2011) 1757–1765. doi:10.1002/bit.23123.

[12] A. Sharif Rohani, P. Mehrani, J. Thibault, Comparison of in-situ recovery methods of gas stripping, pervaporation, and vacuum separation by multi-objective optimization for producing biobutanol via fermentation process, Can. J. Chem. Eng. 93 (2015) 986–997. doi:10.1002/cjce.22186.

[13] H. Azimi, F.H. Tezel, J. Thibault, Effect of nano-activated carbon on the performance of Polydimethylsiloxane (PDMS) membrane for pervaporation separation of butanol from binary aqueous solutions., Submitt. J. Chem. Technol. Biotechnol. (2016).

[14] X. Yang, Z. Wu, F. Manquan, L. Jiding, Nonequilibrium Dissolution-diffusion Model for PDMS Membrane Pervaporation of ABE Water Binary System, J. Membr. Sci. Technol. 6 (2016) 143. doi:10.4172/2155-9589.1000143.

[15] R. Abedini, A. Nezhadmoghadam, Application of membrane in gas separation processes: Its suitability and mechanisms, Pet. Coal. 52 (2010) 69–80.

[16] P.D. Chapman, T. Oliveira, A.G. Livingston, K. Li, Membranes for the dehydration of solvents by pervaporation, J. Membr. Sci. 318 (2008) 5–37. doi:10.1016/j.memsci.2008.02.061.

[17] F. Lipnizki, S. Hausmanns, G. Laufenberg, R. Field, B. Kunz, Use of Pervaporation-Bioreactor Hybrid Processes in Biotechnology, Chem. Eng. Technol. 23 (2000) 569–577. doi:10.1002/1521-4125(200007)23:7<569::AID-CEAT569>3.0.CO;2-1.

[18] S.-Y. Li, R. Srivastava, R.S. Parnas, Study of in situ 1-butanol pervaporation from A-B-E fermentation using a PDMS composite membrane: Validity of solution-diffusion model for pervaporative A-B-E fermentation, Biotechnol. Prog. 27 (2011) 111–120. doi:10.1002/btpr.535.

[19] S.-Y. Li, R. Srivastava, R.S. Parnas, Separation of 1-butanol by pervaporation using a novel tri-layer PDMS composite membrane, J. Membr. Sci. 363 (2010) 287–294. doi:10.1016/j.memsci.2010.07.042.

[20] T.-S. Chung, L.Y. Jiang, Y. Li, S. Kulprathipanja, Mixed matrix membranes (MMMs) comprising organic polymers with dispersed inorganic fillers for gas separation, Prog. Polym. Sci. 32 (2007) 483–507. doi:10.1016/j.progpolymsci.2007.01.008.

[21] D. Hua, Y.K. Ong, Y. Wang, T. Yang, T.-S. Chung, ZIF-90/P84 mixed matrix membranes for pervaporation dehydration of isopropanol, J. Membr. Sci. 453 (2014) 155–167. doi:10.1016/j.memsci.2013.10.059.

[22] E.A. Fouad, X. Feng, Pervaporative separation of n-butanol from dilute aqueous solutions using silicalite-filled poly(dimethyl siloxane) membranes, J. Membr. Sci. 339 (2009) 120–125. doi:10.1016/j.memsci.2009.04.038.

[23] H. Vinh-Thang, S. Kaliaguine, Predictive Models for Mixed-Matrix Membrane Performance: A Review, Chem. Rev. 113 (2013) 4980–5028. doi:10.1021/cr3003888.

[24] J. Ahn, W.-J. Chung, I. Pinnau, M.D. Guiver, Polysulfone/silica nanoparticle mixed-matrix membranes for gas separation, J. Membr. Sci. 314 (2008) 123–133. doi:10.1016/j.memsci.2008.01.031.

[25] A.B. Yadav, M.L. Lind, J.Y. Lin, D.R. Nielsen, Arizona State University, Pervaporation Of Ethanol/Water mixtures using PDMS mixed matrix membranes, in: ASU Electron. Diss. Theses, Arizona State University, 2012. http://hdl.handle.net/2286/R.I.15095.

[26] D.P. Suhas, T.M. Aminabhavi, A.V. Raghu, Mixed matrix membranes of H-ZSM5-loaded poly(vinyl alcohol) used in pervaporation dehydration of alcohols: Influence of silica/alumina ratio, Polym. Eng. Sci. 54 (2014) 1774–1782. doi:10.1002/pen.23717.

[27] M. Hussain, A. König, Mixed-Matrix Membrane for Gas Separation: Polydimethylsiloxane Filled with Zeolite, Chem. Eng. Technol. 35 (2012) 561–569. doi:10.1002/ceat.201100419.

[28] R. Binning, R. Lee, J. Jennings, E. Martin, Separation of Liquid Mixtures by Permeation, Ind. Eng. Chem. 53 (1961) 45–50. doi:10.1021/ie50613a030.

[29] O. Kedem, The role of coupling in pervaporation, J. Membr. Sci. 47 (1989) 277–284. doi:10.1016/S0376-7388(00)83080-X.

[30] T. Okada, T. Matsuura, A new transport model for pervaporation, J. Membr. Sci. 59 (1991) 133–149. doi:10.1016/S0376-7388(00)81179-5.

[31] E.A. Mason, L.A. Viehland, Statistical–mechanical theory of membrane transport for multicomponent systems: Passive transport through open membranes, J. Chem. Phys. 68 (1978) 3562–3573. doi:10.1063/1.436213.

[32] F. Lipnizki, G. Trägårdh, Modelling of Pervaporation: Models to Analyze and Predict the Mass Transport in Pervaporation, Sep. Purif. Methods. 30 (2001) 49–125. doi:10.1081/SPM-100102985.

[33] P. Shao, R.Y.M. Huang, Polymeric membrane pervaporation, J. Membr. Sci. 287 (2007) 162–179. doi:10.1016/j.memsci.2006.10.043.

[34] R. Petrychkovych, K. Setnickova, P. Uchytil, The influence of water on butanol isomers pervaporation transport through polyethylene membrane, Sep. Purif. Technol. 107 (2013) 85–90. doi:10.1016/j.seppur.2013.01.014.

[35] Y. Shen, A.C. Lua, Theoretical and experimental studies on the gas transport properties of mixed matrix membranes based on polyvinylidene fluoride, AIChE J. 59 (2013) 4715–4726. doi:10.1002/aic.14186.

[36] P. Izák, L. Bartovská, K. Friess, M. Šípek, P. Uchytil, Description of binary liquid mixtures transport through non-porous membrane by modified Maxwell–Stefan equations, J. Membr. Sci. 214 (2003) 293–309. doi:10.1016/S0376-7388(02)00580-X.

[37] U.K. Ghosh, L. Teen, Application of modified Maxwell-Stefan equation for separation of aqueous phenol by pervaporation, Int. J. Chem. Mol. Nucl. Mater. Metall. Eng. 6 (2012) 526–531.

[38] H.J.C.T. Hennepe, C.A. Smolders, D. Bargeman, M.H.V. Mulder, Exclusion and Tortuosity Effects for Alcohol/Water Separation by Zeolite-Filled PDMS Membranes, Sep. Sci. Technol. 26 (1991) 585–596. doi:10.1080/01496399108050492.

[39] A. Erdem-şenatalar, M. Tatlier, Ş.B. Tantekin-Ersolmaz, Questioning the validity of present models for estimating the performances of zeolite-polymer mixed matrix membranes, Chem. Eng. Commun. 190 (2003) 677–692. doi:10.1080/00986440302109.

[40] E.A. Feijani, H. Mahdavi, A. Tavasoli, Poly(vinylidene fluoride) based mixed matrix membranes comprising metal organic frameworks for gas separation applications, Chem. Eng. Res. Des. 96 (2015) 87–102. doi:10.1016/j.cherd.2015.02.009.

[41] S.A. Hashemifard, A.F. Ismail, T. Matsuura, Prediction of gas permeability in mixed matrix membranes using theoretical models, J. Membr. Sci. 347 (2010) 53–61. doi:10.1016/j.memsci.2009.10.005.

[42] M.R. Othman, H. Mukhtar, A.L. Ahmad, Gas Permeation Characteristics across Nano-Porous Inorganic Membranes, IIUM Eng. J. 5 (2004) 17–33.

[43] J. Kärger, Determination of Diffusion Coefficients in Porous Media, in: Handb. Heterog. Catal., Wiley-VCH Verlag GmbH & Co. KGaA, 2008. doi:10.1002/9783527610044.hetcat0093.

[44] J. Kärger, J. Caro, P. Cool, M.-O. Coppens, D. Jones, F. Kapteijn, F. Rodríguez-Reinoso, M. Stöcker, D. Theodorou, E.F. Vansant, J. Weitkamp, Benefit of Microscopic Diffusion Measurement for the Characterization of Nanoporous Materials, Chem. Eng. Technol. 32 (2009) 1494–1511. doi:10.1002/ceat.200900160.

[45] R.H.B. Bouma, A. Checchetti, G. Chidichimo, E. Drioli, Permeation through a heterogeneous membrane: the effect of the dispersed phase, J. Membr. Sci. 128 (1997) 141–149. doi:10.1016/S0376-7388(96)00303-1.

[46] D. a. G. Bruggeman, Berechnung verschiedener physikalischer Konstanten von heterogenen Substanzen. I. Dielektrizitätskonstanten und Leitfähigkeiten der Mischkörper aus isotropen Substanzen, Ann. Phys. 416 (1935) 636–664. doi:10.1002/andp.19354160705.

[47] T.B. Lewis, L.E. Nielsen, Dynamic mechanical properties of particulate-filled composites, J. Appl. Polym. Sci. 14 (1970) 1449–1471. doi:10.1002/app.1970.070140604.

[48] L.E. Nielsen, Thermal conductivity of particulate-filled polymers, J. Appl. Polym. Sci. 17 (1973) 3819–3820. doi:10.1002/app.1973.070171224.

[49] R. Pal, New Models for Thermal Conductivity of Particulate Composites, J. Reinf. Plast. Compos. 26 (2007) 643–651. doi:10.1177/0731684407075569.

[50] G.M. Monsalve-Bravo, S.K. Bhatia, Extending effective medium theory to finite size systems: Theory and simulation for permeation in mixed-matrix membranes, J. Membr. Sci. 531 (2017) 148–159. doi:10.1016/j.memsci.2017.02.029.

[51] A.-C. Yang, C.-H. Liu, D.-Y. Kang, Estimations of effective diffusivity of hollow fiber mixed matrix membranes, J. Membr. Sci. 495 (2015) 269–275. doi:10.1016/j.memsci.2015.08.030.

[52] T. Singh, D.-Y. Kang, S. Nair, Rigorous calculations of permeation in mixed-matrix membranes: Evaluation of interfacial equilibrium effects and permeability-based models, J. Membr. Sci. 448 (2013) 160–169. doi:10.1016/j.memsci.2013.08.010.

Chapter 2: Mass transport in dense polymeric membranes

Description of Butanol Aqueous Solution Transport through Commercial PDMS Membrane via Pervaporation Process Using Extended Maxwell–Stefan Model

Arian Ebneyamini, Hoda Azimi, Jules Thibault and Handan Tezel*

Department of Chemical and Biological Engineering

University of Ottawa, Ottawa, Ontario, Canada K1N 6N5

Corresponding author: Handan.Tezel@uOttawa.ca

Abstract

The mass transport of components during the pervaporation of binary butanol aqueous solutions using commercial PDMS membranes has been investigated. The effect of temperature and concentration on the selectivity and flux of pervaporation has been studied. A simplified approach of the Maxwell-Stefan model was extended to include the effect of membrane swelling and temperature on the diffusion coefficient and sorption properties into the model. Partial permeate fluxes obtained at different temperatures and concentrations have been fitted to determine the extended model parameters. The sorption properties, component diffusion coefficients and coupled diffusion coefficient of butanol and water have been estimated using fitted parameters at different temperatures and concentrations. Predicted values of the solubility and diffusivity were used to calculate and compare the permeability of the components under different operating conditions.

Keywords: Pervaporation, Butanol, Extended Maxwell-Stefan Equation, Effect of Swelling

2.1. Introduction

Butanol has been considered as a potential biofuel for the partial replacement of liquid fuel obtained from fossil fuels [1–4]. Biobutanol produced from Acetone-Butanol-Ethanol (ABE) bacterial fermentation was a century ago the second largest biotechnological industrial process after ethanol in term of production capacity [5,6]. Its bacterial production was later completely replaced by petroleum-based butanol for economic reasons. In recent decades with large fluctuations in the price of fossil fuels and the desire to develop renewable and more sustainable fuels, a resurgence in the production of biobutanol has occurred. However, there are some major challenges to overcome to make the production of biobutanol from ABE fermentation economically viable. The main challenges are the low final butanol concentration in the fermentation broth and the toxic effect of this alcohol on microorganisms [7,8]. To enhance butanol production from ABE fermentation, it has been suggested to selectively remove a portion of the butanol produced during the course of fermentation to alleviate its toxicity via integrated recovery technologies such as vacuum fermentation, gas stripping, adsorption, liquid-liquid extraction and pervaporation [9–13].

One of the most promising solvent recovery methods is the pervaporation separation, which is a rapidly developing membrane-based process [14,15]. In this process, a liquid feed containing the chemical species to be separated is contacted with a dense membrane while the other side of membrane is kept under vacuum or a sweeping gas is used to maintain a very low concentration of the permeating components [16]. In comparison to distillation, adsorption, gas stripping, liquid-liquid extraction and other traditional separation methods, pervaporation has some advantages such as high selectivity, low energy consumption and ease of design [17,18]. Moreover, the pervaporation process does not have a detrimental effect on microorganisms such that it can be used for in situ solvent recovery [19].

Membranes made out of a variety of polymeric materials such as styrene butadiene rubber (SBR), ethylene propylene diene rubber (EPDM), polytetrafluoroethylene (PTFE), polypropylene (PP), polyurethane (polyether based) (PUR), polyether block-amide (PEBA), poly(vinylidinedifluoride) (PVDF), poly(methoxy siloxane) (PMS), polydimethylsiloxane (PDMS), poly(1-(trimethylsilyl)-1-propyne) (PTMSP) and polyamide-imide (PAI) containing cyclodextrin (CD) have been used in butanol separation using pervaporation [14]. Among these polymers, PDMS membranes are the

most often used ones for butanol separation due to their high level of hydrophobicity, high flux and selectivity, their good thermal, chemical and mechanical stability [20]. In this study, commercial PDMS membranes were used to investigate the pervaporation separation of butanol from binary aqueous solutions.

Modelling the mass transfer through membranes in the pervaporation process is important in order to gain a more comprehensive engineering understanding of the permeation process, to efficiently design membrane separation processes and to improve the membrane performance [21]. Different models such as solution-diffusion model, thermodynamics of irreversible process (TIP), pore flow model, and Maxwell-Stefan model have been used to describe the transport phenomena through membranes in pervaporation processes [21]. According to the solution-diffusion theory, there are three major steps for the transport of species from the feed side to the permeate side of the membrane [16,21,22]: (1) sorption on the surface of membrane at the feed side, (2) diffusion through the membrane, and (3) desorption from the permeate side.

In this study, a model based on the solution-diffusion theory using the Maxwell-Stefan model has been developed to predict the separation performance of membrane pervaporation of butanol from binary aqueous solutions. While the model was used to predict the performance of commercial PDMS membranes, it can be easily adapted for other pervaporation membranes. In addition, the effect of membrane swelling has been incorporated in the estimation of the component diffusion coefficients using an exponential relation between the diffusion coefficient and the degree of swelling at a fixed temperature. Moreover, Arrhenius-type equations were used to estimate the solubility and diffusivity parameters at different operating temperatures.

2.2. Materials and methods

2.2.1. Membrane and materials

Commercial PDMS membranes (PDMS A4 size flat sheet membranes) were obtained from Pervatech B.V. (Rijssen, Netherlands). Even though the exact manufacturing details are not available, SEM image analysis of this commercial membrane (Figure 2.1) revealed that it consists of three layers: a thin PDMS active layer of approximately 5 µm thick mounted on a two-layer porous support (100 µm Polyimide (PI) thick and 100-150 µm thick Polyethylene (PET) as the

first and second layer, respectively[1]). Butanol (99% pure, Acros) was obtained from Fisher Scientific (Fair Lawn, NJ, USA). Deionized distilled water was used to prepare all binary aqueous solutions.

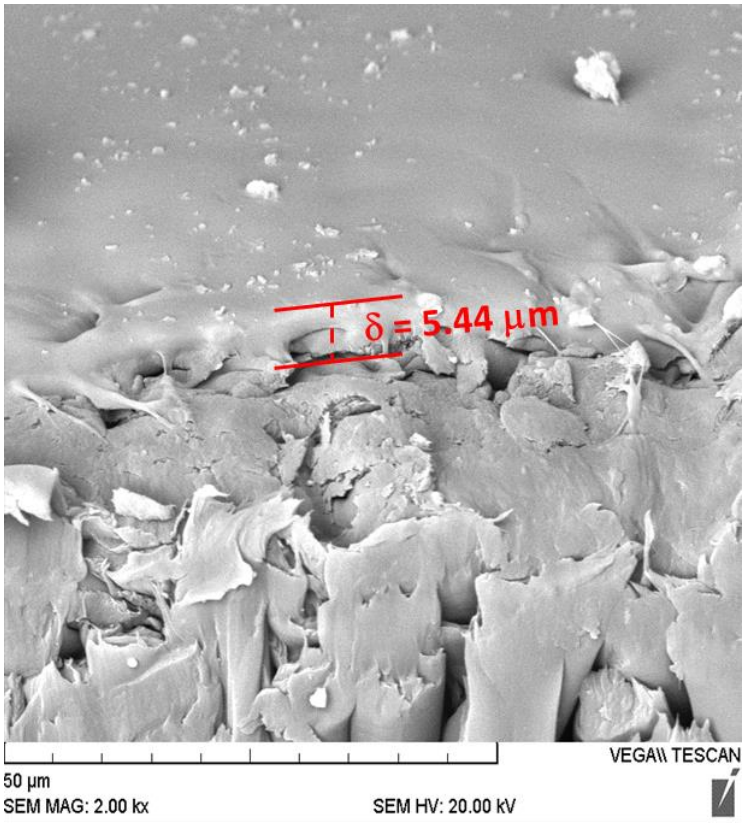

Figure 2.1.SEM picture of the cross section of the Pervatech commercial PDMS

2.2.2. Three-membrane Pervaporation Experimental System

Figure 2.2 presents the schematic diagram of the experimental system that was used to carry out all pervaporation tests. The experimental system is comprised of three flat membrane modules placed in series where the retentate flow of the first module is the feed of the second module and the retentate flow of the second module is the feed of the third module. A peristaltic pump (Cole-Parmer Instrument Company, Montreal, Canada) was used to pump the butanol aqueous solution from feed tank to the feed side of the first membrane module. The retentate flow of the third membrane module was returned to the feed tank. The flow rate was high enough to ensure nearly zero-stage cut condition (permeate flow rate was on average 2.5×10^4 times smaller than the feed

[1] These thickness values for the commercial PDMS membrane were provided by Pervatech B. V.

flow rate). The three-module assembly was placed in a temperature-controlled oven. Prior to entering the first membrane module, the feed stream flowed through a long stainless steel coil located in the oven to be pre-heated to the desired temperature. A thermocouple was used to measure and record the temperature of the feed flow before entering membrane modules.

The vapour permeate from each of the three modules was condensed, each using its own cold trap to independently measure the performance of each membrane. The three cold traps were immersed into a liquid nitrogen Dewar flask. The level of liquid nitrogen in the Dewar flask was controlled using an automatic time-fill controller. A vacuum pump (Scroll Pump, 78603-11, Cole-Parmer, Montreal, Quebec, Canada) was used to keep the permeate side of the membrane under very low pressure (~3 Torr). The cumulative permeate samples were collected at the end of the experiment for each membrane module, weighed and analyzed individually for their concentration using high performance liquid chromatography (HPLC). The average values of experimentally obtained partial permeate fluxes of the two species have been reported in Section 2.4.2.

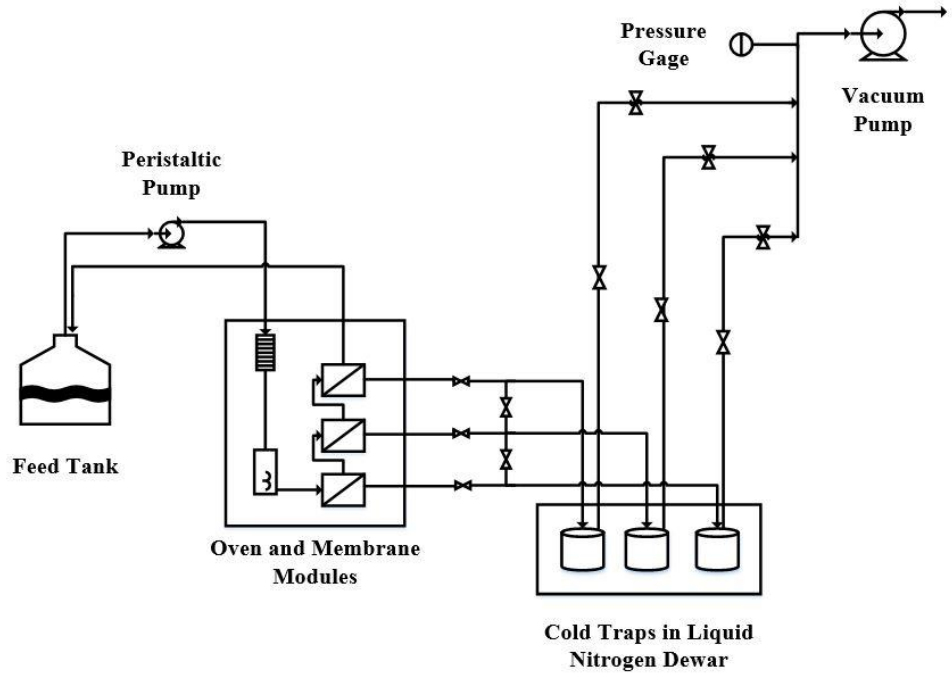

Figure 2.2. Schematic diagram of the three-module pervaporation experimental set up.

To investigate the effect of the operating temperature and feed concentration on the membrane performance, commercial PDMS membranes were tested for three different feed concentrations

(5, 20 and 50 g L^{-1}) of butanol over a temperature range of 37-57°C. The first level of temperature was chosen based on the typical temperature under which an ABE fermentation is performed.

Membrane performance in the pervaporation separation process is typically defined in terms of selectivity and total permeate flux. The permeate molar flux of species *i* is calculated using Equation (2.1) [14,23].

$$J_i = \frac{m_t y_i}{t A_M M_i} \tag{2.1}$$

where J_i is the mole flux of component *i*, m_t is the total mass of the permeate collected in an experiment, y_i is the permeate mass fraction of component *i*, A_M is the membrane area, M_i is the molecular weight of component *i* and *t* is the duration of the specific experiment.

Selectivity of component *i* is defined as a function of mass or mole fraction of a specific species in the feed and permeate side of the membrane as shown in Equation (2.2), generalized for a multicomponent system [24]. Under the assumption of steady state, the permeate stream mass or mole fraction can be calculated using the permeate mass or mole flux of the components as presented in Equation (2.3).

$$\alpha_i = \frac{\left(\frac{y_i}{1-y_i}\right)}{\left(\frac{x_i}{1-x_i}\right)} \tag{2.2}$$

$$y_i = \frac{J_i}{\sum_{i=1}^{n} J_i} \tag{2.3}$$

where α_i is the membrane selectivity for component *i*, *n* is the number of components in the mixture and x_i is the mass or mole fraction of component *i* in the liquid feed.

The pervaporation separation index (PSI) is a parameter used to compare the performance of different membranes under different operating conditions. For a specific component, this parameter is defined in Equation (2.4) [14]:

$$PSI = J_i\left(\alpha_i - 1\right) \tag{2.4}$$

2.3. Pervaporation modeling method

In this section, a simplified approach of Maxwell-Stefan [15] model is briefly described and then used to represent the experimental data for the pervaporation of aqueous butanol solutions using a commercial PDMS membrane. The model was also extended to include the effect of the operating conditions on the solubility and diffusivity parameters.

2.3.1. Maxwell-Stefan model

The Maxwell–Stefan theory assumes that the movement of a species in a multicomponent mixture is caused by a concentration driving force, which is balanced by the friction of one species with the other species in the solution and its surrounding [23,25]. A simplified approach of the model was used by Aguilar-Valencia et al. to simulate the pervaporation process for the separation of ethanol from aqueous solutions using PDMS membranes [15]. According to the concept of irreversible thermodynamic, Equation (2.5) is applicable for the relationship between the chemical potential and friction resistances in multicomponent mixtures where *n* applies for all penetrants as well as the membrane material [23,26].

$$\frac{x_i}{RT}\nabla(T,P)\mu_i = \sum_{j=1}^{n}\frac{x_i x_j\left(u_j - u_i\right)}{D_{ij}} \tag{2.5}$$

Based on momentum conservation, the coupling diffusion coefficients for the permeating species D_{ij} and D_{ji} in the Maxwell-Stefan equation are identical [23]. Therefore, for a one-directional transport of species of a binary solution through the membrane (b: Butanol, w: Water, M: Membrane), Equation (2.5) reduces to Equation (2.6) for the description of butanol transport within the membrane. An equivalent expression can be written for the water transport, as well.

$$\frac{x_b}{RT}\frac{d\mu_b}{dz} = \frac{x_b x_w\left(u_w - u_b\right)}{D_{bw}} + \frac{x_b x_M\left(u_M - u_b\right)}{D_{bM}} \tag{2.6}$$

According to Hittorf frame of reference [23], the membrane velocity can be set to zero. Moreover, velocities of species have been rewritten in terms of their fluxes and concentrations while the

expression x_M / D_{bM} was replaced by $1/\bar{D}_{bM}$ where $\bar{D}_{bM}$ is the Maxwell-Stefan diffusion coefficient of butanol in the membrane.

$$\frac{x_b}{RT}\frac{d\mu_b}{dz} = \frac{x_b J_w - x_w J_b}{C_T D_{bw}} + \frac{J_b}{C_T \bar{D}_{bM}} \tag{2.7}$$

where C_T is the total molar concentration of the membrane. Equation (2.8) was used to relate the gradient of the chemical potential of component *i* within the membrane to the temperature and to its partial pressure gradient as the prevailing driving force for the pervaporation separation process. The calculation of the partial pressure in the liquid feed is given in Section 2.4.1 while a perfect vacuum was assumed on the permeate side of the membrane. Moreover, due to the low butanol concentration in the feed, it was assumed that Henry's law is dominating as the sorption mechanism of butanol in the polymer. In addition, it has been reported that water sorption from binary ethanol aqueous solutions in PDMS membranes follows Henry's law mechanism [15]. Similarly, also assuming non-competitive sorption of species for butanol-water binary solutions, water sorption in binary butanol-water solutions should follow the Henry's law mechanism in PDMS membranes. Hence, the two differential equations, as shown in Equations (2.9) and (2.10), can be written in terms of the partial pressures to account for the mass transport of both butanol and water through the membrane [15].

$$\frac{d\mu_i}{dz} = \frac{RT}{p_i}\frac{dp_i}{dz} \tag{2.8}$$

$$H_b \frac{dp_b}{dz} = \frac{p_b J_w H_b - p_w J_b H_w}{C_T D_{bw}} - \frac{J_b}{\bar{D}_{bM}} \tag{2.9}$$

$$H_w \frac{dp_w}{dz} = \frac{p_w J_b H_w - p_b J_w H_b}{C_T D_{bw}} - \frac{J_w}{\bar{D}_{wM}} \tag{2.10}$$

According to Krishna's method [15,26], it is assumed that the concentration profiles of both species across the membrane are linear and the Maxwell-Stefan diffusivities are constant throughout the membrane. Moreover, to simplify the integration of the equations and, without loss

of generality, the partial pressure of component *i* throughout the membrane is considered to be constant and equal to the average partial pressure between the retentate and the permeate streams [15]. The butanol and water fluxes were obtained by integrating the two differential equations as presented in Equations (2.11) and (2.12).

$$J_b = \frac{\left(-\Delta p_b\right) - \left(\frac{K_3\,\bar{p}_b\,\Delta p_w}{K_4\bar{p}_b + K_5}\right)}{K_1\bar{p}_b + K_2 - \left(\frac{\left(K_3^2\right)\bar{p}_b\bar{p}_w}{K_4\bar{p}_b + K_5}\right)} \tag{2.11}$$

$$J_w = \frac{\left(-\Delta p_w\right) + K_3\bar{p}_w J_b}{K_4\bar{p}_b + K_5} \tag{2.12}$$

where parameters K_m (m =1 to 5) are defined in Equations (2.13)-(2.17).

$$K_1 = \frac{H_w\delta}{H_b D_{bw} C_T} \tag{2.13}$$

$$K_2 = \frac{\delta}{H_b \bar{D}_{bM}} \tag{2.14}$$

$$K_3 = \frac{\delta}{D_{bw} C_T} \tag{2.15}$$

$$K_4 = \frac{H_b\delta}{H_w D_{bw} C_T} \tag{2.16}$$

$$K_5 = \frac{\delta}{H_w \bar{D}_{wM}} \tag{2.17}$$

The numerical values of these parameters were determined by performing a simultaneous nonlinear regression to minimize the sum of squares of the differences between the experimental

butanol and water fluxes (J_b and J_w, respectively) obtained at different temperatures and concentrations and the ones predicted by the models (by Eqs. (2.11) and (2.12)).

2.3.2. Extended Maxwell-Stefan model based on the concentration and temperature effect

Although the simplified Maxwell-Stefan model showed relatively good agreement with experimental data in the case of ethanol separation [15], the fact that the diffusion coefficients and the solubility factors are changing with the operating conditions indicates that values of parameters K_m cannot be constant at different temperature and feed concentration. In order to extend Equations (2.13)-(2.17) for different operating conditions, the effect of temperature and concentration on the solubility and diffusion coefficients was investigated.

2.3.2.1. Solubility

An Arrhenius-type equation (Van't Hoff equation) was used to account for the effect of temperature on the Henry's law constant [27,28].

$$H_i^* = H_{i0}^* e^{\frac{-\Delta H_i}{RT}} \tag{2.18}$$

where ΔH_i is the heat of sorption and H_i^* is the Henry's law constant $\left(g.m^{-3}/g.m^{-3}\right)$. Equation (2.19) was used to convert the Henry's law constant to the solubility factor from $\left(g.m^{-3}/g.m^{-3}\right)$ to $\left(mole.m^{-3}.bar^{-1}\right)$ which has been used in Equations (2.13)-(2.17). This equation considers both concentration and temperature dependency of the solubility factor of component *i* in the membrane.

$$H_i = \frac{H_i^* C_{fi}}{p_i M_i} = \frac{H_{i0}^* C_{fi}}{p_i M_i} e^{\frac{-\Delta H_i}{RT}} \tag{2.19}$$

2.3.2.2. Diffusivity

Swelling of the membrane leads to an increase in the free volume of the polymer which results in an increase of the membrane diffusivity. Since the concentration of each species varies linearly across the membrane, swelling of a polymeric membrane will be higher on the feed side and will

progressively decrease to nearly no swelling at the permeate side of the membrane. In practice, the variation in the degree of swelling across the membrane implies that the diffusion coefficient will also vary. In the case of a dilute aqueous solution of butanol in contact with a PDMS membrane, the degree of swelling will be relatively small because of the low concentration of butanol and the low solubility of water in PDMS. As a result, the variation of the diffusion coefficients will be small. Therefore, it is assumed that the diffusion coefficients are constant within the membrane and equal to their average values for a given feed condition. To account for the variation of the degree of swelling as a function of the feed composition, an exponential relationship was used to express the diffusion coefficient of each component as a function of the degree of swelling (ϕ) of the membrane at a fixed temperature (Eq. (2.20)). A similar type of expression was used by Shao and Huang to relate the diffusion coefficient to the feed concentration [29].

$$D_{iM} = D_{i0}\, e^{A_i \phi_{(C_{fi},T)}} \tag{2.20}$$

where A_i is a dimensionless constant. Assuming non-competitive sorption of the species in the membrane, the degree of swelling was calculated by dividing the summation of the sorbed phase concentrations of the two diffusing species of the binary feed solution by the density of the neat PDMS membrane (Eq. (2.21)).

$$\phi_{(C_{fi},T)} = \frac{C_{fi} H_i^* + C_{fj} H_j^*}{\rho_M} = \frac{C_{fi} H_{i0}^* e^{\frac{-\Delta H_i}{RT}} + C_{fj} H_{j0}^* e^{\frac{-\Delta H_j}{RT}}}{\rho_M} \tag{2.21}$$

Furthermore, the diffusion coefficient also follows an Arrhenius-type relation with respect to temperature at a constant feed concentration [21].

$$D_{iM} = D_{i0}^*\, e^{\frac{-\Delta E_{di}}{RT}} \tag{2.22}$$

where E_{di} is the energy of activation for the diffusion of component i in the membrane. By assuming that A_i and E_{di} are independent of temperature and concentration, the diffusion coefficient

of component *i* at any feed concentration and at an arbitrary reference temperature was estimated using Equation (2.20).

$$D_{iM(C_{fi},T_R)} = D_{i0(T_R)} e^{A_i \phi_{(C_{fi},T_R)}} \tag{2.23}$$

Using Equations (2.21)–(2.23), an extended expression for the diffusion coefficient at various concentrations and temperatures was derived and resulted in Equations (2.24) and (2.25).

$$D_{iM(C_{fi},T)} = D_{iM(C_{fi},T_R)} \frac{D_{iM(C_{fi},T)}}{D_{iM(C_{fi},T_R)}} = D_{i0(T_R)} \left[e^{A_i \phi_{(C_{fi},T_R)}} \right] \left[e^{\left(\frac{-\Delta E_{di}}{R}\right)\left(\frac{1}{T}-\frac{1}{T_R}\right)} \right] \tag{2.24}$$

or

$$D_{iM(C_{fi},T)} = D_{i0(T_R)} e^{\left(A_i \left(\frac{C_{fi} H^*_{i0} e^{\frac{-\Delta H_i}{RT_R}} + C_{fj} H^*_{j0} e^{\frac{-\Delta H_j}{RT_R}}}{\rho_M} \right) - \left[\frac{\Delta E_{di}}{R} \left(\frac{1}{T} - \frac{1}{T_R} \right) \right] \right)} \tag{2.25}$$

The term of the coupling effect ($c_T D_{bw}$) in Equation (2.7) represents the effect of one component on the mass transport of the other component for the diffusion penetration of butanol-water binary mixture through the membrane [23]. According to Maxwell-Stefan theory, increasing the coupled diffusion coefficient (D_{ij}) results in a decrease in the frictional effect exerted by component *i* on component *j*. Moreover, in the case of a system with negligible coupling effect, the coupled diffusion coefficient tends towards infinity [21,30]. D_{ij} is typically estimated using the diffusion coefficients of the components in the membrane [31] with respect to the experimental partial fluxes of the components [23,30]. In this study, it was assumed that the coupled diffusion coefficient is a linear weighted combination of the component diffusion coefficients as given by Equation (2.26).

$$D_{ij} = Q_i D_{iM} + Q_j D_{jM} \tag{2.26}$$

The total molar concentration of the membrane is assumed equal to the molar density of the swelled membrane. By considering that the effect of the change in volume due to swelling is negligible on the membrane density, the molar density of the swelled membrane was determined with the number of moles of the adsorbed phase, the molecular weights and the density of the polymer, as given in Equation (2.27).

$$C_T = \frac{C_{fi} H_i^*}{M_i} + \frac{C_{fj} H_j^*}{M_j} + \frac{\rho_M}{M_M} \tag{2.27}$$

The expressions for the diffusion coefficients, Henry's law constants and the total molar concentration of the membrane, written in terms of concentration and temperature, have been inserted into Equations (2.13)-(2.17) to express the K_m values as functions of concentration and temperature. Then a non-linear regression was performed to optimize the parameters listed in Table 2.1 to minimize the sum of the squared residuals between the calculated and the experimental values for J_b and J_w in Equations (2.11) and (2.12).

Table 2.1. List of the parameters determined in the Extended Maxwell-Stefan model

Unknown Parameters	
$D_{b0(T_R)}$	$D_{w0(T_R)}$
E_{db}	E_{dw}
A_b	A_w
H_{b0}^*	H_{w0}^*
ΔH_b	ΔH_w
Q_b	Q_w

2.4. Results and discussion

2.4.1. Feed partial pressure calculation

The extended Raoult's law was used to predict the partial pressure of components in equilibrium with the feed solution to be used in Equations (2.11), (2.12) and (2.19) [15,30]:

$$p_i = x_i \gamma_i p_i^S \tag{2.28}$$

Margules model (Eqs. (2.29)-(2.30)) was used to estimate the activity coefficients for both components [32].

$$Ln(\gamma_1) = x_2^2 \left[Ln(\gamma_1^\infty) + 2x_1 \left(Ln(\gamma_2^\infty) - Ln(\gamma_1^\infty) \right) \right] \tag{2.29}$$

$$Ln(\gamma_2) = x_1^2 \left[Ln(\gamma_2^\infty) + 2x_2 \left(Ln(\gamma_1^\infty) - Ln(\gamma_2^\infty) \right) \right] \tag{2.30}$$

The infinite dilution activity coefficients for vapour-liquid equilibrium for butanol in aqueous solutions were obtained from the literature [33]. The infinite dilution activity coefficient for butanol as a function of temperature is presented in Figure 2.3. Values for butanol can be sufficiently well approximated by a linear relation with respect to temperature in the range of 303-333 K. On the other hand, the infinite dilution activity coefficient for water in a butanol aqueous mixture is 5.06 at room temperature and progressively decreases to 3.27 at 343 K [34]. Since the initial feed is a dilute aqueous solution with a very small concentration of butanol, the activity coefficients of butanol and water are not sensitive to the infinite dilution activity coefficient for water under the operating conditions encountered in this investigation. Hence, this value for water was set equal to unity for the range of temperatures used in this investigation.

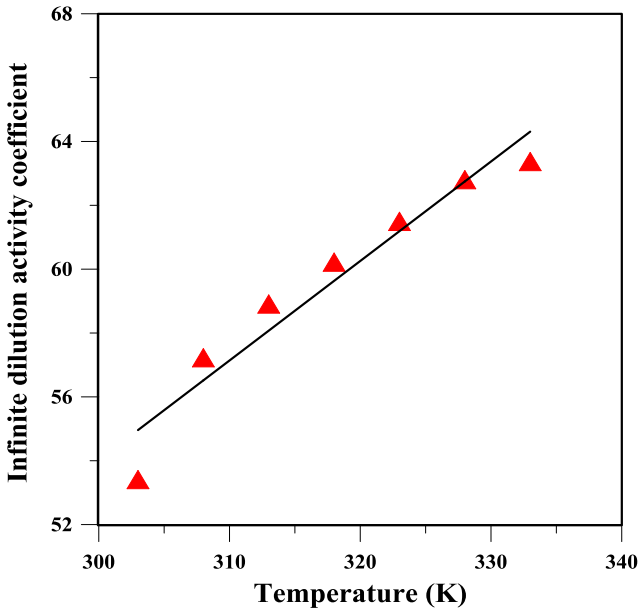

Figure 2.3. Experimental (▲) and calculated (—) values of infinite dilution activity coefficient of butanol in water as a function of temperature [33].

Antoine equation was used to predict the saturation vapour pressures of butanol and water at different temperatures [35].

$$Ln\left(p^{S}_{(kPa)}\right) = \bar{A} - \frac{\bar{B}}{\bar{C} + T_{(^{0}C)}} \tag{2.31}$$

The parameters of Antoine equation for butanol and water were obtained from the literature [36]. The values of these parameters are given in Table 2.2.

Table 2.2. Antoine coefficients for vapour pressure of butanol and water [36]

Parameter	Butanol	Water
$\bar{A}$	15.3144	16.3872
$\bar{B}$	3212.43	3885.70
$\bar{C}$	182.739	230.170

2.4.2. Modeling of membrane performance

The Maxwell-Stefan (MS) and the extended Maxwell-Stefan (Extended MS) approaches were used to describe the transport of both butanol and water through a commercial PDMS membrane. A 310 K reference temperature was used in the extended model. Moreover, since the molecular weight of the PDMS layer of the commercial membrane used in this investigation was not available, an assumed approximate value of 30 000 g.mol^{-1} was used[(2)]. A value of 970 kg.m^{-3} was used as the density of PDMS layer of the membrane [37]. Given the large number of parameters that need to be determined by the nonlinear regression for the extended MS model, it is paramount to use the right order of magnitude for the initial guess values for these parameters. Table 2.3 presents a set of Henry's law constants of pure butanol and water in PDMS which were obtained from isotherms and sorption capacities available in the literature at different temperatures.

The data in Table 2.3 were used in Equation (2.18) to estimate the parameters of the Arrhenius equation for the sorption of butanol and water in the PDMS membrane. These estimated values are presented in Table 2.4 and they were used as the initial guesses for the extended Maxwell-Stefan model.

Curve fitting was performed using the experimental data obtained at different temperatures for both Maxwell-Stefan and extended Maxwell-Stefan models by minimizing the differences between the calculated and experimental component fluxes to determine the parameters of each

[2] The value of PDMS molecular weight could vary from 162 to 116 500 g.mol^{-1} based on the viscosity of the polymer [37]

model separately. The obtained parameters of both models are given in Tables 2.5 and 2.6, respectively.

Table 2.3. Henry's law constants of butanol and water in PDMS at different temperatures from literature.

Component	Temperature (K)	Henry's Law constant ($g.L^{-1}/g.L^{-1}$)
Butanol	313	0.277 [38]
Butanol	373	0.194[3]
Water	283	0.00113 [39]
Water	298	0.00134 [39]
Water	298	0.00134 [40]
Water	313	0.00152 [39]
Water	333	0.00173 [39]

Table 2.4. Initial guesses for the coefficients of Arrhenius equation for the solubility of butanol and water in PDMS.

Component	H_0^* ($g.L^{-1}/g.L^{-1}$)	ΔH ($J.mol^{-1}$)
Butanol	0.03	-5785
Water	0.022	6928

[3] Isotherm was obtained from butanol adsorption isotherm at 313 K [38] and using the ratio of the maximum sorption capacity (pure component sorption) obtained from the Flory-Huggins parameters at 373 K [37] and 313 K [38]

Table 2.5. Values of the parameters for the Maxwell-Stefan model.

K_1 ($m^2.h.mol^{-1}$)	K_2 ($m^2.h.bar.mol^{-1}$)	K_3 ($m^2.h.mol^{-1}$)	K_4 ($m^2.h.mol^{-1}$)	K_5 ($m^2.h.bar.mol^{-1}$)
0.00073	0.05033	0.0041	0.0227	0.0197

Table 2.6. Values of parameters determined from the extended Maxwell-Stefan model.

Parameter	Value	Parameters	Value
$D_{b0(Tr)}$ ($m^2.h^{-1}$)	8.02×10^{-9}	$D_{w0(Tr)}$ ($m^2.h^{-1}$)	8.12×10^{-8}
E_{db} ($J.mol^{-1}$)	26853.9	E_{dw} ($J.mol^{-1}$)	29692.25
A_b (-)	9.99×10^{-5}	A_w (-)	16.3
H^*_{b0} ($g.m^{-3}/g.m^{-3}$)	0.032	H^*_{w0} ($g.m^{-3}/g.m^{-3}$)	0.0238
ΔH_b ($J.mol^{-1}$)	-6362.76	ΔH_w ($J.mol^{-1}$)	4949.5
Q_b	9.91	Q_w	17.11

To evaluate the performance of the Maxwell-Stefan and the extended Maxwell-Stefan models, the predicted butanol and water fluxes obtained with both models as a function of butanol concentration at three different temperatures were compared with the experimental data. Results, presented in Figure 2.4, show that the permeate fluxes for both butanol and water increase with the concentration of butanol in the feed. According to the extended Raoult's law (Equation (2.28)), by increasing the butanol concentration in the feed, the equilibrium partial pressure of butanol increases which results in a higher driving force for the mass transfer of butanol across the membrane. In addition, butanol has a higher affinity for PDMS which leads to a higher solubility in comparison to water [14]. Therefore, by increasing the butanol concentration in the feed stream,

a higher sorption of butanol in the PDMS membrane occurs accompanied by a higher degree of swelling. An increase in the degree of swelling of the membrane results in a higher free volume available for diffusion of components and consequently an increase in the permeate fluxes of both butanol and water [41]. In this investigation, because of the highly diluted butanol concentration in the feed (5-50 $g.L^{-1}$), the water driving force remains essentially constant such that the observed increase in water flux is due to membrane swelling. The effect of membrane swelling on the diffusivity and flux is much more significant for water because of its smaller molecular size in comparison to butanol [42] (1.48 Å for water in comparison to 2.53 Å for butanol [43]). Altogether, the butanol flux increases with an increase in the butanol feed concentration due to the increasing concentration driving force. On the other hand, the membrane swelling, even though small, is the main reason for the increased water flux with the increase in the butanol feed concentration.

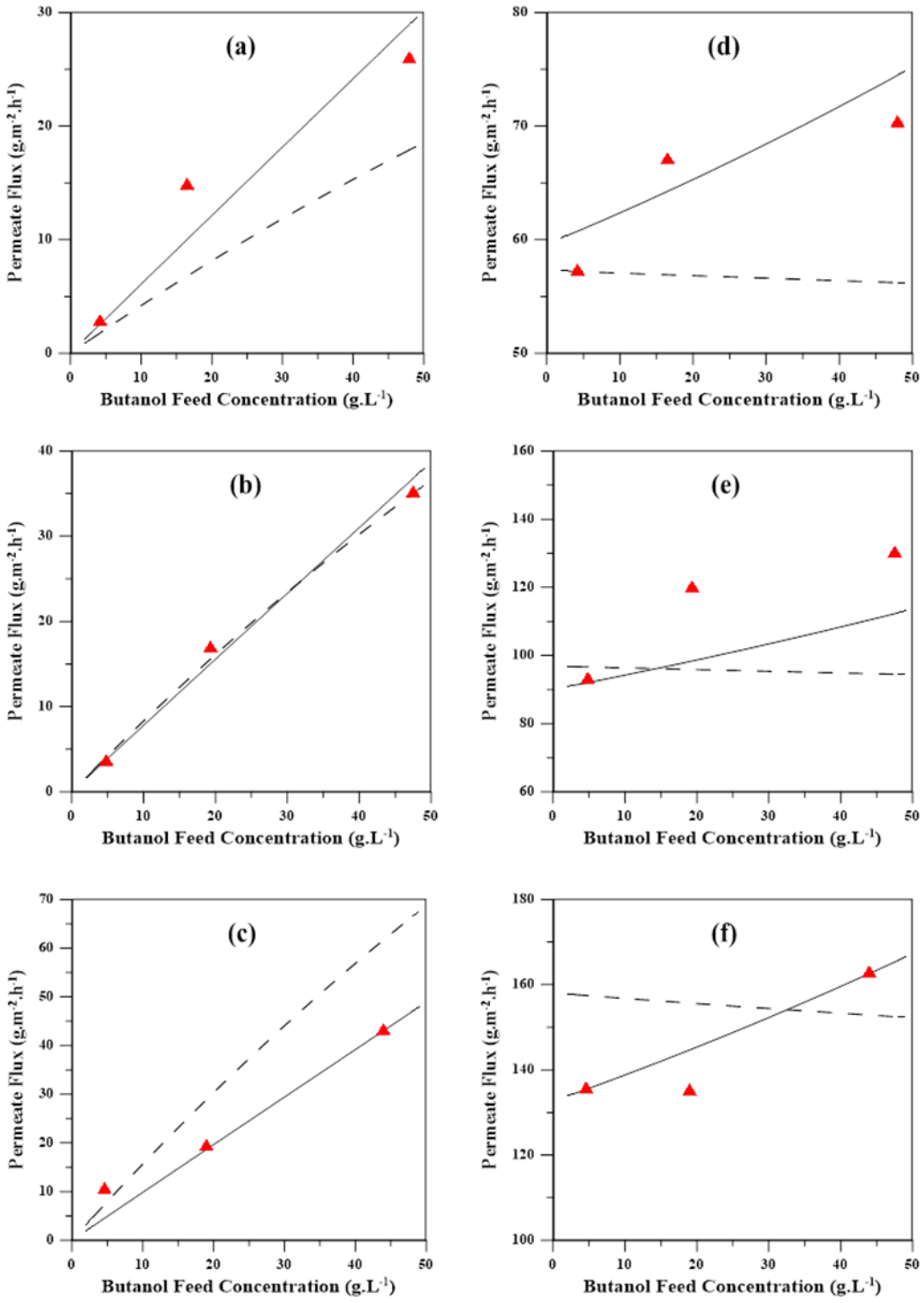

Figure 2.4. Estimated (MS Model — —, Extended MS Model —) and experimental (▲) butanol ((a) 310 K, (b) 320 K, (c) 330 K) and water fluxes ((d) 310 K, (e) 320 K, (f) 330 K) vs butanol feed concentration at different temperatures.

Figure 2.5 shows the effect of temperature on butanol and water fluxes at a feed concentration of 20 $g.L^{-1}$. According to the heat of sorption presented in Table 2.4, the sorption of butanol and water in PDMS membrane are exothermic and endothermic, respectively. Hence, as it will be shown in the next section, increasing the temperature reduces the sorption of butanol in PDMS while the sorption capacity of water slightly increases with temperature. At the same time, the increase of the chain motion of the polymeric membrane with an increase in temperature leads to a higher free volume and consequently higher diffusivity of both species within the membrane [14]. Equation (2.32) expresses the permeate flux of component *i* in terms of both partial pressure and concentration difference as the driving force for the transport of species in a system without coupling effect. According to the experimental data in Figures 2.4 and 2.5, the permeate fluxes of both species have increased with increasing temperature. For butanol, this is due to the higher temperature sensitivity of the diffusion coefficient than the sorption properties of this component. The increase of the water flux with increasing temperature would be due to both its diffusion and sorption (H^*) (endothermic sorption) increase with temperature.

$$J_i = \frac{H_i D_{iM}\left(\Delta p_i\right)}{\delta} = \frac{H_i^* D_{iM}\left(\Delta C_i\right)}{\delta} \tag{2.32}$$

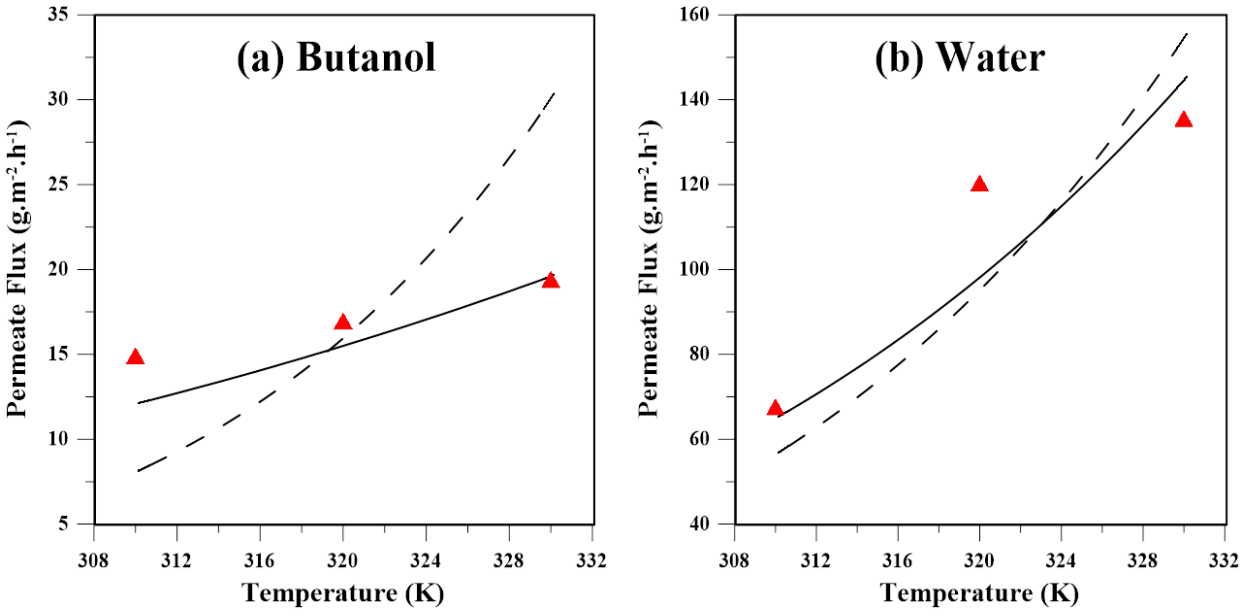

Figure 2.5. Effect of temperature on butanol (a) and water (b) permeation fluxes at a feed butanol concentration of 20 $g.L^{-1}$ (MS Model — —, Extended MS Model —, Experimental ▲)

2.4.3. Simulation of membrane properties

2.4.3.1. Sorption properties

The fitted parameters for the estimation of the solubility factors in the extended MS model were used in Equations (2.18) and (2.19) to estimate the sorption properties of the components in a PDMS layer in term of Henry's law constant (H^*) and solubility factor (H), respectively. Results of Figure 2.6 show that the Henry's law constant of butanol slightly decreases with an increase in temperature whereas the water Henry's law constant smoothly increases with temperature. These trends are in agreement with the data reported in the literature for pure water and butanol sorption in PDMS membrane presented in Table 2.3. Moreover, the higher Henry's law constant for butanol in comparison to the one for water shows a higher solubility of butanol in the hydrophobic PDMS membrane. This can be explained via the Hansen's solubility parameters, which consist of hydrogen bonding interactions, polar interactions and dispersion interactions. The distance between two substances based on their partial solubility parameter (called distance parameter) is a metrics usually used to investigate the affinity between the materials. A smaller value of the distance parameter indicates a higher mutual affinity of the pair of materials. It has been reported that the distance parameter of water-PDMS is larger than the one for butanol-water (41.4 in comparison to 13.0 $MPa^{1/2}$, respectively) which indeed indicates higher affinity of butanol for PDMS membrane [14].

Figure 2.6 also presents the predicted values for the solubility factor (H) of butanol and water in PDMS membrane at different operating conditions. According to Equation (2.19), the solubility factor is a function of the Henry's law constant as well as the equilibrium partial pressure of the species on the feed side of the membrane. As it is mentioned previously, Henry's law constants of butanol and water decrease and increase with increasing temperature, respectively. However, due to the exponential increase in the equilibrium partial pressure with temperature, the solubility factor for both species decreases (refer to Eq. 2.19). Moreover, due to the small change in activity coefficient (γ) with concentration, a small increase was predicted for the solubility factor of butanol as well as smoothly decreasing solubility factor for water in the commercial PDMS membrane.

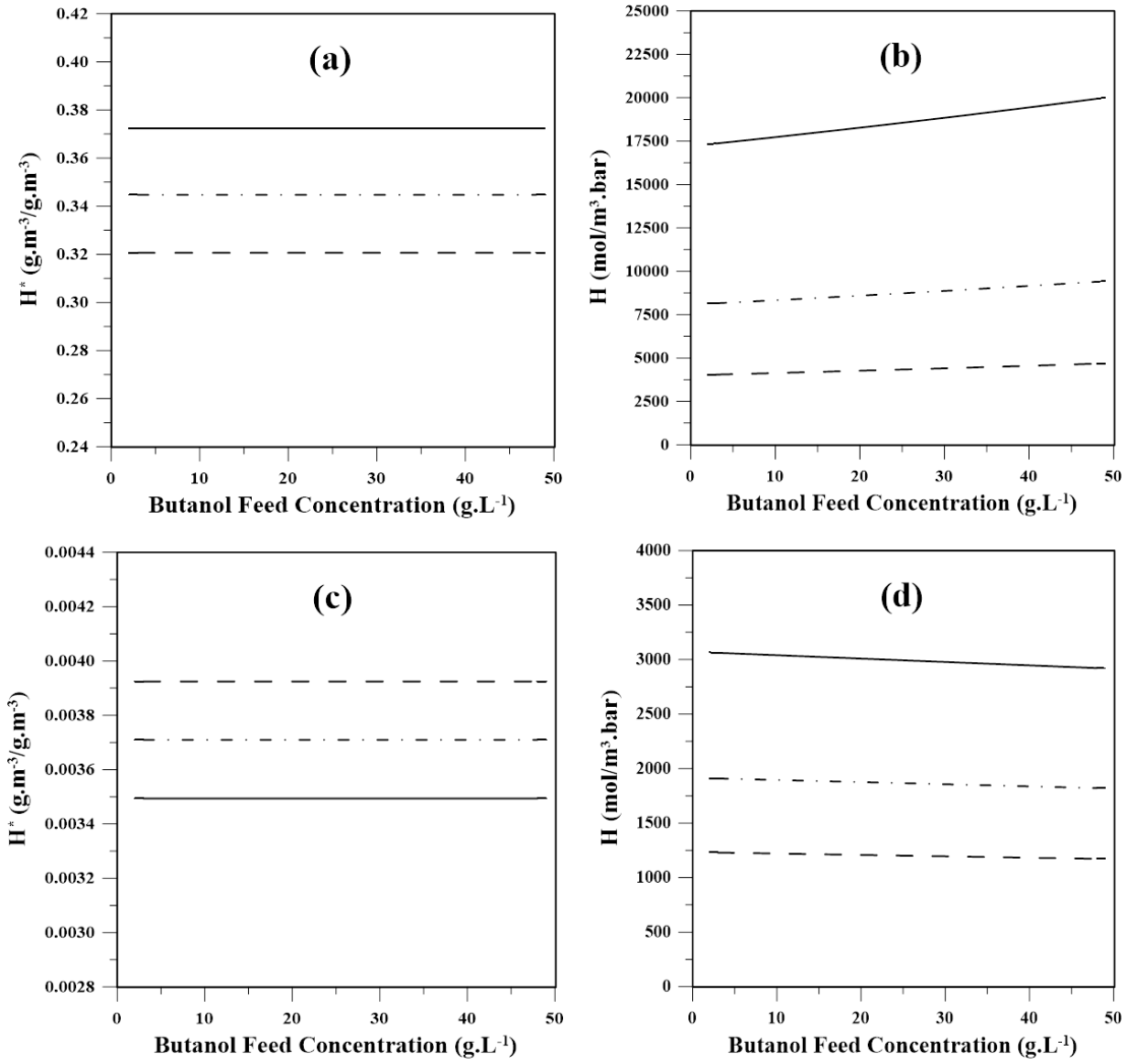

Figure 2.6. Simulated Henry's law constant (H^*) and solubility factor (H) of butanol ((a) for H^* and (b) for H) and water ((c) for H^* and (d) for H)) in a commercial PDMS membrane vs butanol feed concentration at different temperatures (310 K ——, 320 K — •, 330 K — —).

Table 2.7 compares the estimated degree of swelling of the Pervatech PDMS membrane in contact with a butanol binary aqueous solution (Equation (2.21)) with data for silicone membranes reported in the literature [4]. The predictions are in agreement with reported literature data. It is believed that the small discrepancies could be due to the variability of swelling experiments and the difference in operating conditions. Although there might be some dissimilarities between the

structure and properties of these polymeric membranes, the first active layer of both membranes is made of silicone, which explains the similarities between their sorption properties.

Table 2.7. Comparison between the estimated degree of swelling of Pervatech PDMS and the ones extracted from a graph for silicone membranes [4].

Butanol wt.% in Feed	Silicone membrane ϕ (wt. %) [4]	Estimated ϕ for Pervatech PDMS (wt. %)
1.4	1.0%	0.9%
3	1.8%	1.5%
4.8	2.7%	2.3%

2.4.3.2. Diffusivity

Equations (2.25) and (2.26) were used to estimate the diffusion coefficients of species in the membrane and the coupled diffusion coefficients, respectively using the parameters determined by the simulation. Figure 2.7 shows the results of the diffusion coefficients as a function of butanol concentration in the feed at different temperatures. It has been observed that water has a much higher diffusion coefficient in comparison to that of butanol which is mainly attributed to its smaller molecular size [42]. Moreover, according to the simulated values for Q_w and Q_b in Table 2.6, the coupled diffusion coefficient is approximately 20 times higher than the diffusion coefficients of water and butanol, which clearly indicates the low impact of coupling effect on the component transportation across the membrane ($C_T D_{ij} \rightarrow \infty$ in comparison to components diffusivity in the membrane). Therefore, the component transportation of butanol and water is dominated by their individual diffusion coefficients relative to the membrane. In addition, increasing the temperature leads to an increase of the polymer chain movement, which results in an increase of the available membrane free volume. Consequently, the diffusion coefficient of species within the membrane increases with temperature. In the case of concentration dependency of diffusion coefficients, diffusivity of water drastically increases with increasing the feed concentration while the butanol diffusion coefficient remains roughly constant. This observation confirms that the diffusion of water as the smaller penetrant is more sensitive to the swelling of the membrane. On the other hand, Figure 2.8 presents the term of the coupling effect ($C_T D_{bw}$) as a

function of butanol feed concentration at different temperatures. It can be observed that increasing both butanol concentration and temperature results in a decrease of the effect of coupling which is in agreement with the previous observation about the negligible coupling effect assumed in this study.

Predictions of the diffusion coefficients were compared with some diffusion coefficients reported in the literature for commercial and laboratory-made membranes and presented in Table 2.8. An exact comparison cannot be made because the diffusion coefficients vary as a function of many factors such as the molecular weight of PDMS, the level of crosslinking and the preparation method.

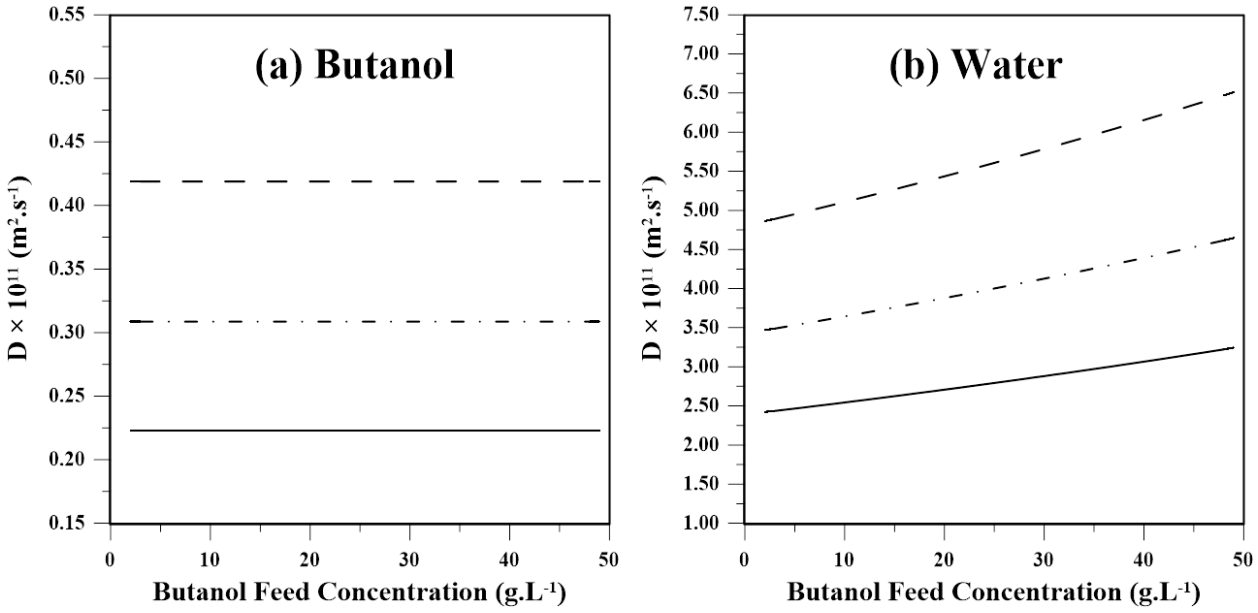

Figure 2.7. Simulated diffusion coefficients of butanol (a) and water (b) vs butanol feed concentration at different temperatures (310 K ___, 320 K — •, 330 K — —)

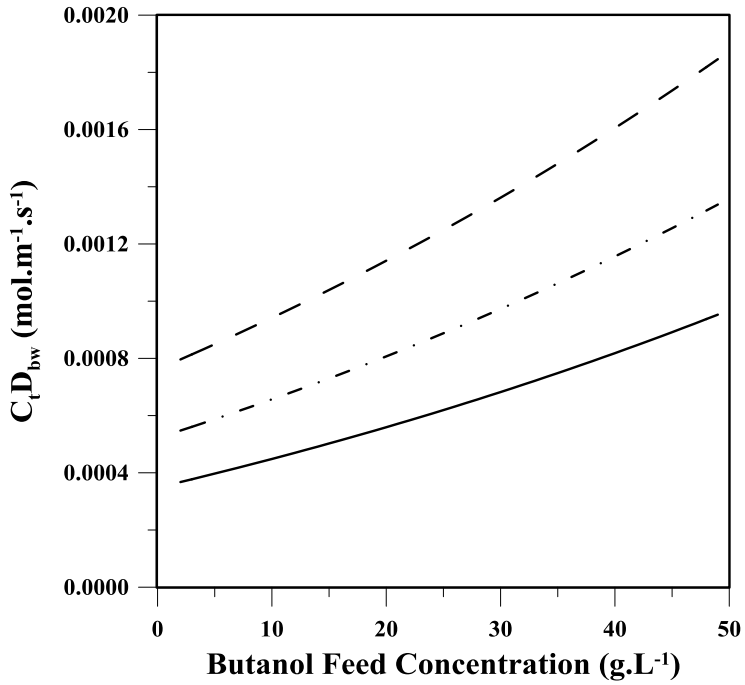

Figure 2.8. Simulated coupling effect vs butanol feed concentration at different temperatures (310 K ___, 320 K — •, 330 K — —).

Table 2.8. Comparison between literature and simulated diffusion coefficients of butanol and water in PDMS.

Component	Temperature (°C)	Reported Diffusion Coefficient (m^2/s)	Estimated Diffusion Coefficient by Extended MS model (m^2/s)
n-Butanol	30	6.5×10^{-11} [44]	1.75×10^{-12}
n-Butanol	35	3×10^{-11} [45]	2.08×10^{-12}
n-Butanol	80	5.5×10^{-10} [44]	7.92×10^{-12}
Water	25	7.8×10^{-10} [46]	1.5×10^{-11}
Water	25	3×10^{-10} [44]	1.5×10^{-11}
Water	35	5.5×10^{-11} [45]	2.22×10^{-11}
Water	80	1.2×10^{-9} [44]	9.7×10^{-11}

According to the results of Table 2.8, the simulated diffusion coefficients for both species are approximately between 3-70 times less than the ones reported in the literature. Differences in the experimental set up, membrane fabrication, polymer properties and operating conditions might be some of the reasons for this range of variation. However, it can be observed that the diffusion coefficients of species in both literature and simulated data in this work follow a similar trend with temperature. Changing the temperature from 30 to 80ºC corresponds to an approximate increase of 8 times in the butanol diffusion coefficient in PDMS membrane. Moreover, the diffusion coefficient of water in PDMS increases 4 times by varying the temperature from room temperature to 80ºC. These ranges of variation were also observed for simulated data where the diffusion coefficient of butanol and water roughly increases by a factor of 4 and 6, respectively, in the same range of temperature.

2.4.3.3. Membrane permeability

The permeability of a chemical species in a membrane, assuming solution-diffusion permeation process, is defined through the Fick's law of diffusion as the product of solubility and diffusivity (Equation (2.33)) of a specific species in the membrane [29,47,48].

$$P_i = S_i D_{iM} \tag{2.33}$$

The permeability of butanol and water in a commercial PDMS membrane was analyzed based on the predicted solubility factors and diffusion coefficients of species in the membrane. As shown in Figure 2.9, the permeability of both components increases with the concentration of butanol in the feed because of the increase in diffusion coefficient due to the swelling of the membrane, which is mainly due to the presence of butanol. Results of Figure 2.9 show that the permeability of the species in PDMS decreases with increasing temperature. As mentioned in previous sections, an increase in temperature leads to an increase in diffusivity for both species in the PDMS membrane. Moreover, although the dimensionless Henry's law constant (H^*) for water increases slightly with increasing temperature, the solubility factor (H) of both species decreases with increasing temperature because of the increase in equilibrium vapour pressure of the components on the feed side. Based on the results of the pervaporation experiments and the mass transport simulations, the rate of decrease in the solubility factor (H) is much more important than the increase in diffusivity with temperature. Hence, the permeability of both components decreases with an increase in the

operating temperature. Moreover, the permeability of butanol is more sensitive to temperature than the permeability of water.

Figure 2.10 shows the butanol selectivity calculated from Equation (2.2) with respect to water as a function of butanol feed concentration for different temperatures. As can be seen from this figure, the selectivity decreases with increasing temperature because the water flux is more sensitive to temperature than the butanol flux is as can be seen in Figure 2.5. Moreover, increasing the butanol feed concentration results in decreasing the membrane selectivity for butanol. This can be explained by the effect of membrane swelling on available free volume for penetrant diffusion as the feed butanol concentration increases. Since water is the smaller molecule compared to butanol, water penetration is more affected by the membrane swelling, increasing its penetration. This decreases the butanol selectivity as the butanol feed concentration is increased.

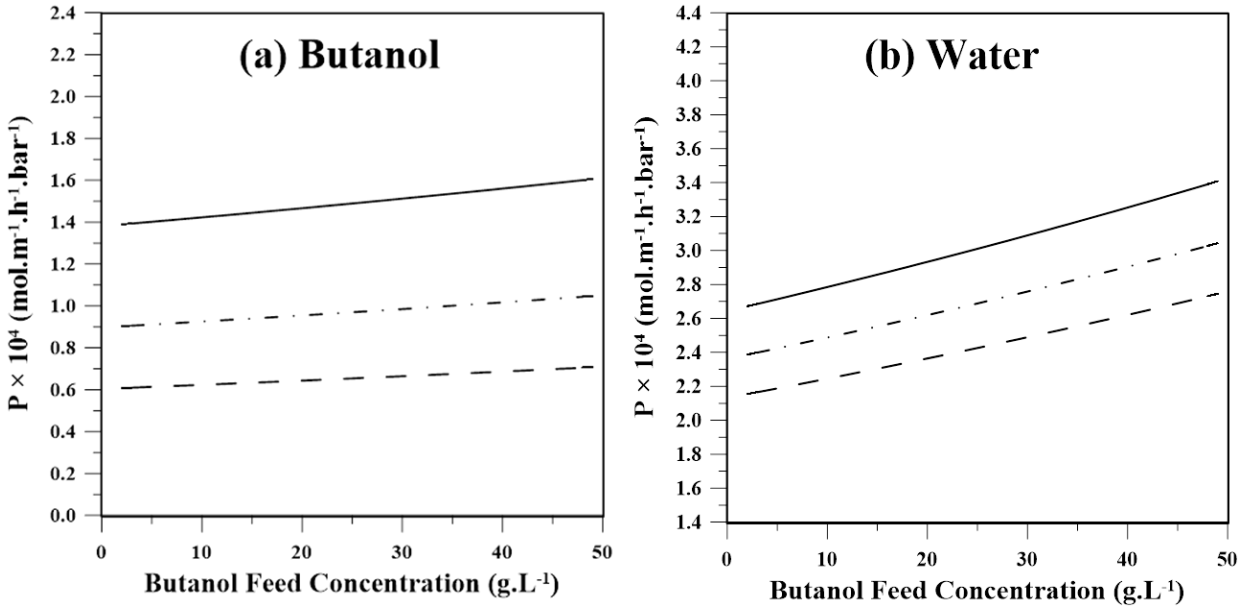

Figure 2.9. Simulated butanol (a) and water (b) permeability vs butanol feed concentration at different temperatures (310 K ___, 320 K ___ •, 330 K ___ ___).

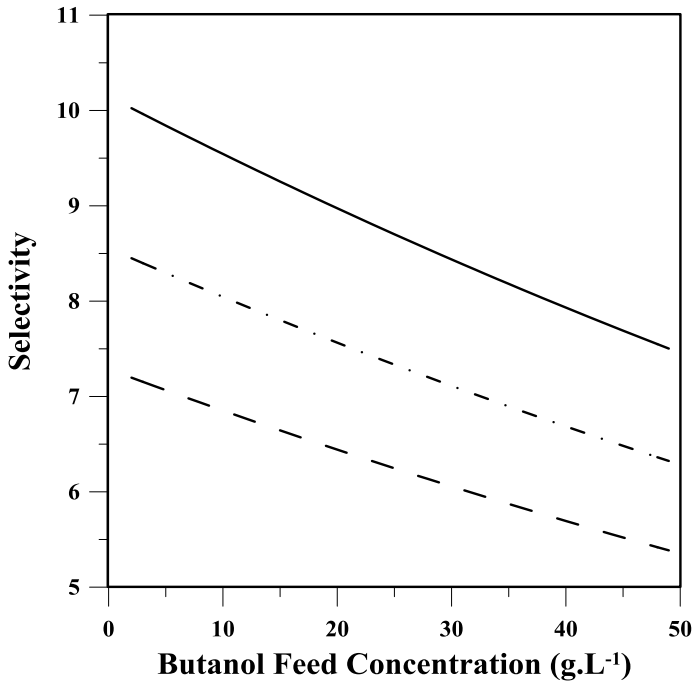

Figure 2.10. Simulated selectivity vs butanol feed concentration at different temperatures (310 K ___, 320 K — •, 330 K — —).

2.4.3.4. Pervaporation Separation Index (PSI)

The pervaporation separation index (PSI) was estimated using the results for the modelling of the membrane performance in Section 2.4.2, using Equation (2.4). Figure 2.11 shows the estimated PSI as a function of butanol concentration at different temperatures. Increasing the concentration and the temperature results in an increase in the butanol permeation flux (Figures 2.4 (a)-2.4(c)) and a decrease in selectivity (Figure 2.10). Although the selectivity decreases with an increase in temperature, a much larger increase in the butanol partial flux leads to an increase in PSI with respect to temperature according to Equation (2.4). Increasing the feed concentration also results in an increase in the PSI for the membrane performance. Within the operating conditions of this study, it was observed that the rate of change of PSI with the butanol feed concentration is considerably more than its change with temperature.

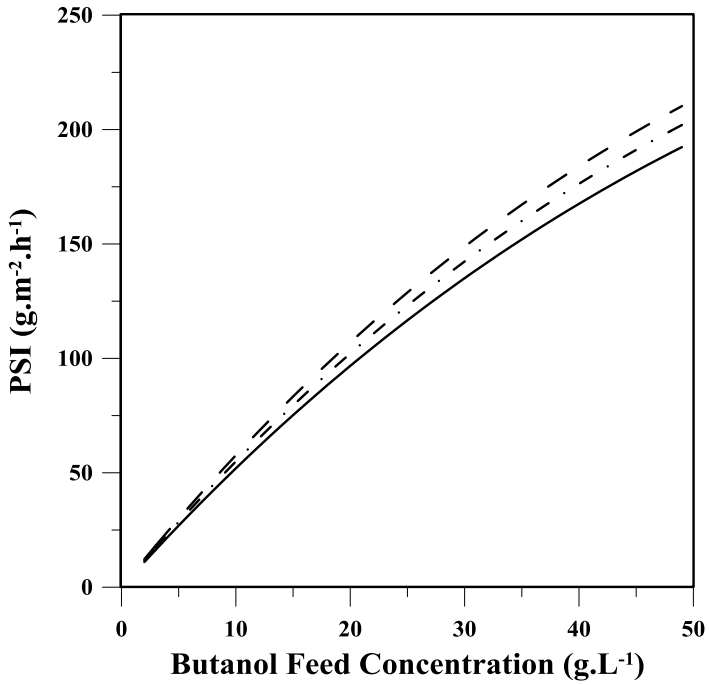

Figure 2.11. Simulated PSI vs butanol feed concentration at different temperatures (310 K ___, 320 K — • —, 330 K — — —).

2.5. Conclusions

Solution-diffusion theory with the assumption of negligible coupling flux, i.e. Fick's equation, is the simplest model to describe the transport of species for the pervaporation separation of species using polymeric membranes. To consider the coupling effect of the permeating components, the Maxwell-Stefan theory was implemented. In this investigation, Maxwell-Stefan model was initially used to describe the mass transport of binary butanol aqueous solutions through a commercial PDMS membrane. A nonlinear least square regression was used to determine the parameters of the model based on the experimental permeate fluxes of each component. It was observed that the calculated butanol and water fluxes had 30% and 14% errors with respect to the experimental data, respectively. To reduce the prediction error, the fitted Maxwell-Stefan model was improved by including the temperature and concentration dependence of the mass transfer parameters for this pervaporation application. The effect of membrane swelling on diffusivities was incorporated via an exponential relationship between the diffusion coefficient and the degree of swelling. Furthermore, an Arrhenius-type equation was used to estimate the effect of temperature on the diffusion coefficients of each species. In addition, Henry's law was used as the dominating sorption mechanism and its temperature dependency was expressed by an Arrhenius-

type equation. The coupled diffusivity of the penetrants was estimated to be a weighted combination of the component diffusion coefficients within the membrane.

This extended Maxwell-Stefan model was fitted based on the experimental data and showed better agreement with experimental data with errors of 15% and 6% on butanol and water permeate fluxes, respectively. In addition, the model was validated using literature experimental values of the Henry's law constant and the diffusivity of species within PDMS membranes. A good agreement was observed with the sorption properties whereas the fluctuation of literature diffusion coefficients makes it difficult to make an exact comparison.

The extended Maxwell-Stefan model was also used to predict the selectivity and pervaporation separation index (PSI) for different butanol feed concentrations and temperatures. Results show that the selectivity of PDMS membranes is decreasing by increasing both temperature and feed concentrations whereas the PSI increases with temperature and concentration. The ultimate decision on the actual operating conditions for this pervaporation application will involve a compromise between the total flux and the selectivity.

Acknowledgements

The authors would like to acknowledge the financial support received from NSERC (Natural Sciences and Engineering Research Council) of Canada for the completion of this study.

Nomenclature

A_i	Dimensionless constant in Equation (2.20) (-)
A_M	Area (m^2)
$\bar{A}$	Parameter in Antoine Equation
$\bar{B}$	Parameter in Antoine Equation
$\bar{C}$	Parameter in Antoine Equation
C	Concentration ($mole.m^{-3}$)
D	Diffusion coefficient ($m^2.s^{-1}$)
$\bar{D}$	Maxwell-Stefan diffusion coefficient ($m^2\ s^{-1}$)
D_{i0}	Pre-exponential parameter of swelling-dependence for diffusion ($m^2\ s^{-1}$)
D_{i0}^*	Pre-exponential parameter of Arrhenius equation for diffusion ($m^2\ s^{-1}$)
E_d	Energy of diffusion $(J.mol^{-1})$
H	Solubility factor ($mole.m^{-3}.bar^{-1}$)

H^*	Dimensionless Henry's law constant *(g.m^{-3}/g.m^{-3})*
H^*_{i0}	Pre-exponential parameter of Arrhenius equation for solubility *(g.m^{-3}/g.m^{-3})*
J	Permeate flux (mole.m^{-2}.h^{-1})
K	Constants defined in Equations (2.13)–(2.17)
M	Molecular weight (g.mole^{-1})
m_t	Total permeate weight (g)
p	Pressure (bar)
P	Permeability (mole.m^{-1}.h^{-1}.bar^{-1})
PSI	Pervaporation separation index (g.m^{-2}.h^{-1})
Q_i	Linear coefficient of coupling diffusion (-)
R	Gas constant (J.K^{-1}.mol^{-1})
S	Solubility factor (mole.m^{-3}.bar^{-1})
t	Time (h)
T	Temperature (K)
u	Velocity (m.h^{-1})
x	Feed mole or mass fraction (-)
y	Permeate mole or mass fraction (-)
α	Selectivity (-)
γ	Activity coefficient (-)
γ^∞	Infinite dilution activity coefficient (-)
δ	Thickness of active layer of the membrane (m)
ΔH	Heat of adsorption *(J.mol^{-1})*
μ	Chemical potential (bar.m^3.mol^{-1})
ρ	Density (g.m^{-3})
ϕ	Degree of swelling (%)

Superscripts

S	Saturation conditions

Subscripts

b	Butanol
f	Feed
i	Chemical species
j	Chemical species
M	Membrane
R	Reference

T	Total
w	Water

Abbreviations

HPLC	High Performance Liquid Chromatography
MS	Maxwell-Stefan
PDMS	Polydimethylsiloxane
SEM	Scanning Electron Microscope

2.6. References

[1] N. Abdehagh, F.H. Tezel, J. Thibault, Separation techniques in butanol production: Challenges and developments, Biomass Bioenergy. 60 (2014) 222–246. doi:10.1016/j.biombioe.2013.10.003.

[2] Y. Zhu, F. Xin, Y. Chang, Y. Zhao, W. Weichong, Feasibility of reed for biobutanol production hydrolyzed by crude cellulase, Biomass Bioenergy. 76 (2015) 24–30. doi:10.1016/j.biombioe.2015.02.013.

[3] P. Dürre, Biobutanol: An attractive biofuel, Biotechnol. J. 2 (2007) 1525–1534. doi:10.1002/biot.200700168.

[4] S. Heitmann, V. Krüger, D. Welz, P. Lutze, Experimental Investigation of Pervaporation Membranes for Biobutanol Separation, J. Membr. Sep. Technol. 2 (2013) 245–262. doi:http://dx.doi.org/10.6000/1929-6037.2013.02.04.5.

[5] V.V. Zverlov, O. Berezina, G.A. Velikodvorskaya, W.H. Schwarz, Bacterial acetone and butanol production by industrial fermentation in the Soviet Union: use of hydrolyzed agricultural waste for biorefinery, Appl. Microbiol. Biotechnol. 71 (2006) 587–597. doi:10.1007/s00253-006-0445-z.

[6] S.B. Jadhav, S. Harde, S.B. Bankar, T. Granström, H. Ojamo, R.S. Singhal, S.A. Survase, A green process for the production of butanol from butyraldehyde using alcohol dehydrogenase: process details, RSC Adv. 4 (2014) 14597–14602. doi:10.1039/C3RA47821A.

[7] M. Kumar, K. Gayen, Developments in biobutanol production: New insights, Appl. Energy. 88 (2011) 1999–2012. doi:10.1016/j.apenergy.2010.12.055.

[8] X. Liu, Q. Gu, C. Liao, X. Yu, Enhancing butanol tolerance and preventing degeneration in Clostridium acetobutylicum by 1-butanol–glycerol storage during long-term preservation, Biomass Bioenergy. 69 (2014) 192–197. doi:10.1016/j.biombioe.2014.07.019.

[9] H. Dong, W. Tao, Z. Dai, L. Yang, F. Gong, Y. Zhang, Y. Li, Biobutanol, Adv. Biochem. Eng. Biotechnol. 128 (2012) 85–100. doi:10.1007/10_2011_128.

[10] W.J. Groot', C.E. van den Qever, N.W.F. Kossen, Pervaporation for simultaneous product recovery in the butanol/isopropanol batch fermentation, Biotechnol. Lett. 6 (1984) 709–714. doi:10.1007/BF00133061.

[11] A.P. Mariano, M.J. Keshtkar, D.I.P. Atala, F. Maugeri Filho, M.R. Wolf Maciel, R. Maciel Filho, P. Stuart, Energy Requirements for Butanol Recovery Using the Flash Fermentation Technology, Energy Fuels. 25 (2011) 2347–2355. doi:10.1021/ef200279v.

[12] A. Sharif Rohani, P. Mehrani, J. Thibault, Comparison of in-situ recovery methods of gas stripping, pervaporation, and vacuum separation by multi-objective optimization for producing biobutanol via fermentation process, Can. J. Chem. Eng. 93 (2015) 986–997. doi:10.1002/cjce.22186.

[13] A.P. Mariano, N. Qureshi, R.M. Filho, T.C. Ezeji, Bioproduction of butanol in bioreactors: new insights from simultaneous in situ butanol recovery to eliminate product toxicity, Biotechnol. Bioeng. 108 (2011) 1757–1765. doi:10.1002/bit.23123.

[14] H. Azimi, F.H. Tezel, J. Thibault, Effect of nano-activated carbon on the performance of Polydimethylsiloxane (PDMS) membrane for pervaporation separation of butanol from binary aqueous solutions., Submitt. J. Chem. Technol. Biotechnol. (2016).

[15] D.M. Aguilar-Valencia, M.Á. Gómez-García, J. Fontalvo, Effect of pH, CO2, and High Glucose Concentrations on Polydimethylsiloxane Pervaporation Membranes for Ethanol Removal, Ind. Eng. Chem. Res. 51 (2012) 9328–9334. doi:10.1021/ie3002765.

[16] X. Yang, Z. Wu, F. Manquan, L. Jiding, Nonequilibrium Dissolution-diffusion Model for PDMS Membrane Pervaporation of ABE Water Binary System, J. Membr. Sci. Technol. 6 (2016) 143. doi:10.4172/2155-9589.1000143.

[17] P.D. Chapman, T. Oliveira, A.G. Livingston, K. Li, Membranes for the dehydration of solvents by pervaporation, J. Membr. Sci. 318 (2008) 5–37. doi:10.1016/j.memsci.2008.02.061.

[18] F. Lipnizki, S. Hausmanns, G. Laufenberg, R. Field, B. Kunz, Use of Pervaporation-Bioreactor Hybrid Processes in Biotechnology, Chem. Eng. Technol. 23 (2000) 569–577. doi:10.1002/1521-4125(200007)23:7<569::AID-CEAT569>3.0.CO;2-1.

[19] S.-Y. Li, R. Srivastava, R.S. Parnas, Study of in situ 1-butanol pervaporation from A-B-E fermentation using a PDMS composite membrane: Validity of solution-diffusion model for pervaporative A-B-E fermentation, Biotechnol. Prog. 27 (2011) 111–120. doi:10.1002/btpr.535.

[20] S.-Y. Li, R. Srivastava, R.S. Parnas, Separation of 1-butanol by pervaporation using a novel tri-layer PDMS composite membrane, J. Membr. Sci. 363 (2010) 287–294. doi:10.1016/j.memsci.2010.07.042.

[21] F. Lipnizki, G. Trägårdh, Modelling of Pervaporation: Models to Analyze and Predict the Mass Transport in Pervaporation, Sep. Purif. Methods. 30 (2001) 49–125. doi:10.1081/SPM-100102985.

[22] H.K. Lonsdale, U. Merten, R.L. Riley, Transport properties of cellulose acetate osmotic membranes, J. Appl. Polym. Sci. 9 (1965) 1341–1362. doi:10.1002/app.1965.070090413.

[23] P. Izák, L. Bartovská, K. Friess, M. Šípek, P. Uchytil, Description of binary liquid mixtures transport through non-porous membrane by modified Maxwell–Stefan equations, J. Membr. Sci. 214 (2003) 293–309. doi:10.1016/S0376-7388(02)00580-X.

[24] M.R. Othman, H. Mukhtar, A.L. Ahmad, Gas Permeation Characteristics across Nano-Porous Inorganic Membranes, IIUM Eng. J. 5 (2004) 17–33.

[25] E.A. Mason, L.A. Viehland, Statistical–mechanical theory of membrane transport for multicomponent systems: Passive transport through open membranes, J. Chem. Phys. 68 (1978) 3562–3573. doi:10.1063/1.436213.

[26] R. Krishna, J.A. Wesselingh, The Maxwell-Stefan approach to mass transfer, Chem. Eng. Sci. 52 (1997) 861–911. doi:10.1016/S0009-2509(96)00458-7.

[27] Mudeer Mubarak Merza, Kinetic and thermodynamics study of heavy metal ions adsorption from aqueous solution using new resin 8-hydroxyquinoline-furfural hydroquinone (HQFH)., J. Coll. Basic Educ. 21 (2015) 169–188.

[28] A.A. Inyinbor, F.A. Adekola, G.A. Olatunji, Kinetics, isotherms and thermodynamic modeling of liquid phase adsorption of Rhodamine B dye onto Raphia hookerie fruit epicarp, Water Resour. Ind. 15 (2016) 14–27. doi:10.1016/j.wri.2016.06.001.

[29] P. Shao, R.Y.M. Huang, Polymeric membrane pervaporation, J. Membr. Sci. 287 (2007) 162–179. doi:10.1016/j.memsci.2006.10.043.

[30] B. Bettens, A. Verhoef, H.M. van Veen, C. Vandecasteele, J. Degrève, B. Van der Bruggen, Pervaporation of binary water–alcohol and methanol–alcohol mixtures through microporous methylated silica membranes: Maxwell–Stefan modeling, Comput. Chem. Eng. 34 (2010) 1775–1788. doi:10.1016/j.compchemeng.2010.03.014.

[31] U.K. Ghosh, L. Teen, Application of modified Maxwell-Stefan equation for separation of aqueous phenol by pervaporation, Int. J. Chem. Mol. Nucl. Mater. Metall. Eng. 6 (2012) 526–531.

[32] K. Zhang, R.P. Lively, M.E. Dose, A.J. Brown, C. Zhang, J. Chung, S. Nair, W.J. Koros, R.R. Chance, Alcohol and water adsorption in zeolitic imidazolate frameworks, Chem. Commun. 49 (2013) 3245–3247. doi:10.1039/C3CC39116G.

[33] V. Dohnal, D. Fenclová, P. Vrbka, Temperature Dependences of Limiting Activity Coefficients, Henry's Law Constants, and Derivative Infinite Dilution Properties of Lower (C1–C5) 1-Alkanols in Water. Critical Compilation, Correlation, and Recommended Data, J. Phys. Chem. Ref. Data. 35 (2006) 1621–1651. doi:10.1063/1.2203355.

[34] Islam, Akand Wahid, Universal Liquid Mixture Models for Vapor-liquid and Liquid-liquid Equilibria in Hexane-butanol-water System, North Carolina Agricultural and Technical State University, 2009.

[35] W.F. Guo, T.-S. Chung, T. Matsuura, R. Wang, Y. Liu, Pervaporation study of water and tert-butanol mixtures, J. Appl. Polym. Sci. 91 (2004) 4082–4090. doi:10.1002/app.13632.

[36] B.E. Poling, J.M. Prausnitz, J.P. O'Connel, Properties of Gases and Liquids, 5th ed., Mc Graw-Hill Education, 2011.

[37] A.C.M. Kuo, Polymer Data Handbook, Oxford University Press, Oxford, 1999.

[38] E. Favre, P. Schaetzel, Q.T. Nguygen, R. Clément, J. Néel, Sorption, diffusion and vapor permeation of various penetrants through dense poly(dimethylsiloxane) membranes: a transport analysis, J. Membr. Sci. 92 (1994) 169–184. doi:10.1016/0376-7388(94)00060-3.

[39] T.-H. Yang, S. Jessie Lue, UNIQUAC and UNIQUAC-HB models for the sorption behavior of ethanol/water mixtures in a cross-linked polydimethylsiloxane membrane, J. Membr. Sci. 415–416 (2012) 534–545. doi:10.1016/j.memsci.2012.05.041.

[40] T.-H. Yang, S.J. Lue, Modeling Sorption Behavior for Ethanol/Water Mixtures in a Cross-linked Polydimethylsiloxane Membrane Using the Flory-Huggins Equation, J. Macromol. Sci. Part B. 52 (2013) 1009–1029. doi:10.1080/00222348.2012.750992.

[41] E.A. Fouad, X. Feng, Pervaporative separation of n-butanol from dilute aqueous solutions using silicalite-filled poly(dimethyl siloxane) membranes, J. Membr. Sci. 339 (2009) 120–125. doi:10.1016/j.memsci.2009.04.038.

[42] G. LIU, D. HOU, W. WEI, F. XIANGLI, W. JIN, Pervaporation Separation of Butanol-Water Mixtures Using Polydimethylsiloxane/Ceramic Composite Membrane, Chin. J. Chem. Eng. 19 (2011) 40–44. doi:10.1016/S1004-9541(09)60174-9.

[43] G. Liu, W.-S. Hung, J. Shen, Q. Li, Y.-H. Huang, W. Jin, K.-R. Lee, J.-Y. Lai, Mixed matrix membranes with molecular-interaction-driven tunable free volumes for efficient bio-fuel recovery, J. Mater. Chem. A. 3 (2015) 4510–4521. doi:10.1039/C4TA05881J.

[44] J.M. Watson, P.A. Payne, A study of organic compound pervaporation through silicone rubber, J. Membr. Sci. 49 (1990) 171–205. doi:10.1016/S0376-7388(00)80786-3.

[45] G. Cocchi, M.G. De Angelis, F. Doghieri, Solubility and diffusivity of liquids for food and pharmaceutical applications in crosslinked polydimethylsiloxane (PDMS) films: I. Experimental data on pure organic components and vegetable oil, J. Membr. Sci. 492 (2015) 600–611. doi:10.1016/j.memsci.2015.04.063.

[46] J.M. Watson, M.G. Baron, The behaviour of water in poly(dimethylsiloxane), J. Membr. Sci. 110 (1996) 47–57. doi:10.1016/0376-7388(95)00229-4.

[47] R. Petrychkovych, K. Setnickova, P. Uchytil, The influence of water on butanol isomers pervaporation transport through polyethylene membrane, Sep. Purif. Technol. 107 (2013) 85–90. doi:10.1016/j.seppur.2013.01.014.

[48] J. Ahn, W.-J. Chung, I. Pinnau, M.D. Guiver, Polysulfone/silica nanoparticle mixed-matrix membranes for gas separation, J. Membr. Sci. 314 (2008) 123–133. doi:10.1016/j.memsci.2008.01.031.

Chapter 3: Mass transfer in mixed matrix membranes (MMM's)

Mixed Matrix Membranes for pervaporation and gas separation applications: A Resistance-Based Model

Arian Ebneyamini, Hoda Azimi, F. Handan Tezel and Jules Thibault*

Department of Chemical and Biological Engineering

University of Ottawa, Ottawa, Ontario, Canada K1N 6N5

***Corresponding author: Jules.Thibault@uottawa.ca, 613-562-5800 Ext. 6094**

Abstract

In this study, a model for the prediction of the mass transport through mixed matrix membranes (MMMs) for pervaporation and gas separation processes has been introduced. A Resistance-Based (RB) model was used in conjunction with a Finite Difference (FD) model to derive an analytical model for calculating the effective permeability of mixed matrix membranes. The proposed model was validated using experimental pervaporation data for the separation of butanol from binary aqueous solutions using Polydimethylsiloxane (PDMS)/activated carbon nanoparticle membranes and using data from the literature for gas separation using mixed matrix membranes.

Keywords: Mixed Matrix Membranes, Effective permeability, Pervaporation, Gas Separation, Resistance-Based Model, Finite Difference Method

3.1. Introduction

Polymeric membranes are the most commonly used ones in membrane-based separation processes due to their good transport properties, ease of processing and low cost [1–3]. However, neat polymeric membranes usually suffer from the trade-off between selectivity and permeate flux [3–6]. It has been reported that embedding proper organic or inorganic filler into the polymer matrix can enhance the separation performance (permeation flux and selectivity) as well as the thermal and mechanical stability of the membranes [1,7–9]. Various types of filler materials such as zeolites, metal organic frameworks (MOF's) and activated carbons have been successfully incorporated within the membrane matrix to improve the separation performance in different applications such as pervaporation and gas separation processes [3,7–11].

The theoretical description of the mass transport through mixed matrix membranes is paramount to optimize the membrane separation processes. According to the solution-diffusion theory, three steps can be used to describe the mass transport of species within the membrane film: (1) sorption of species on the feed side of the membrane, (2) diffusion of components through the membrane, and (3) desorption from the permeate side of the membrane [12–15]. Therefore, the permeate flux of a component for pervaporation and gas separation processes is proportional to the partial pressure gradient (or concentration gradient) as the driving force, the membrane thickness and the permeability of the component. Moreover, the permeability is the product of the solubility and the diffusion coefficient of penetrants through the membrane. Equation (3.1) gives the expression of the permeate flux of component *m.* Solubility of a species in a membrane could be defined based on the equilibrium vapour pressure (S with units of $mol.m^{-3}.bar^{-1}$) or the mass concentration of the component (S^* with units of $g.m^{-3}/g.m^{-3}$ where the first concentration is in the membrane whereas the latter one is in the feed solution). Therefore, the permeability of component *m* in the membrane could be expressed using different units ($mol.m^{-1}.h^{-1}.bar^{-1}$ and $m^2.h^{-1}$) for which the permeability would obviously have different values. However, the type of driving force (partial pressure or concentration gradient) is the determining factor to select the proper units to express permeability without any impact on the estimation of partial permeate fluxes (See Equation (3.1) where the permeate flux is expressed in $g.m^{-2}h^{-1}$).

$$J_m = \frac{\left(D_m S_m\right) M_m \, \Delta p_m}{\delta} = \frac{P_m M_m \, \Delta p_m}{\delta} = \frac{\left(D_m S_m^*\right) \Delta C_m}{\delta} = \frac{P_m^* \Delta C_m}{\delta} \tag{3.1}$$

Various models such as Maxwell [16], Bruggeman [17], Lewis-Nielson [18,19] and Pal [20] have been introduced to estimate the effective permeability of ideal mixed matrix membranes for gas separation processes. These models are based on the permeability of the continuous phase, permeability of the dispersed phase and the volume fraction of the solid fillers within the polymer matrix [2]. Maxwell model is the most common model that is widely used for the prediction of the effective permeability of MMMs for gas separation applications (Equation (3.2)). The Maxwell model was originally presented to describe the dielectric properties of composite materials containing spherical particles. However, the Maxwell model is only applicable for low amounts of filler loading within the polymer matrix (less than 0.2 volume fraction of the filler) based on the assumption that diffusion in and around a particle is not affected by the diffusion streamlines around the neighbouring particles [2].

$$P_{Eff} = P_c \frac{P_d + 2P_c - 2\phi(P_c - P_d)}{P_d + 2P_c + \phi(P_c - P_d)} \tag{3.2}$$

In addition, a resistance-based model has been proposed by Hennepe et al. to predict the effective permeability of the species in a mixed matrix membrane for pervaporation separation (Equation (3.3)) [21,22]. The model was able to predict the separation performance for the pervaporation of some alcohols from water using zeolite-PDMS mixed matrix membranes.

$$P_{Eff} = \frac{1}{\frac{1 - \phi^{1/3}}{P_c} + \frac{1.5\,\phi^{1/3}}{P_c\left(1-\phi\right) + 1.5 P_d \phi}} \tag{3.3}$$

The factor 1.5 in Equation (3.3) was added to account for the tortuosity factor due to the presence of the particles. As a result, the permeability prediction of the Hennepe's model for an identical permeability of the components in both phases ($P_c = P_d$) deviates from the asymptotic permeability, and the prediction of the effective permeability is still a function of the filler volume fraction [22]. In addition, a small error for the determination of the diffusional area in the derivation of this equation was also made. Indeed, the denominator of the second term of Equation (3.3) should be $P_c\left(1-\phi^{2/3}\right) + P_d\phi^{2/3}$ while excluding at the same time the tortuosity factor of 1.5 [22].

In this work, it was desired to resort to a simple predictive model such that a Resistance-Based (RB) model has been introduced to estimate the effective permeability of migrating components in a homogenously dispersed mixed matrix membrane with the assumption of ideal polymer-filler interface morphology. In addition, an accurate solution was obtained by Finite Differences (FD) to predict the effective permeability of the mixed matrix membranes for different ratios of the respective permeability in the two phases and different volumetric filler contents within the polymer matrix. The results of these two models were compared to modify the RB model by a correction factor to account for the three-directional (3D) diffusional pathways. The new model was validated with different sets of experimental data for pervaporation and gas separation processes obtained from previously published studies.

3.2. Modelling of the Mass Transport through MMMs

3.2.1. Resistance-Based (RB) Model

The resistance of a membrane for the permeation of a species *m* is a function of the diffusion pathway, the area available for permeation and species permeability (Equation (3.4)).

$$R_m = \frac{d_m}{P_m A_m} \tag{3.4}$$

Assuming a homogenous dispersion of the particles within the polymeric membrane, a mixed matrix membrane can be described as the repetition of a basic element, which consists of two different phases: the continuous and dispersed phases. Figure 3.1 presents a schematic diagram of a mixed matrix membrane with uniformly dispersed three-dimensional cubical filler particles (Fig. 3.1(a)) and a basic repeatable unit where the cubical filler particle is located at the center of a cubical polymeric matrix unit element (Fig. 3.1(b)). Figure 3.1(b) shows that each repeatable unit of the mixed matrix membrane has four distinct regions: (1) the continuous phase above the filler, (2) the cubical filler particle located in the center of the unit, (3) the continuous phase below the filler and, (4) the continuous phase which surrounds Regions 1, 2 and 3.

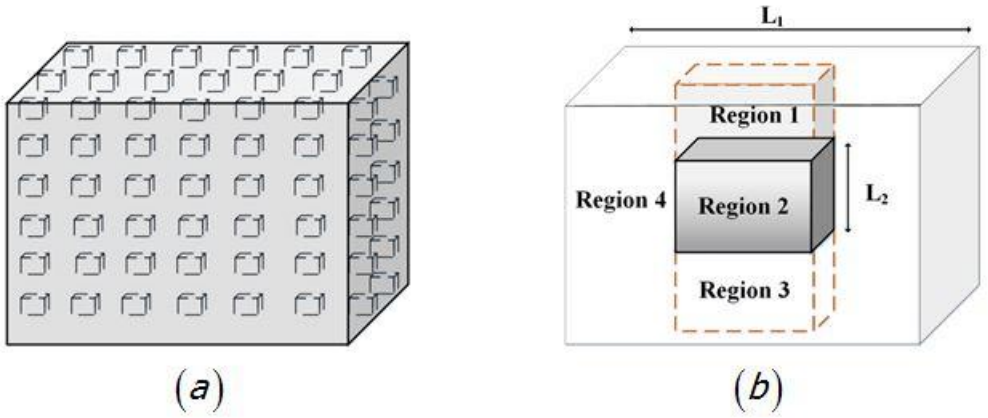

Figure 3.1. Schematic diagram for (a) the mixed matrix membrane with uniformly dispersed cubical filler particles, and (b) a basic repeatable unit consisting of a cubical filler particle centered in a cubical polymeric matrix unit element.

Considering the four regions of the repeatable basic unit of Figure 3.1(a), the effective resistance of a repeatable element for the permeation of a species is a combination of parallel and series resistances of the different regions where species permeation occurs. The equivalent electrical circuit representing the permeation resistances of a repeatable unit is presented in Figure 3.2. Using the Kirchhoff's rule to determine the effective resistance of the basic element, Equation (3.5) is obtained.

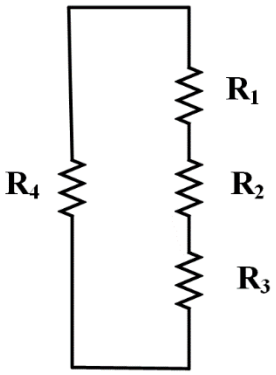

Figure 3.2. Equivalent electrical resistance circuit in a repeatable basic element.

$$R_{Eff} = \frac{1}{\frac{1}{R_1 + R_2 + R_3} + \frac{1}{R_4}} \tag{3.5}$$

Table 3.1 indicates the parameters that were used to determine each of the resistances (Equation (3.4)) of the four regions within a repeatable cubic element based on the phase material, size of the element and the size of the filler particle (Figure 3.1(b)).

Table 3.1.Parameters of Equation (4) for each of the resistances required to calculate R_{eff}.

Region	d_m	A_m	P_m
Region 1	$0.5\ (L_1 - L_2)$	$(L_2)^2$	P_c
Region 2	L_2	$(L_2)^2$	P_d
Region 3	$0.5\ (L_1 - L_2)$	$(L_2)^2$	P_c
Region 4	L_1	$(L_1)^2 - (L_2)^2$	P_c

For a homogenous dispersion of the filler throughout the polymeric matrix, the volume fraction (ϕ) of the filler in each basic element should be equal to the one prevailing within the whole membrane. Therefore, Equation (3.6) defines the relation between the dimensions of the cubical element with the volume fraction ϕ of the filler.

$$L_2 = L_1\left(\phi\right)^{1/3} = L_1 H \tag{3.6}$$

where *H* is used to designate the cubic root of the filler volume fraction. Equations (3.6) and the resistance parameters (Table 3.1) were substituted into Equation (3.4) and, in turn, the resistances of each region were inserted in Equation (3.5) to develop an expression for the effective resistance of the repeatable element of the membrane (Equation (3.7)). As previously shown in Equation (3.4), the permeability of an element is a function of the resistance, the area and the diffusional pathway or thickness of the element. Therefore, Equation (3.8) defines the effective permeability of the repeatable unit and, consequently, the effective permeability of the mixed matrix membrane.

$$R_{Eff} = \frac{L_1}{{L_1}^2 P_{Eff,RB}} = \frac{1}{\left(\frac{{L_1}^2}{L_1}\right)\left(\left(1-H^2\right)P_c + \frac{P_c P_d H^2}{HP_c + \left(1-H\right)P_d}\right)} \tag{3.7}$$

$$P_{Eff,RB} = \frac{L_1}{L_1^2 R_{Eff}} = \left(1-H^2\right)P_c + \frac{P_c P_d H^2}{HP_c + \left(1-H\right)P_d} \tag{3.8}$$

Equation (3.8) could be rearranged to estimate relative permeability of a MMM ($P_r = P_{eff}/P_c$) based on the ratio of the permeability of the two phases (P_d/P_c) and the volume fraction of the

filler content (ϕ). Since the relative permeability is independent of the units of the permeability ($P_d/P_c = P_d^*/P_c^*$), the estimated effective permeability of a MMM will have identical units to those of the permeability of the continuous and the dispersed phases.

3.2.2. Finite difference method

One of the main assumptions for the RB model is the one-directional transport of the components through a mixed matrix membrane. For a neat polymeric membrane with a constant permeability or with a solid filler with identical permeability as the polymeric membrane, the concentration profile for a given component through the membrane is indeed one-directional and perfectly linear [23–25]. However, the presence of solid fillers within the matrix of the membrane will usually result in the deviation of the concentration profile from linear to a more tortuous diffusional pathway depending on the permeability of each phase. If the permeability of the dispersed phase (solid filler) is larger than the permeability of the continuous phase, the solid particles will act as an attractor, which will make the concentration streamlines to deviate toward the solid particles. On the other hand, if the permeability of the dispersed phase is smaller than the one of the continuous phase, the concentration streamlines will deviate away from the solid particles. As a result, the driving force becomes three-dimensional even though the predominant driving force across the membrane still prevails. Because of the presence of the solid particles will favour or inhibit the overall component permeation flux across the membrane, an increase or a decrease of the effective membrane permeability will be observed based on the ratio of the respective permeability in the two phases.

Our objective was to use a simple RB model to predict analytically the permeation flux of each species. To satisfy this objective, it was decided to retain the simple RB model (Equation (3.8)) with the addition of a correction factor to include the effect of the three-dimensional pathway. The correction factor, which should be a function of the permeability ratio and the volume fraction of particles within the membrane, will be obtained by comparing the permeation rate obtained by solving the diffusion equation by finite differences with the one obtained with the simple RB model.

An ideal mixed matrix membrane with perfectly homogenous dispersion of cubical filler particles can be described by the repetition of a unique basic element. Therefore, the permeability of the

membrane will be equal to the permeability of the repeatable basic unit, which has been referred to as a "RB element" in this section. The finite difference three-directional mass transfer solution will therefore consider a single cubical RB element. The RB element can be described by a finite cube ($0 \leq x, y, z \leq L_1$) containing at its center a cubical solid filler ($\left(L_1 - L_2\right)/2 \leq x, y, z \leq \left(L_1 + L_2\right)/2$). The RB element was discretized into a sufficiently large number of mesh points to generate small cubical elements, each consisting of only one phase (continuous or dispersed phase) (Fig. 3.3(a)). Other finite difference simulations were performed with centered spheres and cylinders of different dimensions instead of cubical elements and it was found that the particles geometry has a negligible effect on the membrane effective permeability for filler volume fractions less than approximately 40-50%, which is much greater than the normal range of volume fraction that prevails in typical MMMs.

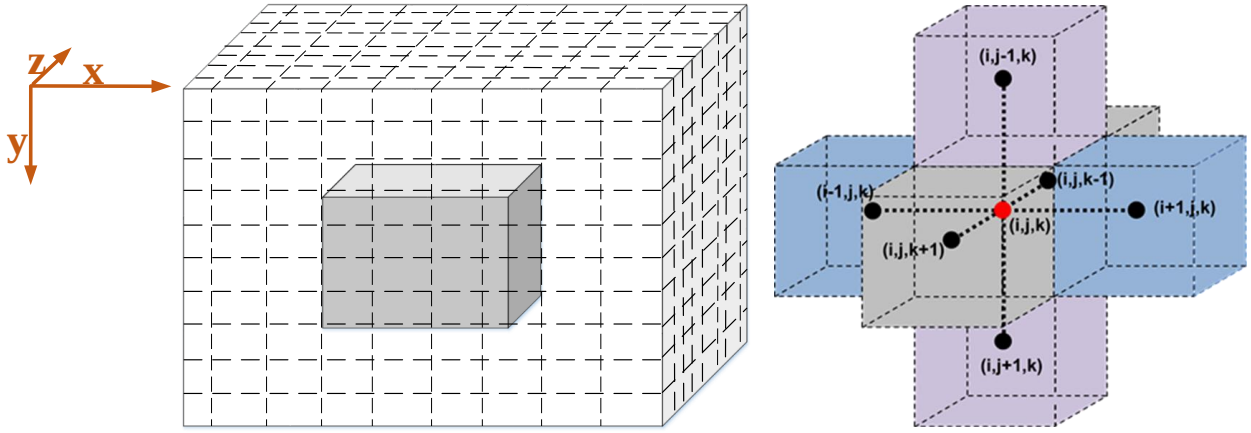

(a) **(b)**

Figure 3.3. Discretized RB element (a) and the (*i*, *j*, *k*) interior mesh point within the element (b).

The concentration profile of each component within the RB element was obtained by solving the Fick's second law (Equation (3.9)). A zero-stage cut condition at the feed side and perfect vacuum at the permeate side of the element were used as the boundary conditions in y-coordinate. Since it is assumed that the membrane is made of a large number of identical RB elements, symmetrical boundary conditions prevail at the two faces perpendicular to the x-axis and the two faces perpendicular to the z-axis. These four symmetrical boundary conditions are often refer to as periodic conditions. To reduce the convergence time to achieve steady state, a linear concentration

profile in the y-direction was used as the initial condition for the numerical solution. Table 3.2 provides a summary of the initial and boundary conditions used in this investigation.

$$\frac{\partial C}{\partial t} = \frac{\partial}{\partial x}\left(D_{x,y,z} \frac{\partial C}{\partial x} \right) + \frac{\partial}{\partial y}\left(D_{x,y,z} \frac{\partial C}{\partial y} \right) + \frac{\partial}{\partial z}\left(D_{x,y,z} \frac{\partial C}{\partial z} \right) \tag{3.9}$$

Table 3.2. Initial and boundary conditions of the FD model

Initial Condition	$C_{(x,y,z)}\Big\|_{t=0} = C_{(x,0,z)} - \frac{C_{(x,0,z)} - C_{(x,L_1,z)}}{N_y - 1}$
BC: At y = 0	$C_{(x,0,z)} = C_f S^*_{(x,0,z)}$
BC: At y = L_1	$C_{(x,L_1,z)} = 0$
BC: At x = 0 and x = L_1	$\frac{\partial C}{\partial x}\Big\|_{x=0} = \frac{\partial C}{\partial x}\Big\|_{x=L_1} = 0$
BC: At z = 0 and z = L_1	$\frac{\partial C}{\partial z}\Big\|_{z=0} = \frac{\partial C}{\partial z}\Big\|_{z=L_1} = 0$

The Fick's second law of diffusion is used to determine iteratively the concentration at each mesh point within the membrane. For a mesh point (*i*, *j*, *k*) located within the membrane, such as in Figure 3.3(b), Equation (3.9) is discretized and the solution of the concentration for each species (*m*) at mesh point (*i*, *j*, *k*) at the next time step ($t+\Delta t$) is obtained using Equation (3.10). The instantaneous change in concentration at mesh point (*i*, *j*, *k*) during the time interval Δt only depends on the concentration at (*i*, *j*, *k*) and the six neighbouring mesh points at time *t*.

$$C_{i,j,k}^{m,t+\Delta t} = C_{i,j,k}^{m,t} + \Delta t \left[\begin{array}{l} - D_{i,j,k}^{LX} \dfrac{(C_{i,j,k}^{m,t} - \dfrac{S_{i,j,k}^{*}}{S_{i-1,j,k}^{*}} C_{i-1,j,k}^{m,t})}{\Delta x^2} + D_{i,j,k}^{RX} \dfrac{(\dfrac{S_{i,j,k}^{*}}{S_{i+1,j,k}^{*}} C_{i+1,j,k}^{m,t} - C_{i,j,k}^{m,t})}{\Delta x^2} \\ - D_{i,j,k}^{LY} \dfrac{(C_{i,j,k}^{m,t} - \dfrac{S_{i,j,k}^{*}}{S_{i,j-1,k}^{*}} C_{i,j-1,k}^{m,t})}{\Delta y^2} + D_{i,j,k}^{RY} \dfrac{(\dfrac{S_{i,j,k}^{*}}{S_{i,j+1,k}^{*}} C_{i,j+1,k}^{m,t} - C_{i,j,k}^{m,t})}{\Delta y^2} \\ - D_{i,j,k}^{LZ} \dfrac{(C_{i,j,k}^{m,t} - \dfrac{S_{i,j,k}^{*}}{S_{i,j,k-1}^{*}} C_{i,j,k-1}^{m,t})}{\Delta z^2} + D_{i,j,k}^{RZ} \dfrac{(\dfrac{S_{i,j,k}^{*}}{S_{i,j,k+1}^{*}} C_{i,j,k+1}^{m,t} - C_{i,j,k}^{m,t})}{\Delta z^2} \end{array} \right] \quad (3.10)$$

Because the solubility of the six neighbouring mesh points may be different than the solubility at mesh point (*i, j, k*), as indicated in Equation (3.10), the concentrations of the neighbouring mesh points are multiplied by the solubility ratio such that all concentrations are defined on the same basis as the center mesh point (*i, j, k*). Equation (3.10) is defined for an interior mesh point. For the boundary mesh points at ($x = 0$ and L_1) and ($z = 0$ and L_1), where symmetry prevails, the mesh points locate outside the boundary is simply replaced by the first interior mesh point. For the boundary mesh points at ($y = 0$ and L_1), the concentrations are set constant according to the boundary conditions specified in Table 3.2.

Because the phases of neighbouring mesh elements may be different and have distinct solubility and diffusivity, it is important to determine the effective diffusivity in order to calculate the mass fluxes at each of the six faces of the mesh element (*i, j, k*). A simple mass balance was used to estimate the effective diffusivity between the central mesh point and its six neighbouring mesh points. Equations (3.11) and (3.12) give the effective diffusivity in the *x*-direction between mesh point (i, j, k) and its left neighbour (*i-1, j, k*), and between mesh point (*i, j, k*) and its right neighbour (*i+1, j, k*), respectively. Similar equations were derived for the effective diffusion coefficients in the other two dimensions. All these effective diffusivities were used in Equation (3.10).

$$\frac{1}{D_{i,j,k}^{LX}} = \frac{S_{i,j,k}^{*}}{S_{i-1,j,k}^{*}} \frac{1}{2D_{i-1,j,k}} + \frac{1}{2D_{i,j,k}} \quad (3.11)$$

$$\frac{1}{D_{i,j,k}^{RX}} = \frac{S_{i,j,k}^{*}}{S_{i+1,j,k}^{*}} \frac{1}{2D_{i+1,j,k}} + \frac{1}{2D_{i,j,k}} \quad (3.12)$$

The finite difference algorithm was programmed in Visual Basic for Applications (VBA). In the current investigation, the cubical RB element was discretized using 21 nodes in each direction ($N_x = N_y = N_z = 21$). The mesh independency was validated for this number of mesh points. The total size of the RB element was 40 nm and the size of the central cubical particle was varied to calculate the concentration profile for different volume fraction of the dispersed phase. It was assumed that the solubility and the diffusivity of each permeating species, different for the continuous and dispersed phases, remained constant throughout the RB element and the membrane. The permeation flux of each component was calculated in the y-direction at the feed side, at the midpoint of the RB element and the permeate side using the Fick's first law. Equations (3.13) and (3.14) provides the equations that were used to calculate the permeation flux at the permeate side of the RB element. Similar equations were used to calculate the permeation flux at the feed side and at the midpoint of the RB element. The simulation was run until the permeation fluxes at the three above-mentioned surfaces of the RB element were the same to within a relative error of 0.01% that is when steady state conditions were achieved. The effective permeability of the MMM was then calculated using the predicted permeate flux, the RB element size and the concentration difference across the RB element (Equation (3.15)).

$$J_{(i,N_y,k)} = -D_{x,y,z}\left.\frac{\partial C}{\partial y}\right|_{y=L_1} \tag{3.13}$$

$$J_{FD}\Big|_{y=L_1} = \sum_{i=1}^{N_x}\sum_{k=1}^{N_z}\frac{\omega_i\omega_k J_{(i,N_y,k)}}{(N_x-1)(N_z-1)} \quad \text{with} \quad \omega_i = \begin{cases} 0.5 \; if \; i = 1 \; or \; i = N_x \\ 1.0 \; for \; i \in [2, N_x - 1] \end{cases} \quad \omega_k = \begin{cases} 0.5 \; if \; k = 1 \; or \; k = N_z \\ 1.0 \; for \; k \in [2, N_z - 1] \end{cases} \tag{3.14}$$

$$P^*_{Eff,FD} = \frac{J_{FD}\, L_1}{\Delta C} \tag{3.15}$$

Contrary to the findings of Singh et al. [26] and Yang et al. [27], for linear solubility factors, the product of the diffusivity and solubility, i.e. permeability, dictates the permeation flux of a species across the membrane and not their individual values. This has been our findings in this investigation and recently corroborated by Monsalve-Bravo and Bhatia [28]. To illustrate this finding, the effective permeability of mixed matrix membranes was obtained numerically for different ratios of the respective diffusivity and solubility of a permeating species of the two phases

of the membrane. In this study, the values of the diffusion coefficient and the solubility factor were varied while the ratio of the permeability of a permeating species in the two phases remained constant. Table 3.3 gives the values of the ratio of the diffusion coefficients and solubility factors along with the estimated relative permeability of the MMM for a 16.6% filler volume fraction. These results clearly indicate that the effective permeability is the permeability of a migrating species in the two phases of the MMM and not on the individual values of diffusivity and solubility.

Table 3.3. Effect of ratio of the diffusion coefficient and solubility factor of the two phases of a mixed matrix membrane on the estimation of the relative permeability for a percentage volume fraction of 16.6%.

$D_d . D_c^{-1}$	$S_d^* . S_c^{*-1}$	$P_d^* . P_c^{*-1}$	$P_{eff}^* . P_c^{*-1}$
0.1	100	10	1.46
1	10	10	1.46
100	0.1	10	1.46
0.2	2500	500	1.68
0.5	1000	500	1.68
10	50	500	1.68
100	5	500	1.68

Moreover, different sizes of elements were used in the computer program to investigate the effect of the particle size on the effective permeability of MMMs. It was observed that the variation in the size of an element, and consequently the size of a particle, does not affect the effective permeability of MMMs. This observation is in agreement with the results of computational simulation for MMMs containing spherical fillers obtained by Singh et al [26]. However, in practice, increasing the particle size could result in a deviation from a homogenous dispersion of the particles within the membrane. In addition, the polymer-particle interface interaction may diverge from ideal morphology when the size of the particle increases [6,26,29]. Therefore, the model may lose its validity since the fundamental assumptions of an ideal mixed matrix membrane would not prevail anymore.

3.2.3. Correction factor of the resistance-based model

To develop a simple and accurate analytical model that could be used to predict rapidly the permeation flux across a mixed matrix membrane, the effective permeability for each numerical FD simulations were compared to the permeability estimated by the resistance-based model under identical conditions for the permeability of the continuous and dispersed phases as well as the volume fraction of the solid filler. This comparison allowed determining a set of correction factors (τ) for the RB model defined in terms of the ratio of the effective permeability obtained by finite differences and the permeability prediction calculated with the RB model (See Equation (3.16)). All the individual correction factors were used to determine a global correlation that could predict the correction factor as a function of the ratio of permeabilities of the dispersed and continuous phases and the volume fraction of the dispersed phase. Two such correlations were obtained: one for high permeable fillers (HPF) and one for low permeable fillers (LPF). Figure 3.4 shows the prediction of the effective permeability using both the RB and FD models as a function of the ratio of the permeabilities of the dispersed and the continuous phases for a fixed volume fraction of the filler ($\phi = 0.42$). Figure 3.4 clearly indicates that the prediction of both models follow a sigmoidal variation as a function of the ratio of the permeabilities at a fixed filler content. For a solid filler with a lower or similar permeability of the dispersed phase relative the continuous phase, the two models are relatively equivalent for the estimation of the effective membrane permeability. For a solid filler with higher permeability, the RB model is underestimating the effective membrane permeability.

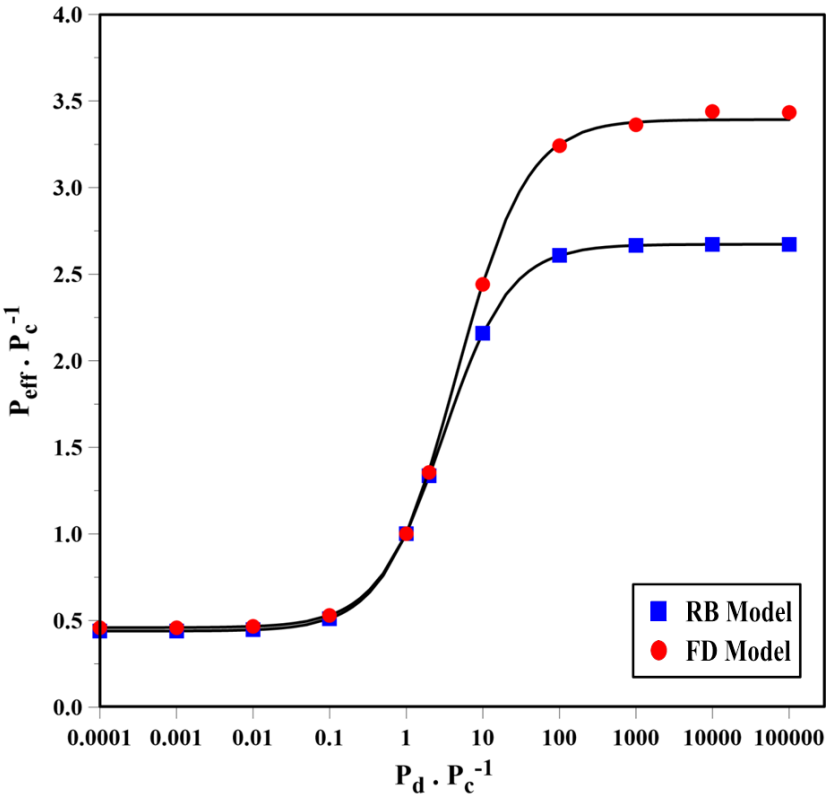

Figure 3.4. Predictions of RB and FD models for different ratios of permeability and for a fixed filler volume fraction (ϕ=0.42).

The correction factor was then used to adjust the predicted effective permeability of the mixed matrix membranes by the RB model (Equation (3.17)).

$$\tau_{(P_c,P_d,\phi)} = \frac{P_{Eff,FD}}{P_{Eff,RB}} = \frac{P^*_{Eff,FD}}{P^*_{Eff,RB}} \tag{3.16}$$

$$P_{Eff} = \tau_{(P_c,P_d,\phi)} \times \left(\left(1-H^2\right)P_c + \frac{P_c P_d H^2}{HP_c + \left(1-H\right)P_d} \right) \tag{3.17}$$

To generalize the RB model, two correlations for the correction factor were developed: one correlation for high permeable solid fillers and one correlation for low permeable solid fillers. It was observed that at a fixed filler volume fraction, a Langmuir-type equation could be used to predict the correction factor as a function of the permeability ratio of the dispersed to the continuous phase (P_d/P_c or P_d^*/P_c^*). Equation (3.18) was therefore used to model the correction factor for the RB model in the MMM containing a solid filler having a higher permeability than

the continuous phase. The parameters b_{HPF} and $C_{M\text{-}HPF}$ of Equation (3.18) were found to be a function of the volumetric filler content only. Two polynomial correlations were obtained by curve fitting the correction factor data set to calculate the parameters b_{HPF} and $C_{M\text{-}HPF}$ as a function of the volumetric filler content (Eqs. (3.19) and (3.20)). Figure 3.5 shows the experimental correction factors obtained from the Equation (3.16) with the ones estimated by Equations (3.18)-(3.20). As can be observed in Figure 3.5, there is a very good agreement between the experimental and the model predictions with an average relative prediction error of less than 0.5%. This indicates the relatively high accuracy of Langmuir-type equation for predicting the correction factor for the effective permeability of a MMM containing a high permeable filler.

$$\tau_{(P_c,P_d,\phi)-HPF} = 1 + \frac{C_{M-HPF}\, b_{HPF}\left(\frac{P_d}{P_c}-1\right)}{1+b_{HPF}\left(\frac{P_d}{P_c}-1\right)} \tag{3.18}$$

$$b_{HPF} = -0.0923\phi^2 - 0.0563\phi + 0.1486 \tag{3.19}$$

$$C_{M-HPF} = 2.2115\phi^3 - 4.2545\phi^2 + 2.043\phi \tag{3.20}$$

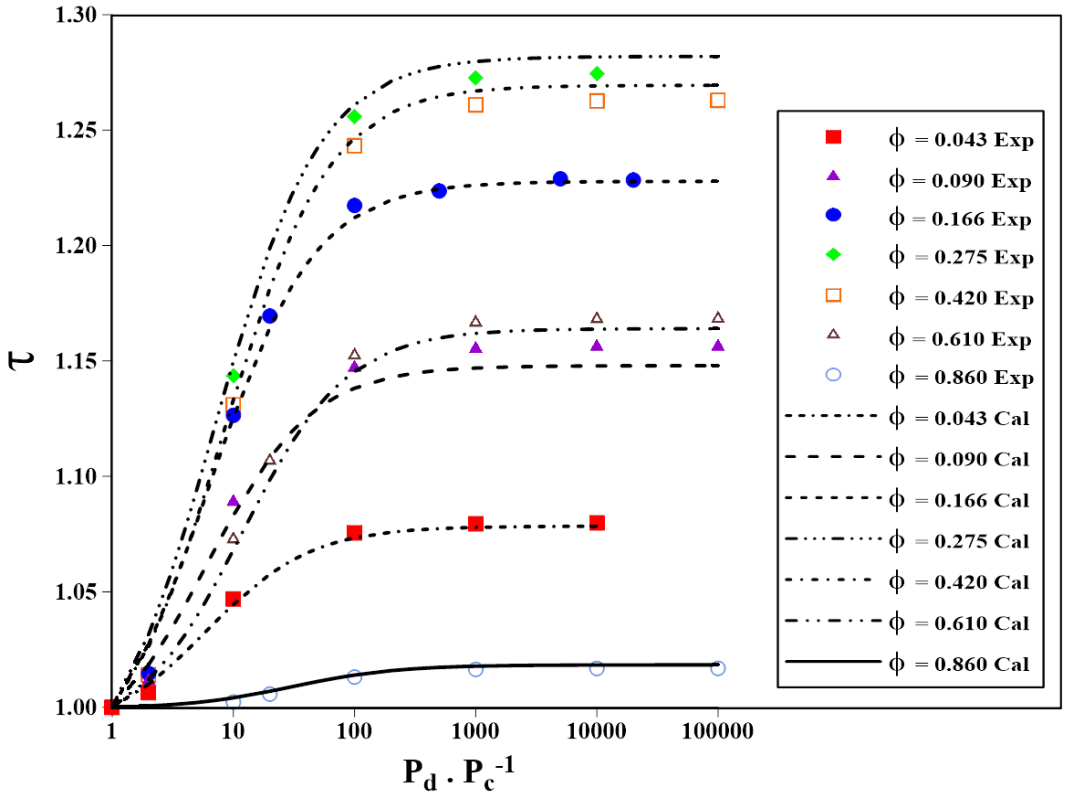

Figure 3.5. Experimental and estimated correction factor for mixed matrix membranes containing a HPF.

Figure 3.6 compares the prediction of the new RB model with the Maxwell and Hennepe models for a MMM containing a high permeable filler for different ratios of the permeability as a function of the volumetric filler loading. Results show that the prediction of the effective permeability as a function of the filler volume fraction obtained with the new model starts to deviate from the Maxwell and Hennepe models at lower filler volume fraction. The magnitude of the deviation is more important in MMMs containing higher permeable particles. Moreover, increasing the volume fraction of the filler within the membrane up to 40%, a larger difference between the model predictions is observed. All three models converge to an identical value of $P_d.P_c^{-1}$ when the volume fraction of filler approached unity. The observed difference is undoubtedly due to the influence of the three-dimensional tortuosity effect of the mass transport of the components through the membrane. Furthermore, the predicted values in this study show similar trends to the simulated values obtained by Singh et al. [26] for a MMM with randomly dispersed particles.

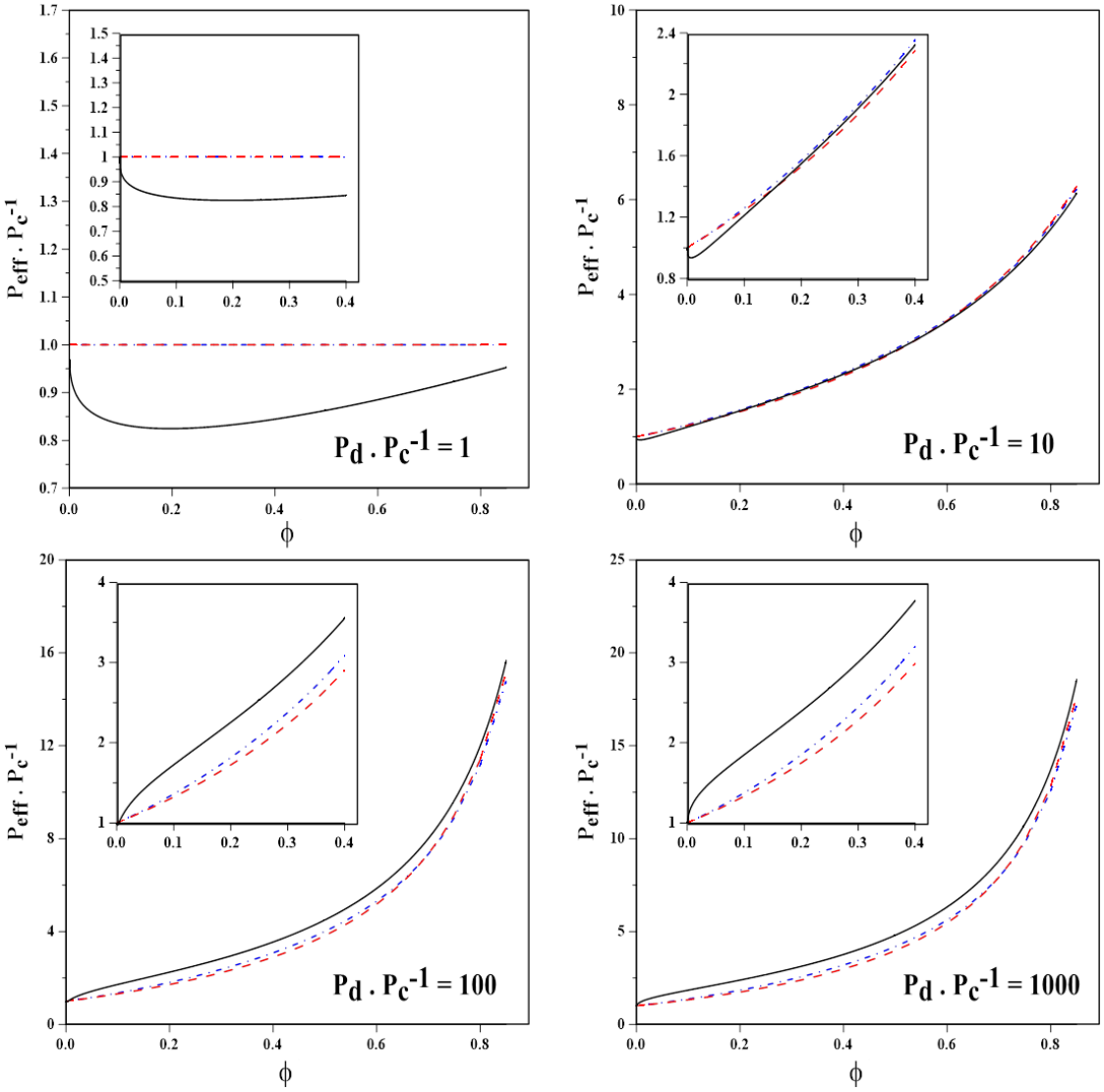

Figure 3.6. Comparison between the predictions of the extended RB model (—·), Maxwell model (— —) and Hennepe model (——) for HPF.

A similar analysis was performed to develop a correlation for the correction factor for the case where the permeability of the solid filler is lower than the permeability of the continuous phase. Akin for the HPF, a Langmuir-type equation (Equation (3.21)) was used to correlate the correction factors for a mixed matrix membrane containing low permeable fillers (LPF). The correlation parameters b_{LPF} and $C_{M\text{-}LPF}$ were modeled via two different polynomial functions (Eqs. (3.22) and (3.23)). Equations (3.21)-(3.23) were used to predict the correction factor for a MMM with low permeable fillers, and results were then compared to the experimental correction factors (Figure 3.7). An average relative prediction error of less than 0.1% was observed between the experimental

and calculated correction factors, which clearly indicates that the RB model along with the correlations for the correction factors can be used with confidence to predict the effective permeability of a mixed matrix membrane.

$$\tau_{(P_c,P_d,\phi)-LPF} = 1 + \frac{C_{M-LPF}\, b_{LPF}\left(\frac{P_c}{P_d}-1\right)}{1+b_{LPF}\left(\frac{P_c}{P_d}-1\right)} \tag{3.21}$$

$$b_{LPF} = 1.6758\phi^3 - 4.4098\phi^2 + 2.734\phi \tag{3.22}$$

$$C_{M-LPF} = -1.2077\phi^4 + 2.7016\phi^3 - 1.995\phi^2 + 0.4593\phi + 0.0418 \tag{3.23}$$

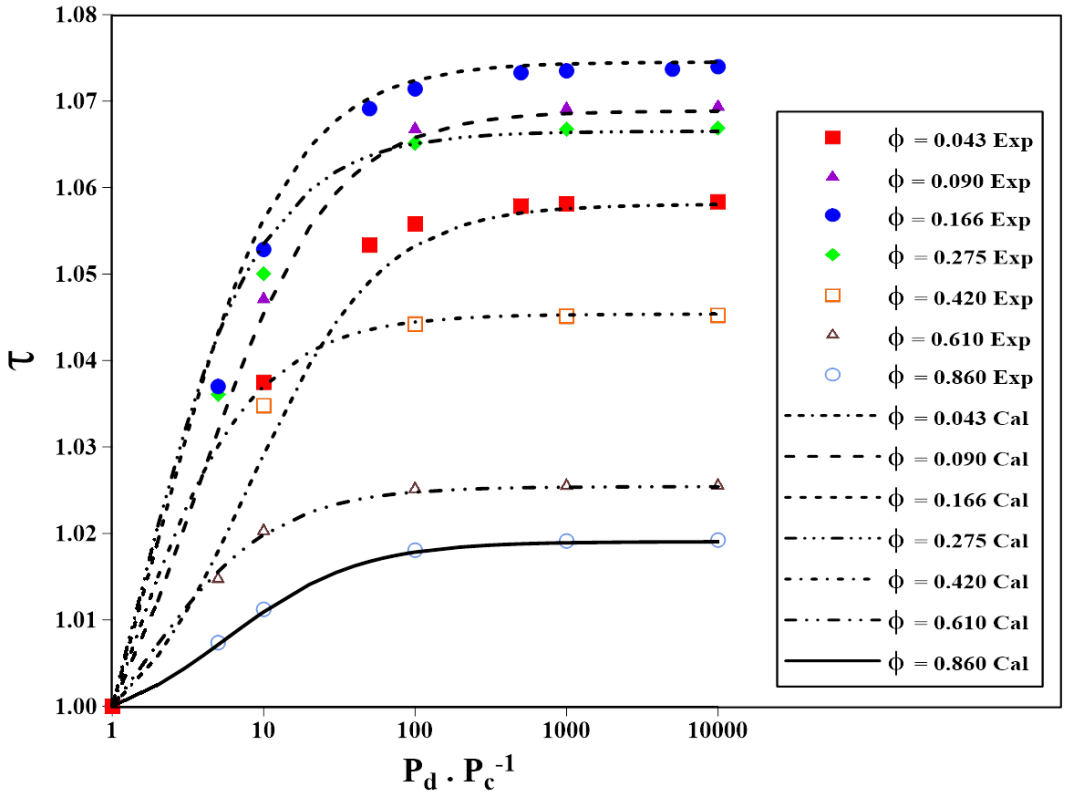

Figure 3.7. Experimental and estimated correction factors for a mixed matrix membrane containing LPF.

The predictions of the effective permeability obtained with the new model for low permeable fillers were compared in Figure 3.8 to the Maxwell and Hennepe models. The deviations observed for the various models for the predictions of the effective permeability of a MMM containing low

permeable fillers are smaller than the deviations observed for the high permeable fillers. It turns out that the Maxwell and Hennepe models are more applicable for MMMs where the dispersed phase is less permeable than the continuous phase. It is interesting to note that the Maxwell model is surprisingly accurate given that, in addition to be simple, it was derived more than a century ago for estimating the effective electrical conductivity of a continuous matrix material in which were embedded spherical solid particles. Greater deviations are observed at higher relative permeability ratio and intermediate filler volume fraction.

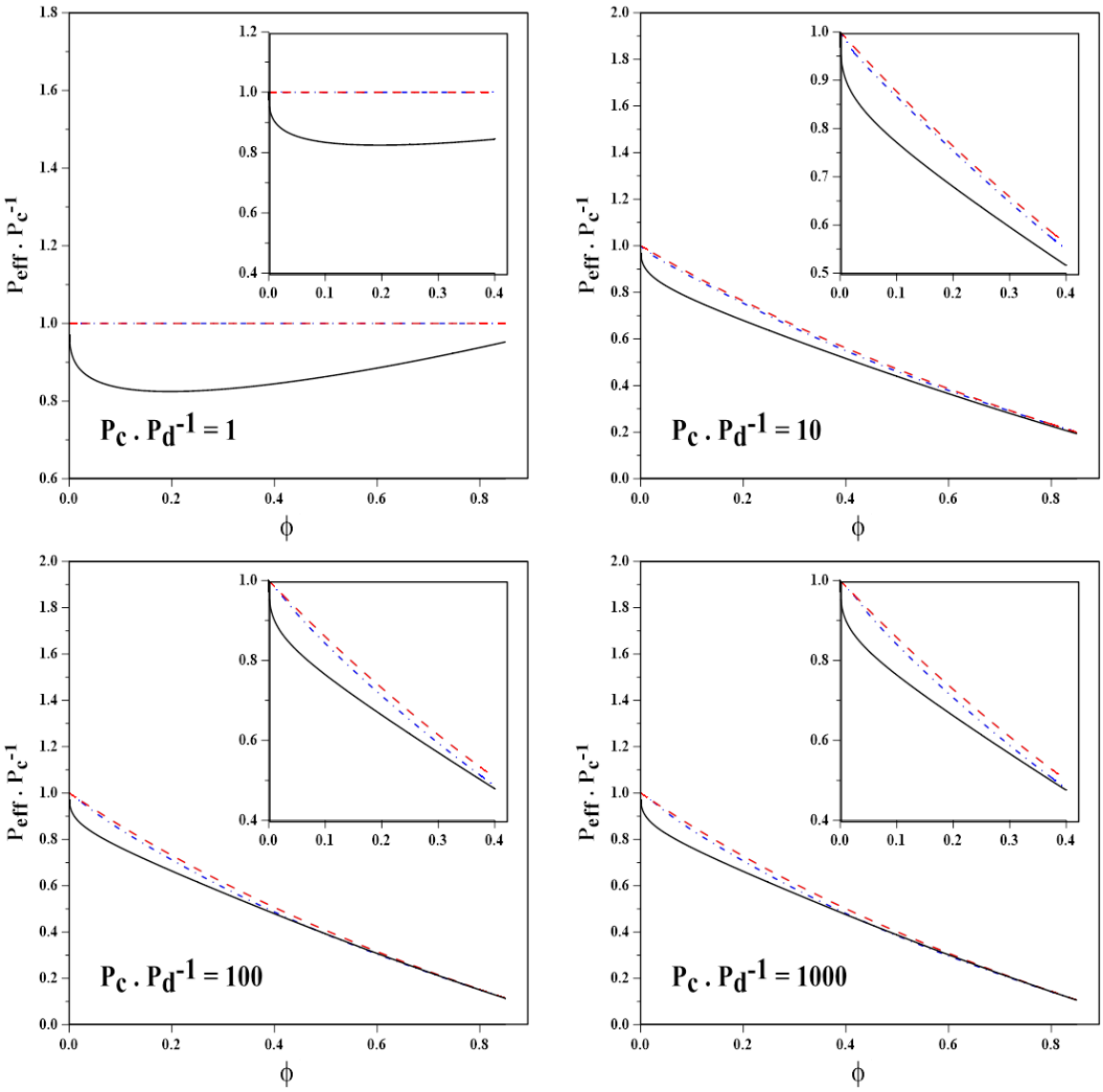

Figure 3.8. Comparison between the predictions of the extended RB model (— ·), Maxwell model (— —) and Hennepe model (——) for LPF.

With the number of numerical nodes (21 for each direction) used in this investigation, simulations with the FD method were limited to a volume fraction of the filler in the membrane of roughly 86%. As a result, the proposed RB model is applicable for the prediction of the effective permeability of ideal mixed matrix membranes in the range of 0-86% of the volumetric filler content. It was desired to cover the widest range possible for the volumetric filler content even though realistically such a filler content cannot be achieved. Indeed, for each particle shape and their orientation, there exists a maximum packing capacity. Moreover, similarly to the original RB model, the prediction of the relative permeability in the extended RB model is independent of the units of permeability.

3.3. Applications

The validation of the extended RB model was first performed using experimental data obtained in our laboratory for the pervaporation separation of butanol from aqueous binary solutions using a PDMS/Super Activated Carbon Powder membrane [7]. The model validation was also performed for gas separation using two different types of mixed matrix membranes reported in the literature [30].

3.3.1. MMM for the Pervaporation Separation

The experimental data presented by Azimi et al. [7] for the separation of butanol from aqueous solutions by pervaporation using PDMS/Super Activated Carbon Powder membranes was first used to validate the extended RB model. It was not possible to find a reliable source for the permeability of the permeating species through the PDMS and the activated carbon such that the permeability of butanol and water in the neat PDMS membrane was estimated based on experimental pervaporation data. In addition, the permeability of both water and butanol in the activated carbon nanoparticles was estimated by combining the theoretical calculation of diffusion coefficients with the experimentally obtained sorption properties of species in the nanoparticles (Sections 3.3.1.1 – 3.3.1.4). Then, the partial permeate fluxes of the species were estimated using the calculated effective permeability of the penetrants through the mixed matrix membrane using the extended RB model (Section 3.3.1.5).

3.3.1.1. Thermodynamic of Vapour-Liquid Equilibrium

The vapour-liquid equilibrium of each permeating species was calculated using the extended Raoult's law (Equation 3.24) [24]. Moreover, Margules model was used to estimate the activity coefficients of the species in binary butanol-water solutions (Eqs. (3.25) and (3.26)) [31].

$$p_m = x_m \gamma_m p_m^S \tag{3.24}$$

$$Ln(\gamma_1) = x_2^2 \left[Ln(\gamma_1^\infty) + 2x_1 \left(Ln(\gamma_2^\infty) - Ln(\gamma_1^\infty) \right) \right] \tag{3.25}$$

$$Ln(\gamma_2) = x_1^2 \left[Ln(\gamma_2^\infty) + 2x_2 \left(Ln(\gamma_1^\infty) - Ln(\gamma_2^\infty) \right) \right] \tag{3.26}$$

According to a previous study, the limiting activity coefficient (activity coefficient at infinite dilution) of butanol in binary aqueous solutions follows a linear relation with respect to temperature over the range of 303-333 K [24]. Moreover, due to the dilute butanol concentration in the feed, it was assumed that the water activity coefficient is equal to unity [24]. In addition, the saturation pressures of butanol and water at different temperatures were predicted using Antoine equation (Equation (3.27)) [32]. Table 3.4 presents the values used in this study for the parameters of Antoine equation for butanol and water [33].

$$Ln\left(p_{(kPa)}^S \right) = \bar{A} - \frac{\bar{B}}{\bar{C} + T_{(^0C)}} \tag{3.27}$$

Table 3.4. Antoine coefficients for calculating the vapour pressure of butanol and water [33]

Parameter	Butanol	Water
$\bar{A}$	15.3144	16.3872
$\bar{B}$	3212.43	3885.70
$\bar{C}$	182.739	230.170

3.3.1.2. Estimation of the Species Permeability in PDMS

According to the solution-diffusion theory, the permeability of component *m* in a membrane is a function of the solubility factor (S) and the diffusion coefficient (D) [12–15]. These two parameters

depend on the properties of the permeating species and the membrane as well as on the operating conditions [12,13,15,24]. Henry's law is the dominating sorption mechanism for both components in dilute butanol aqueous solutions in PDMS membranes [24]. Moreover, Henry's law constant follows an Arrhenius-type relation with respect to temperature (Equation (3.28)) [24,34]. Therefore, Equation (3.29) was used to represent the solubility factor of butanol and water in the PDMS membrane at different temperatures.

$$H_m^* = H_{m0}^* \, \mathrm{e}^{\frac{-\Delta H_m}{RT}} \tag{3.28}$$

$$S_m = H_m^* \frac{C_{fm}}{M_m p_{fm}} = \frac{C_{fm} H_{m0}^*}{M_m p_{fm}} \, \mathrm{e}^{\frac{-\Delta H_m}{RT}} \tag{3.29}$$

The diffusion coefficient also follows an Arrhenius-type relation with respect to the temperature at a constant feed concentration (Equation (3.30)) [9,15]. Therefore, assuming zero-stage cut condition, perfect vacuum on the permeate side and a constant butanol concentration on the feed side, the partial permeate fluxes of each species can be estimated by an Arrhenius-type relation (Equation (3.31)) [15,35].

$$D_m = D_{m0} \, \mathrm{e}^{\frac{-E_{dm}}{RT}} \tag{3.30}$$

$$J_m = \frac{P_m \Delta p_m M_m}{\delta} = \frac{M_m D_m S_m \Delta p_m}{\delta} = \frac{D_{m0} C_{fm} H_{m0}^*}{\delta} \, \mathrm{e}^{\frac{-(\Delta H_m + E_{dm})}{RT}} = J_{m0} \, \mathrm{e}^{\frac{-E_{pm}}{RT}} \tag{3.31}$$

Table 3.5 presents the calculated values for the activation energy of permeation ($E_{pm} = E_{dm} + \Delta H_m$) and the pre-exponential permeation flux parameter (J_{m0}) for the separation of butanol from aqueous solutions by pervaporation using the laboratory-made neat PDMS membranes [7]. Figure 3.9 compares the experimental partial flux data with the partial flux values estimated using Equation (3.31).

Table 3.5. Estimated values for the parameters of Arrhenius equation for the partial permeate fluxes.

	Butanol	**Water**
E_p (J.mol^{-1})	66124	50033
J_0 (g.m^{-2}.h^{-1})	8.74×10^{10}	2.66×10^{9}

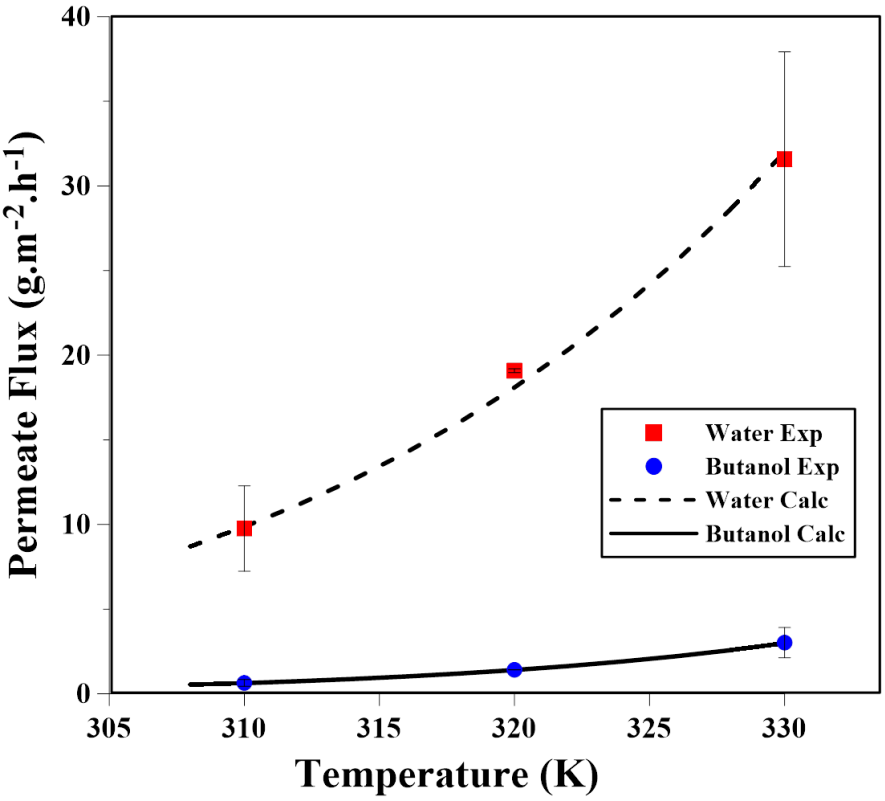

Figure 3.9. Experimental and calculated partial permeate fluxes of the butanol and water for the separation of a 5 $g.L^{-1}$ butanol binary aqueous solution by pervaporation using neat PDMS membranes.

Equation (3.31) was then used to predict the butanol and water permeabilities in neat PDMS membranes at different temperatures. Results of Figure 3.10 show that the permeability of both components in PDMS slightly increases with an increase in temperature. This is due to the increase in the diffusion coefficient and in the species partial pressure whereas the solubility factor decreases with an increase in temperature. It seems that for the permeation of butanol and water in PDMS, the rate of change in diffusivity is moderately greater than the rate of change in the solubility and partial pressure following an increase in temperature. As a result, the permeability of both components increases as a function of temperature. Moreover, according to Figure 3.10, the permeability of water in neat PDMS membranes is higher than the permeability of butanol when the partial pressure gradient is used as the driving force. However, the permeability of butanol would be higher than the one of water if the concentration gradient is used as the driving force of the mass transport. This phenomenon is due to the difference in the vapour-liquid

equilibrium properties of the components, which would affect the solubility factor and consequently the permeability of species. As it was mentioned in the introduction, although the values and units of the permeability are different depending on the selected driving force, the final estimated permeate flux remains independent of the selected units. Table 3.6 gives the values of the permeability of water and butanol in the two sets of units. It seems that the ratio of the permeability of the two components in a membrane is not a suitable pervaporation performance metrics since it is dependent on the type of driving force used. Therefore, it seems to be more practical to use the composition of components on two side of the membrane to investigate the membrane selectivity since they are independent on the chosen driving force.

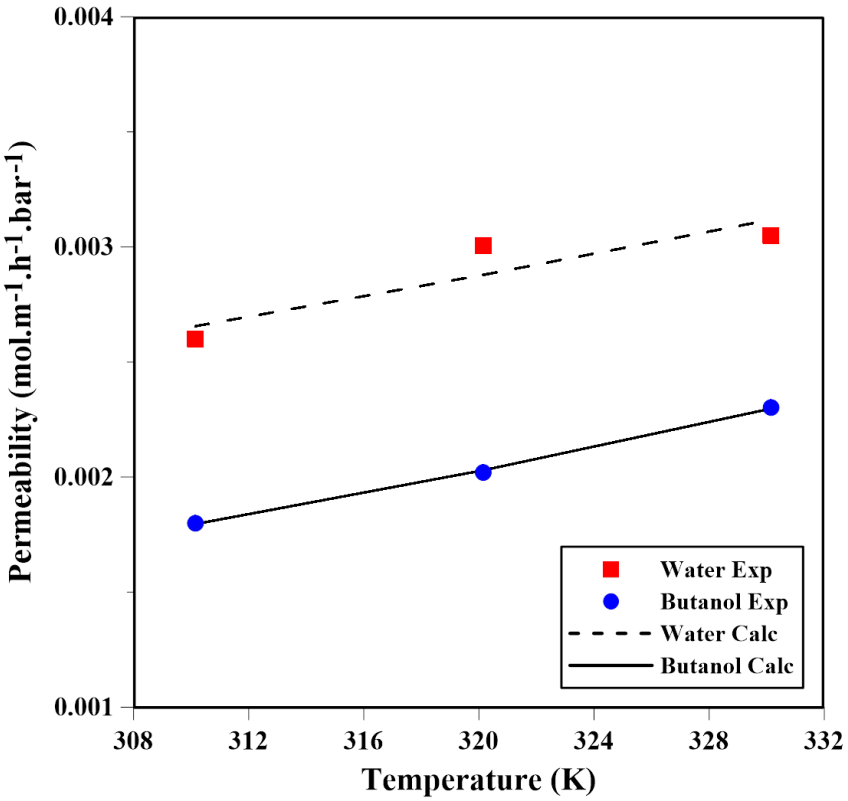

Figure 3.10. Experimental and calculated permeabilities of butanol and water in PDMS as a function of temperature at a fixed feed concentration of 5 $g.L^{-1}$.

Table 3.6. Estimated values of the permeability of butanol and water in neat PDMS membranes expressed in two different sets of units.

Temperature (K)	Butanol		Water	
	($m^2.h^{-1}$)	**($mol.m^{-1}.h^{-1}.bar^{-1}$)**	**($m^2.h^{-1}$)**	**($mol.m^{-1}.h^{-1}.bar^{-1}$)**
310	$3.83x10^{-8}$	0.0018	$3.036x10^{-9}$	0.00266
320	$8.53x10^{-8}$	0.002	$5.6x10^{-9}$	0.00288
330	$1.81x10^{-7}$	0.0023	$9.97x10^{-9}$	0.00312

3.3.1.3. Estimation of Permeabilities in Activated Carbon

The determination of the permeability of the two migrating species in the filler of the mixed matrix membrane was achieved by estimating separately their solubility factor and diffusion coefficient. The solubility factor of butanol on the activated carbon was obtained experimentally through a series of batch adsorption tests to determine the adsorption isotherm. It was not possible to measure the solubility factor of water in the dispersed phase such that it was assumed identical to the continuous phase. On the other hand, the diffusion coefficients were estimated theoretically by considering the combination of possible diffusion mechanisms in porous material.

3.3.1.3.1. Solubility Factor

The sorption property of butanol in the super activated carbon powder was investigated by performing liquid batch adsorption tests over the temperature range of 310-330 K. Experiments were performed by adding an accurately weighted amount of adsorbent (1 g) to 5 flasks. Each flask contained 50 mL of binary butanol aqueous solution of different concentrations (1, 3, 5, 10, 15, 20 and 25 $g.L^{-1}$). An automatic thermostat shaker was used to keep the temperature constant throughout the experiments. Agitation was provided for 48 h, which was much larger than the time needed to reach equilibrium. Samples were taken every 6 h and analyzed using gas chromatography (GC). A mass balance was performed for each flask to determine the amount of butanol adsorbed.

Figure 3.11 presents the butanol isotherms on activated carbon at three different temperatures (310-330 K). Butanol activity (p/p^s) was obtained using the vapour liquid equilibrium discussed in Section 3.3.1.1. Moreover, the Sips isotherm model (Equation (3.32)) was used to represent the

very favourable adsorption behaviour of butanol on the AC nanoparticles [9,36,37]. Table 3.7 gives the parameters (n, b^* and q^*) of the Sips isotherm equation for the adsorption of butanol on the activated carbon at different temperatures.

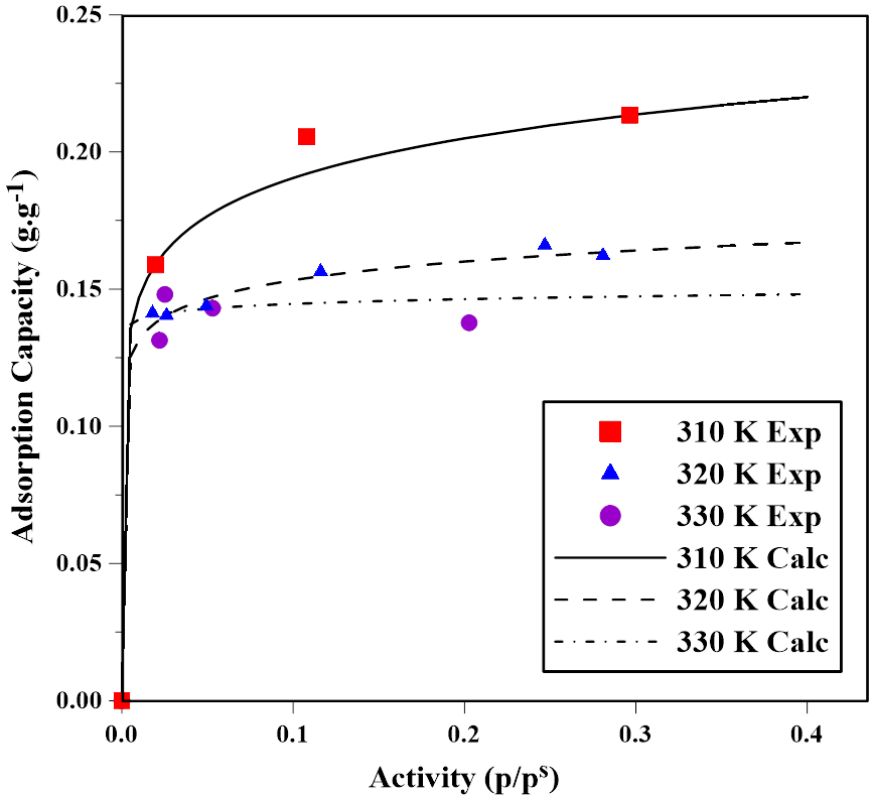

Figure 3.11. Experimental and modelled adsorption isotherms of butanol on AC nanoparticles at different temperatures.

$$q = \frac{q^* b^* p^n}{1 + b^* p^n} \tag{3.32}$$

Table 3.7. Fitted Sips parameters for the prediction of butanol sorption isotherm at different temperatures

Temperature (K)	b^*	q^*	n
310	1.136	0.625	0.154
320	1.046	0.41	0.101
330	1.044	0.307	0.033

Hashemifard et al. suggested a combination of Fick's law, Darken equation and adsorption isotherm to represent the solubility of the dispersed phase inside mixed matrix membranes for

Langmuir, dual-site Langmuir and Sips adsorption models [9]. Equation (3.33) can be used to predict the solubility of a species in the dispersed phase while the Sips isotherm is used to predict the amount of component *m* adsorbed in the filler.

$$S_m = \frac{q_m^* \rho_d}{n_m M_m \left(p_{fm} - p_{pm} \right)} \left(Ln \left(\frac{\left(1 + b_m^* \left(p_{fm} \right)^{n_m} \right)}{\left(1 + b_m^* \left(p_{pm} \right)^{n_m} \right)} \right) \right) \tag{3.33}$$

Equation (3.33) was used in this study to calculate the solubility of butanol in the solid filler. Sorption of water in both PDMS and activated carbon is assumed small in comparison to butanol. Therefore, it was assumed that the filler had the same water sorption properties as the neat PDMS membrane. Table 3.8 gives the parameters of an Arrhenius equation for the sorption of water in PDMS [24]. Equation (3.28) was used to approximate the solubility of water in the filler.

Table 3.8. Parameters of Arrhenius equation for the sorption of water in neat PDMS membranes [24]

Parameter	Value
H_{w0}^*	2.38×10^{-2}
ΔH_w^* $(J.mol^{-1})$	4949.5

3.3.1.3.2. Diffusion Coefficient

The effective diffusivity of component *m* in a porous filler is a function of the porosity, the tortuosity and the intrinsic diffusion coefficient of the component in the mobile phase within the pores of the filler (Equation (3.34)) [38]. The intrinsic diffusion coefficient is a combination of the different diffusion mechanisms such as Knudsen diffusion, molecular diffusion and surface diffusion [9,38,39]. However, surface diffusion is only significant at high pressures and temperatures, which does not prevail in the case of the pervaporation process [39].

$$D_{d,m} = \frac{D_{\text{int},m} \varepsilon}{\tau_d} \tag{3.34}$$

Equations (3.35) and (3.36) have been commonly used to calculate the Knudsen and molecular diffusion coefficients, respectively [9,40–42].

$$D_{K,m} = \frac{d_{pore}}{3}\left(\frac{8RT}{\pi M_m}\right)^{1/2} \tag{3.35}$$

$$D_M = \frac{1.858\times10^{-3}T^{3/2}\sqrt{\left(\frac{1}{M_m}\right)+\left(\frac{1}{M_n}\right)}}{p\sigma_{mn}{}^2\Omega} \tag{3.36}$$

Table 3.9 gives the parameters that were used to calculate the Knudsen and the molecular diffusion coefficient of butanol and water in the super activated carbon powder.

Table 3.9. Some parameters for the calculation of Knudsen and molecular diffusion coefficients [41]

Parameter	Reported Value
$(\varepsilon/k)_{butanol}$	454 K
$\sigma_{butanol}$	5.27 Å
$(\varepsilon/k)_{water}$	356 K
σ_{water}	2.649 Å
d_{pore} [41]	3.5 nm

The intrinsic diffusion coefficient of the permeating species as a function of pressure was calculated using Equation (3.37) [9,38]. According to Equations (3.35) and (3.36), only the molecular diffusion coefficient depends on pressure. The intrinsic diffusion coefficient was calculated as a function of pressure and temperature. The results of Figure 3.12 show that the intrinsic diffusion coefficient is independent of the pressure up to atmospheric pressure, which corresponds to the range of pressure within the membrane for the pervaporation separation process. Hence, it was assumed that Knudsen diffusion coefficient is the main mechanism to determine the intrinsic diffusion coefficient of both species in the solid filler embedded within the membrane.

$$D_{\text{int},m} = \left(\frac{1}{D_{K,m}} + \frac{1}{D_M} \right)^{-1} \tag{3.37}$$

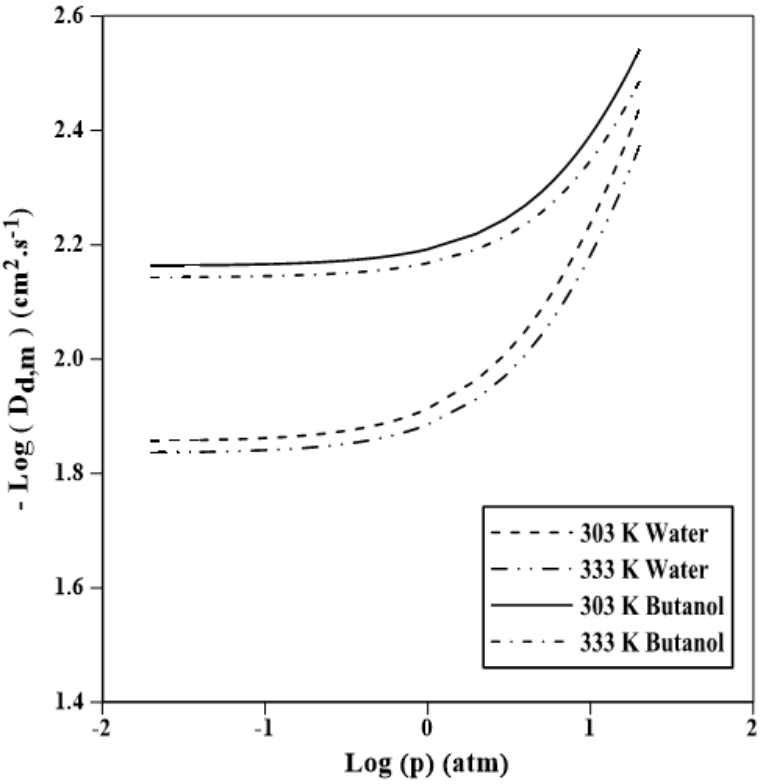

Figure 3.12. Variation of the intrinsic diffusion coefficient for butanol and water in the activated carbon powder.

Equation (3.34) was used to calculate the effective diffusion coefficient of the species in the filler where Knudsen diffusion was used to determine the intrinsic diffusivity of each component (Equation (3.35)). Moreover, a tortuosity factor of 5 was assumed for the transport of the components within the pores inside the filler and the porosity of activated carbon nanoparticles was calculated to be roughly 44% based on the information provided by the manufacturer [44].

3.3.1.4. Estimation of MMMs Thickness and Volume Fraction of Filler in MMMs

Equation (3.38) was used to predict the thickness of a MMM by assuming a constant membrane area and ideal interaction between the polymer and the particles. The addition of the filler into the polymer matrix of the membrane can result in a change of density of the MMMs, which leads to a change in the total volume of the membrane.

$$\delta_{MMM} = \delta_c \left(1 + \frac{\rho_c \, w_d}{\rho_d \left(1 - w_d\right)} \right) \tag{3.38}$$

Figure 3.13 compares the thickness measure experimentally with the estimated values for the thickness of PDMS/Activated Carbon mixed matrix membranes as a function of the weight fraction of the filler content. Results show that the values of the predicted thickness are in good agreement with the experimentally measured thickness.

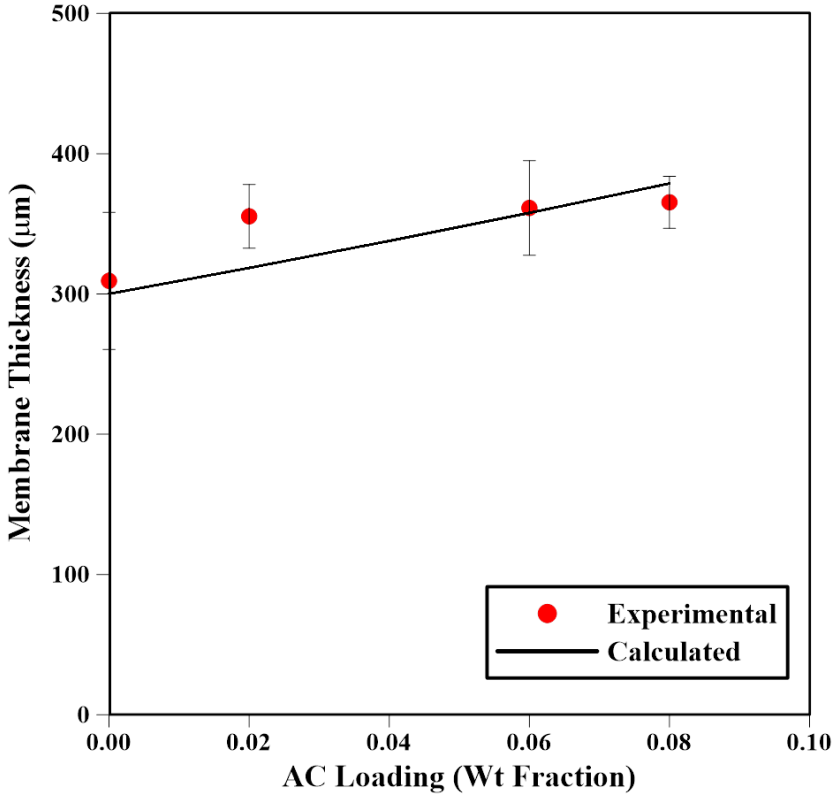

Figure 3.13. Comparison of the experimental and estimated values of the thickness of MMMs as a function of the activated carbon nanoparticle content.

The volume fraction of the filler is also a function of the density of two phases as well as the weight fraction of the filler content. Equation (3.39) was used to estimate the volume fraction of the filler within an ideal mixed matrix membrane. The predicted volume fractions were then used in the extended RB model to calculate the effective permeability of components in MMMs for different filler volume fractions.

$$\phi = \left(\frac{\rho_c w_d}{\rho_c w_d + \rho_d \left(1 - w_d\right)} \right) \tag{3.39}$$

3.3.1.5. Model Validation

The extended RB model was used to estimate the effective permeability of butanol and water in PDMS/Super Activated Carbon Powder Mixed Matrix Membranes. Equation (3.31) was used to predict the permeability of both species in the continuous phase using the parameters presented in Table 3.4. The permeability of the migrating species in the filler was calculated using the diffusion coefficient and the solubility factor as per Sections 3.3.1.3.1 and 3.3.1.3.2. According to Equation (3.33), the solubility of butanol is a function of the partial pressure of butanol in both the feed and the permeate sides of the membrane. The partial pressure of the species in the permeate side of the membrane was calculated using Dalton's law (Equation (3.40)) while the partial pressure of butanol in the feed side obtained from Section 3.3.1.1.

$$p_{pm} = y_m p^{vac} = \frac{J_m}{J_m + J_n} p^{vac} \tag{3.40}$$

A VBA program was used to predict the solubility factor of the components in the activated carbon nanoparticles and the effective permeability of the MMM simultaneously. The estimated effective permeability of MMMs were then used in Equation (3.1) to predict the partial permeate fluxes of both components at different temperatures and weight fractions of the filler. Figure 3.14 presents the comparison between the experimental and estimated values for the partial permeate fluxes for butanol and water for a series of pervaporation experiments conducted with different solid mass fraction. A good agreement was observed between the experimental and estimated values with an average error of almost 13%.

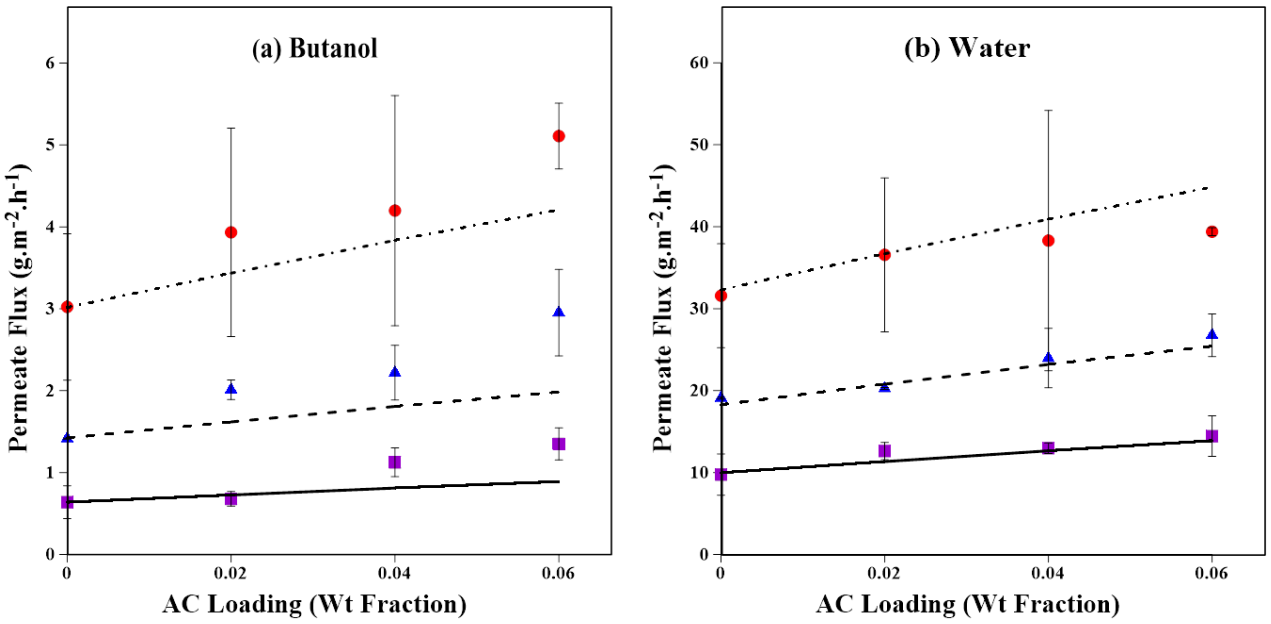

Figure 3.14. Comparison between the experimental (310 K (■), 320 K (▲) and 330 K (●)) and predicted permeate fluxes (310 K (——), 320 K (— —) and 330 K (— .)) of butanol (a) and water (b) as a function of the nanoparticle mass fraction at different temperatures.

Figure 3.15 presents the parity plot of the permeation flux for the pervaporation experimental data and the predicted values with the proposed RB model. The value of the regression coefficient R^2 exceeds 0.8, which indicates a relatively high accuracy of the model for the prediction of the pervaporation separation performance using mixed matrix membranes.

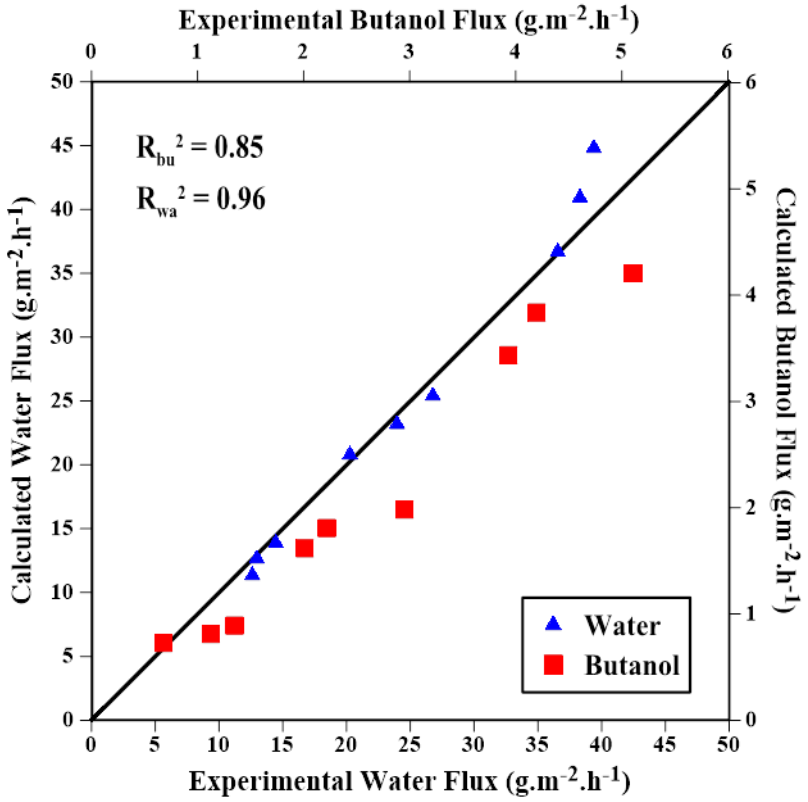

Figure 3.15. Parity plot between experimental and estimated partial fluxes for the separation of butanol using a pervaporation MMM

3.3.2. Mixed Matrix Membranes for Gas Separation

In this section, the extended RB model is validated for gas separation processes. Experimental data for the permeation of different gases through the Polyvinylidene fluoride (PVDF)/MCM-41 and PVDF/Zeolite 4A mixed matrix membranes were obtained from the literature [30]. Table 3.10 presents the literature values that were obtained for the permeability of the various permeating gases in the continuous and dispersed phases.

Table 3.10. Permeabilities of gases through the continuous and dispersed phases of MMMs [30].

Component	Material	Permeability (Barrer)
He	PVDF	3.94
He	MCM-41	1510000
He	Zeolite A4	1255.5
CO_2	PVDF	1.18
CO_2	MCM-41	320000
CO_2	Zeolite A4	139.5
O_2	PVDF	0.14
O_2	MCM-41	380000
O_2	Zeolite A4	2
N_2	PVDF	0.04
N_2	MCM-41	400000
N_2	Zeolite A4	0.048

The proposed RB model was used to predict the effective permeability of different permeating gases through mixed matrix membranes. Figure 3.16 compares the estimated and literature permeability of the various gases in mixed matrix membranes for different filler volume fractions[4]. Although there are some deviations between the predicted values and the experimental data, especially for the permeation of N_2 through PVDF/Zeolite A4 MMMs, results show a relatively good agreement between the predicted and literature effective permeability. These results validate the use of the extended RB model for the prediction of the gas separation performance using mixed matrix membranes. In addition, some researchers have used a three-phase Maxwell model to take into account the non-ideal particle-polymer interface morphology within a MMM [30]. However, based on the results obtained in this study, the experimental data are in good agreement with the results obtained with the model assuming ideal mixed matrix membrane. Furthermore, Figure 3.17 presents the parity plot between the estimated and literature permeability where a coefficient of regression R^2 equal to 0.98 was obtained.

[4] The values of effective permeabilities were obtained from the graphs published in the literature [30]

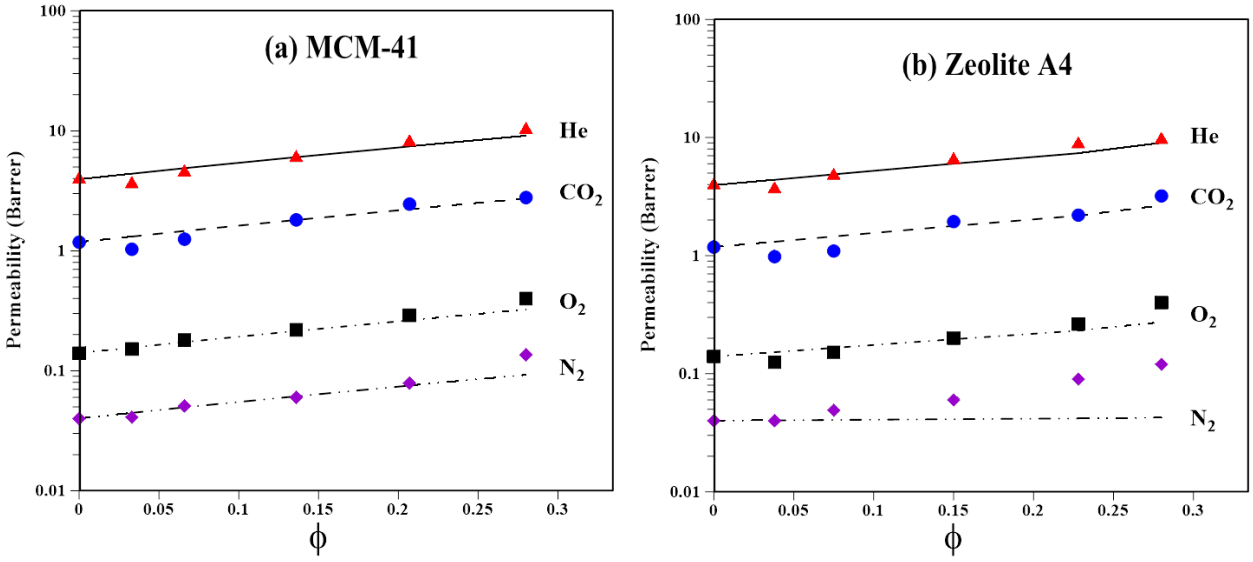

Figure 3.16. Comparison between the experimental (He (▲), CO_2 (●), O_2 (■) and N_2 (◆)) [30] and predicted permeabilities in PVDF/MCM-41 (a) and PVDF/Zeolite 4A (b) as a function of the volume fraction of the filler in polymer matrix

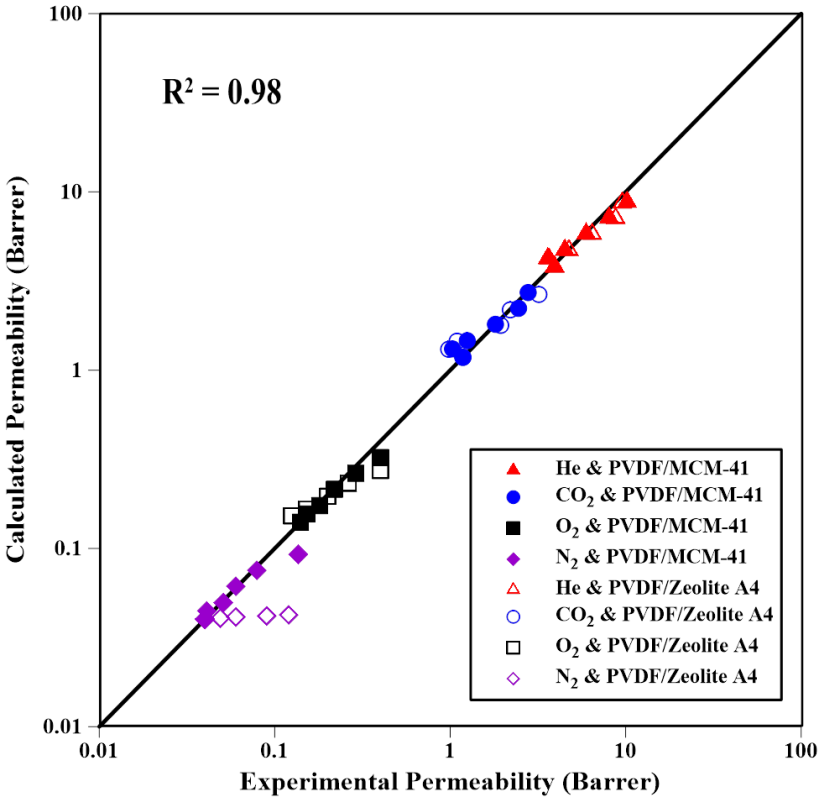

Figure 3.17. Parity plot between the experimental and estimated permeabilities of gases in mixed matrix membranes.

Figure 3.18 compares the average prediction error of the model presented in this study with the ones estimated by the Maxwell and Hennepe models. According to this figure, the extended RB model shows the best agreement with experimental data for both pervaporation and gas separation applications. Moreover, model prediction of the permeability for all sets of data for both pervaporation and gas separation processes were also compared and an average prediction error for each model was calculated as shown in Figure 3.18(c). This figure shows that the best agreement with an average error of 13.5% was obtained with the extended RB model.

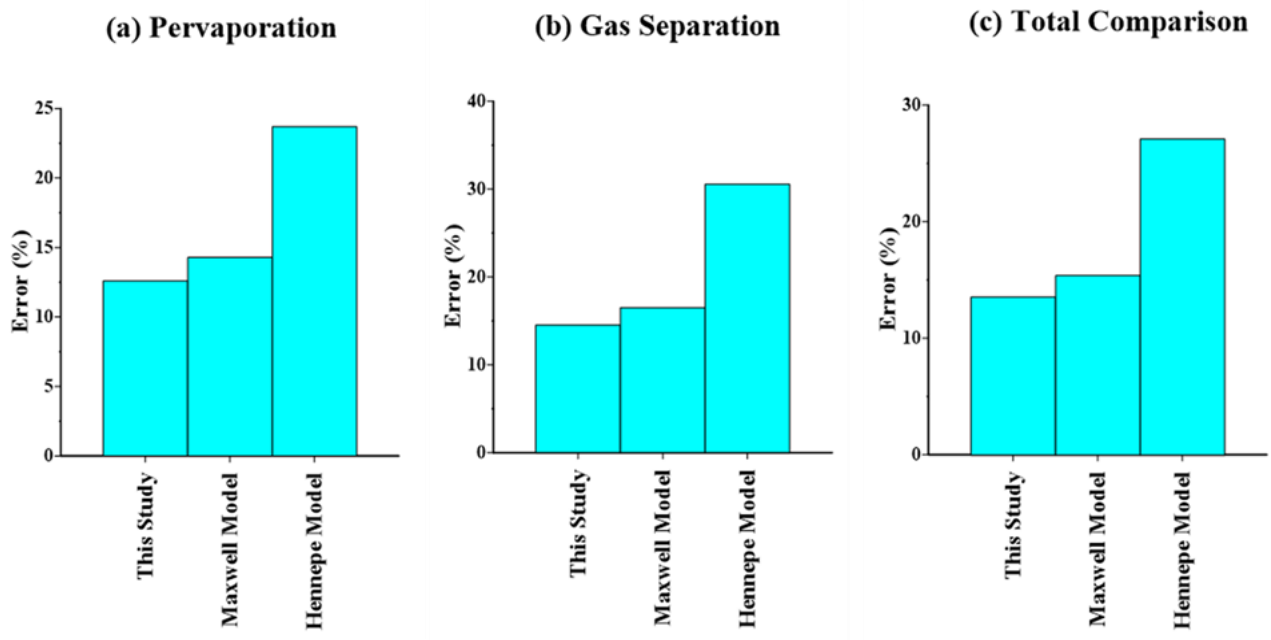

Figure 3.18. Comparison between the error of predictive models for pervaporation (a) and gas separation (b) processes and the total comparison between predictive models (c).

3.4. Conclusions

Despite the high accuracy of the finite difference method to estimate the mass transport within the mixed matrix membranes, long computation time is an important limitation for the application of this method for various applications. Instead, in this investigation, it was desired to develop a simple resistance-based model with a correction factor based on the results of the finite difference numerical simulations to represent more accurately and more rapidly the effective permeability of mixed matrix membranes. The correction factor takes into account the deviation of the concentration streamlines due to presence of a more or less permeable dispersed phase within the matrix of the polymeric membrane. When the dispersed phase has a higher permeability than the

continuous phase, the effective permeability is greater than the permeability of the neat continuous phase, and vice-versa for the less permeable dispersed phase. The correction factors were modeled successfully using a Langmuir-type relation with the model parameters obtained by performing data curve fitting on the set of predicted correction factors. The correction factor is function of the ratio of the dispersed phase permeability to the permeability of the continuous phase, and the volume fraction of the dispersed phase. The extended RB model was verified with experimental data for pervaporation and gas separation processes. High precision for the prediction of the effective permeability was observed with a reasonable coefficient of regression.

Acknowledgment

The authors would like to acknowledge the financial support of the Natural Science and Engineering Research Council of Canada (NSERC).

Abbreviations

AC	Activated Carbon
MMM	Mixed Matrix Membrane
PDMS	Polydimethylsiloxane
PVDF	Polyvinylidenefluoride

Nomenclature

A	Area (m^2)
$\overline{A}$	Parameter of Antoine Equation
b	Parameter of Correction Factor Equation (-)
b^*	Parameter of Sips Equation (bar^{-1})
$\overline{B}$	Parameter of Antoine Equation
C	Concentration $(g.m^{-3})$
C_M	Parameter of Correction Factor Equation (-)
$\overline{C}$	Parameter of Antoine Equation
d	Diffusion Pathway (m)
d_p	Diameter of Filler Nanoparticle (m)
D	Diffusion Coefficient $(m^2.h^{-1})$

D_0	Pre-Exponential Parameter of Arrhenius Equation for Diffusion $(m^2.s^{-1})$
E_d	Energy of Diffusion $(J.mol^{-1})$
E_p	Activation Energy of Permeation $(J.mol^{-1})$
H	Variable Defined in Equation 3.6
H^*	Henry's Law constant ($g.m^{-3}/g.m^{-3}$)
H^*_0	Pre-Exponential Parameter of Arrhenius Equation for Solubility ($g.m^{-3}/g.m^{-3}$)
J	Permeate Flux $(g.m^{-2}.h^{-1})$
J_0	Pre-Exponential Parameter of Arrhenius Equation for Permeate Flux $(g.m^{-2}.h^{-1})$
K	Boltzmann Constant $(m^2.kg.s^{-2}.K^{-1})$
L_1	Size of the RB Element (m)
L_2	Size of the Filler (m)
M	Molecular Weight ($g.mol^{-1}$)
n	Parameter of Sips Equation (-)
N	Number of Nodes
p	Pressure $(bar\ or\ kPa)$
P	Permeability $(mole.m^{-1}.h^{-1}.bar^{-1})$
P^*	Permeability ($m^2.h^{-1}$)
q	Sorption Capacity ($g.g^{-1}$)
q^*	Parameter of Sips Equation ($g.g^{-1}$)
R	Gas Constant $(J.K^{-1}.mol^{-1})$
R_i	Resistance $(h.bar.mole^{-1})$
S	Solubility Factor $(mole.m^{-3}.bar^{-1})$
S^*	Solubility Factor $(g.m^{-3}/g.m^{-3})$
t	Time (h)
T	Temperature (K)
w_d	Mass Fraction of Filler in Mixed Matrix Membrane (-)
x	x Coordinate or Liquid Mole Fraction
y	y Coordinate or Vapor Mole Fraction
z	z Coordinate
δ	Thickness (m)

ε	Porosity of the Filler Particle (-)
ϕ	Volumetric Filler Content (-)
γ	Activity Coefficient (-)
γ^{∞}	Limiting Activity Coefficient (-)
ρ	Density $(g.m^{-3})$
σ_{mn}	Average Collision Diameter (^{0}A)
τ	Correction Factor (-)
τ_d	Tortuosity Factor
Ω	Temperature Dependent Parameter of Collision Integral (-)
ΔH	Heat of sorption $(J.mol^{-1})$

Superscripts

L	Left
R	Right
s	Saturation conditions
vac	Vacuum

Subscripts

c	Continuous Phase
d	Dispersed Phase
Eff	Effective
f	Feed
FD	Finite-Difference Method
HPF	High Permeable Filler
i	x Coordinate for Node Position in FD Model
int	Intrinsic
j	y Coordinate for Node Position in FD Model
k	z Coordinate for Node Position in FD Model
K	Knudsen Diffusion

LPF	Low Permeable Filler
m	Component
M	Molecular Diffusion
MMM	Mixed Matrix Membrane
n	Component
p	Permeate
pore	Pore of the Filler
r	Relative
RB	Resistance-Based Model
t	total

3.5. References

[1] S.A. Hashemifard, A.F. Ismail, T. Matsuura, A new theoretical gas permeability model using resistance modeling for mixed matrix membrane systems, J. Membr. Sci. 350 (2010) 259–268. doi:10.1016/j.memsci.2009.12.036.

[2] H. Vinh-Thang, S. Kaliaguine, Predictive Models for Mixed-Matrix Membrane Performance: A Review, Chem. Rev. 113 (2013) 4980–5028. doi:10.1021/cr3003888.

[3] E.A. Feijani, H. Mahdavi, A. Tavasoli, Poly(vinylidene fluoride) based mixed matrix membranes comprising metal organic frameworks for gas separation applications, Chem. Eng. Res. Des. 96 (2015) 87–102. doi:10.1016/j.cherd.2015.02.009.

[4] D. Hua, Y.K. Ong, Y. Wang, T. Yang, T.-S. Chung, ZIF-90/P84 mixed matrix membranes for pervaporation dehydration of isopropanol, J. Membr. Sci. 453 (2014) 155–167. doi:10.1016/j.memsci.2013.10.059.

[5] J. Ahn, W.-J. Chung, I. Pinnau, M.D. Guiver, Polysulfone/silica nanoparticle mixed-matrix membranes for gas separation, J. Membr. Sci. 314 (2008) 123–133. doi:10.1016/j.memsci.2008.01.031.

[6] T.-S. Chung, L.Y. Jiang, Y. Li, S. Kulprathipanja, Mixed matrix membranes (MMMs) comprising organic polymers with dispersed inorganic fillers for gas separation, Prog. Polym. Sci. 32 (2007) 483–507. doi:10.1016/j.progpolymsci.2007.01.008.

[7] H. Azimi, F.H. Tezel, J. Thibault, Effect of nano-activated carbon on the performance of Polydimethylsiloxane (PDMS) membrane for pervaporation separation of butanol from binary aqueous solutions., Submitt. J. Chem. Technol. Biotechnol. (2016).

[8] G. Liu, W.-S. Hung, J. Shen, Q. Li, Y.-H. Huang, W. Jin, K.-R. Lee, J.-Y. Lai, Mixed matrix membranes with molecular-interaction-driven tunable free volumes for efficient bio-fuel recovery, J. Mater. Chem. A. 3 (2015) 4510–4521. doi:10.1039/C4TA05881J.

[9] S.A. Hashemifard, A.F. Ismail, T. Matsuura, Prediction of gas permeability in mixed matrix membranes using theoretical models, J. Membr. Sci. 347 (2010) 53–61. doi:10.1016/j.memsci.2009.10.005.

[10] D.P. Suhas, T.M. Aminabhavi, A.V. Raghu, Mixed matrix membranes of H-ZSM5-loaded poly(vinyl alcohol) used in pervaporation dehydration of alcohols: Influence of silica/alumina ratio, Polym. Eng. Sci. 54 (2014) 1774–1782. doi:10.1002/pen.23717.

[11] E. Okumus, T. Gurkan, L. Yilmaz, Development of a Mixed-Matrix Membrane for Pervaporation, Sep. Sci. Technol. 29 (1994) 2451–2473. doi:10.1080/01496399408002203.

[12] P. Shao, R.Y.M. Huang, Polymeric membrane pervaporation, J. Membr. Sci. 287 (2007) 162–179. doi:10.1016/j.memsci.2006.10.043.

[13] F. Lipnizki, G. Trägårdh, Modelling of Pervaporation: Models to Analyze and Predict the Mass Transport in Pervaporation, Sep. Purif. Methods. 30 (2001) 49–125. doi:10.1081/SPM-100102985.

[14] X. Yang, Z. Wu, F. Manquan, L. Jiding, Nonequilibrium Dissolution-diffusion Model for PDMS Membrane Pervaporation of ABE Water Binary System, J. Membr. Sci. Technol. 6 (2016) 143. doi:10.4172/2155-9589.1000143.

[15] R. Petrychkovych, K. Setnickova, P. Uchytil, The influence of water on butanol isomers pervaporation transport through polyethylene membrane, Sep. Purif. Technol. 107 (2013) 85–90. doi:10.1016/j.seppur.2013.01.014.

[16] R.H.B. Bouma, A. Checchetti, G. Chidichimo, E. Drioli, Permeation through a heterogeneous membrane: the effect of the dispersed phase, J. Membr. Sci. 128 (1997) 141–149. doi:10.1016/S0376-7388(96)00303-1.

[17] D. a. G. Bruggeman, Berechnung verschiedener physikalischer Konstanten von heterogenen Substanzen. I. Dielektrizitätskonstanten und Leitfähigkeiten der Mischkörper aus isotropen Substanzen, Ann. Phys. 416 (1935) 636–664. doi:10.1002/andp.19354160705.

[18] T.B. Lewis, L.E. Nielsen, Dynamic mechanical properties of particulate-filled composites, J. Appl. Polym. Sci. 14 (1970) 1449–1471. doi:10.1002/app.1970.070140604.

[19] L.E. Nielsen, Thermal conductivity of particulate-filled polymers, J. Appl. Polym. Sci. 17 (1973) 3819–3820. doi:10.1002/app.1973.070171224.

[20] R. Pal, New Models for Thermal Conductivity of Particulate Composites, J. Reinf. Plast. Compos. 26 (2007) 643–651. doi:10.1177/0731684407075569.

[21] H.J.C.T. Hennepe, C.A. Smolders, D. Bargeman, M.H.V. Mulder, Exclusion and Tortuosity Effects for Alcohol/Water Separation by Zeolite-Filled PDMS Membranes, Sep. Sci. Technol. 26 (1991) 585–596. doi:10.1080/01496399108050492.

[22] A.B. Yadav, M.L. Lind, J.Y. Lin, D.R. Nielsen, Arizona State University, Pervaporation Of Ethanol/Water mixtures using PDMS mixed matrix membranes, in: ASU Electron. Diss. Theses, Arizona State University, 2012. http://hdl.handle.net/2286/R.I.15095.

[23] D.M. Aguilar-Valencia, M.Á. Gómez-García, J. Fontalvo, Effect of pH, CO2, and High Glucose Concentrations on Polydimethylsiloxane Pervaporation Membranes for Ethanol Removal, Ind. Eng. Chem. Res. 51 (2012) 9328–9334. doi:10.1021/ie3002765.

[24] A. Ebneyamini, H. Azimi, J. Thibault, F.H. Tezel, Description of Butanol Aqueous Solution Transport through Commercial PDMS Membrane via Pervaporation Process Using Extended Maxwell–Stefan Model, To be Submitted.

[25] R. Krishna, J.A. Wesselingh, The Maxwell-Stefan approach to mass transfer, Chem. Eng. Sci. 52 (1997) 861–911. doi:10.1016/S0009-2509(96)00458-7.

[26] T. Singh, D.-Y. Kang, S. Nair, Rigorous calculations of permeation in mixed-matrix membranes: Evaluation of interfacial equilibrium effects and permeability-based models, J. Membr. Sci. 448 (2013) 160–169. doi:10.1016/j.memsci.2013.08.010.

[27] A.-C. Yang, C.-H. Liu, D.-Y. Kang, Estimations of effective diffusivity of hollow fiber mixed matrix membranes, J. Membr. Sci. 495 (2015) 269–275. doi:10.1016/j.memsci.2015.08.030.

[28] G.M. Monsalve-Bravo, S.K. Bhatia, Extending effective medium theory to finite size systems: Theory and simulation for permeation in mixed-matrix membranes, J. Membr. Sci. 531 (2017) 148–159. doi:10.1016/j.memsci.2017.02.029.

[29] D. Bastani, N. Esmaeili, M. Asadollahi, Polymeric mixed matrix membranes containing zeolites as a filler for gas separation applications: A review, J. Ind. Eng. Chem. 19 (2013) 375–393. doi:10.1016/j.jiec.2012.09.019.

[30] Y. Shen, A.C. Lua, Theoretical and experimental studies on the gas transport properties of mixed matrix membranes based on polyvinylidene fluoride, AIChE J. 59 (2013) 4715–4726. doi:10.1002/aic.14186.

[31] K. Zhang, R.P. Lively, M.E. Dose, A.J. Brown, C. Zhang, J. Chung, S. Nair, W.J. Koros, R.R. Chance, Alcohol and water adsorption in zeolitic imidazolate frameworks, Chem. Commun. 49 (2013) 3245–3247. doi:10.1039/C3CC39116G.

[32] W.F. Guo, T.-S. Chung, T. Matsuura, R. Wang, Y. Liu, Pervaporation study of water and tert-butanol mixtures, J. Appl. Polym. Sci. 91 (2004) 4082–4090. doi:10.1002/app.13632.

[33] B.E. Poling, J.M. Prausnitz, J.P. O'Connel, Properties of Gases and Liquids, 5th ed., Mc Graw-Hill Education, 2011.

[34] A.A. Inyinbor, F.A. Adekola, G.A. Olatunji, Kinetics, isotherms and thermodynamic modeling of liquid phase adsorption of Rhodamine B dye onto Raphia hookerie fruit epicarp, Water Resour. Ind. 15 (2016) 14–27. doi:10.1016/j.wri.2016.06.001.

[35] G. Jyoti, A. Keshav, J. Anandkumar, Review on Pervaporation: Theory, Membrane Performance, and Application to Intensification of Esterification Reaction, J. Eng. 2015 (2015). doi:10.1155/2015/927068.

[36] B. Samiey, S. Abdollahi Jonaghani, A New Approach for Analysis of Adsorption from Liquid Phase: A Critical Review, J. Pollut. Eff. Control. (2015) 1–9. doi:10.4172/2375-4397.1000139.

[37] G.P. Jeppu, T.P. Clement, A modified Langmuir-Freundlich isotherm model for simulating pH-dependent adsorption effects, J. Contam. Hydrol. 129–130 (2012) 46–53. doi:10.1016/j.jconhyd.2011.12.001.

[38] J.M. Zalc, S.C. Reyes, E. Iglesia, The effects of diffusion mechanism and void structure on transport rates and tortuosity factors in complex porous structures, Chem. Eng. Sci. 59 (2004) 2947–2960. doi:10.1016/j.ces.2004.04.028.

[39] M.R. Othman, H. Mukhtar, A.L. Ahmad, Gas Permeation Characteristics across Nano-Porous Inorganic Membranes, IIUM Eng. J. 5 (2004) 17–33.

[40] W. He, W. Lv, J. Dickerson, Gas Transport in Solid Oxide Fuel Cells, Springer Science+Business Media, 2014.

[41] J. Yuan, B. Sundén, On mechanisms and models of multi-component gas diffusion in porous structures of fuel cell electrodes, Int. J. Heat Mass Transf. 69 (2014) 358–374. doi:10.1016/j.ijheatmasstransfer.2013.10.032.

[42] E.S. Kikkinides, M.G. Politis, Linking pore diffusivity with macropore structure of zeolite adsorbents. Part II: simulation of pore diffusion and mercury intrusion in stochastically reconstructed zeolite adsorbents, Adsorption. 20 (2014) 21–35. doi:10.1007/s10450-013-9545-0.

[43] J.R. Welty, C.E. Wicks, R.E. Wilson, G.L. Rorrer, Fundamentals of Momentum, Heat and Mass Transfer, 4th ed., John Wiley & Sons, Inc., United States of America, 2001.

[44] Super Activated Porous Carbon (C) Nanopowder / Nanoparticles (C, 20-40nm, Plant as Raw Materials), (n.d.). http://www.us-nano.com/inc/sdetail/758 (accessed February 4, 2017).

Chapter 4: Conclusions and recommendations

Pervaporation is one of the promising membrane-based solvent recovery methods. Pervaporation system could be integrated to the Acetone-Butanol-Ethanol (ABE) fermentation process to increase butanol productivity by selectively removing of this alcohol from fermentation broth and to partly alleviate butanol inhibition. Based on a literature survey, among the various types of polymeric membranes, Polydimethylsiloxane (PDMS) membranes show the best performance for the separation of butanol from aqueous ABE model solutions and fermentation broths. However, PDMS membranes suffer from the typical membrane trade-off between selectivity and permeation flux. To partly overcome this limitation, mixed matrix membranes (MMMs) can potentially increase both the selectivity and permeation flux. In mixed matrix membranes, filler materials are embedded within the polymer matrix. Solid fillers with a different permeability than the polymeric matrix modify the concentration profile within the membrane and consequently the overall permeability of components through the membrane. If the permeability of a migrating species in the solid filler is greater than the permeability of the polymeric membrane, the permeation flux and potentially the selectivity should increase. The theoretical description of the mass transport of species through mixed matrix membranes leads to a better understanding of the pervaporation process. To gain a better understanding of the permeation process in MMMs, the mass transport through neat polymeric membranes and mixed matrix membranes were investigated using two different approaches: (1) Maxwell-Stefan model adapted to include the effect of swelling and temperature on the pervaporation separation using neat polymeric membranes, and (2) an extended resistance-based model to determine the permeate fluxes of components in a pervaporation separation process as a function of permeability of the polymeric matrix and the solid filler as well as the solid filler volume fraction.

In Chapter 2, a new approach of the Maxwell-Stefan model was implemented to describe the mass transport of butanol and water through a commercial PDMS membrane. The effect of membrane swelling and operating temperature on the sorption property and diffusion coefficient of the permeating species through the membrane was considered. An exponential relationship between the diffusion coefficient and the degree of swelling of the membrane was used to estimate the diffusion coefficient for different butanol feed concentrations at fixed temperature. Moreover, an Arrhenius-type equation was incorporated to the diffusion coefficient equation to extend the

prediction range for different operating temperatures. It was assumed that Henry's law is the dominating sorption mechanism and an Arrhenius-type equation was used to investigate the temperature dependency of Henry's law constant. The coupled diffusivity of the penetrants was estimated to be a weighted combination of the component diffusion coefficients within the membrane. The numerical values of the model parameters were determined by performing an overall nonlinear regression to minimize the sum of squares of the differences between the experimental butanol and water fluxes obtained at different temperatures and concentrations and the ones predicted by the models. It was observed that the estimated fluxes are in agreement with the experimental values with an average prediction error of roughly 10.5%. The parameters of the model were then used to predict the sorption properties and diffusion coefficients of species through the PDMS membrane. It was observed that the sorption properties are in relatively good agreement with the literature values considering the wide fluctuation in reported diffusion coefficients, which makes it difficult to make an exact comparison. The model was also used to estimate the membrane separation performances in terms of selectivity and pervaporation separation index (PSI) for different butanol feed concentrations and operating temperatures. It was observed that the selectivity of PDMS membranes is decreasing when increasing both temperature and feed concentration whereas the PSI increases with temperature and butanol feed concentration.

In Chapter 3, a resistance-based (RB) model was initially introduced to predict the effective permeability of species through ideal mixed matrix membranes containing homogenously dispersed cubical particles. The model was derived based on the assumption of uni-directional mass transport within the membranes. To consider the three-directional mass transport, the RB model was extended by adding a correction factor, which was obtained by comparing the permeation flux using a simple RB model with an accurate value of the permeation flux obtained by solving the diffusion coefficient by finite differences. The correction factor takes into account the deviation of the concentration streamlines due to presence of a more or less permeable dispersed phase within the matrix of the polymeric membrane. It was observed that the correction factor is only a function of the permeability ratio of the two phases and the volume fraction of the solid filler within the polymer matrix. The correction factors were then correlated successfully using a Langmuir-type relation. The proposed extended RB model was validated with experimental data for pervaporation and gas separation processes. Good precision for the predicted values was observed with a reasonable coefficient of regression.

Future works should be directed towards considering non-homogenous distribution of particles with various particle shapes and orientations within the membrane. Moreover, in this study, it was assumed that the solubility of both phases are independent of concentration (Henry's law domination); therefore, another case of study would be the estimating the effective permeability of MMMs while one or both phases sorption properties follows non-linear sorption isotherms.

In this study, solubility of butanol in the dispersed phase was estimated by liquid batch adsorption test whereas the water solubility was assumed to be identical in both phases. However, these methods lack precision for the estimation of solubility factor and, consequently, the permeability in the filler material. Therefore, it would be highly desirable to use Temperature Gravimetric Adsorption (TGA) as a more accurate measurement method to obtain the sorption properties of the permeating components on the solid filler content as well as on polymeric materials.

A. Appendix

Appendix A contains three figures which provide the concentration profile through the RB element obtained by the finite difference method. The concentration data was obtained for a 5 $g.L^{-1}$ feed butanol aqueous solution. An identical solubility factor was set for both the dispersed and continuous phases while the filler diffusivity was chosen to be more 1000 times more than the diffusivity of the continuous phase. As a result, the permeability of the dispersed phase is 1000 times larger than the one of the continuous phase in the simulation. Figure A.1 shows the 3D concentration profile of component through the RB element (40 nm element size and a volume fraction of 0.166 filler material within the polymer matrix).

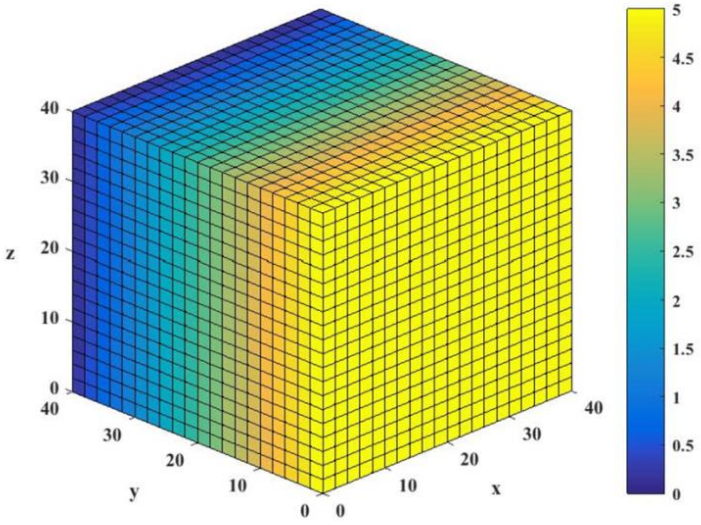

Figure A.1. Overall concentration profile within a RB element for a permeability ratio $P_d.P_c^{-1}$ = 1000, solubility ratio $S_d.S_c^{-1}$ = 1 and a filler volume fraction of 0.166 for a butanol feed concentration of C_f = 5 $g.L^{-1}$)

Figure A.2 presents a contour plot of the concentration profile in two directions (x and y) at the central node of the z direction. Moreover, Figure A.3 presents a surface plot of the concentration profile with the identical properties used for Figures A.1 and A.2.

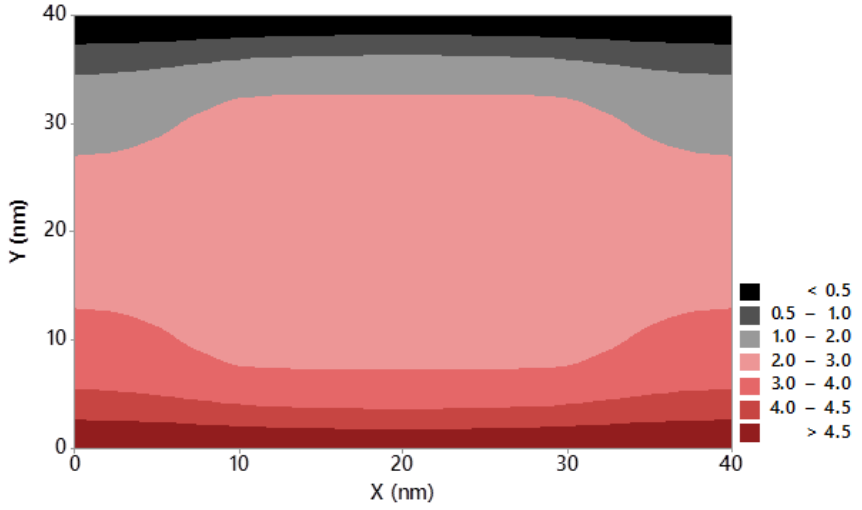

Figure A.2. Contour plot of the concentration profile in two directions of x and y at central position of z direction for a permeability ratio $P_d.P_c^{-1}$ = 1000, solubility ratio $S_d.S_c^{-1}$ = 1 and a filler volume fraction of 0.166 for a butanol feed concentration of C_f = 5 g.L^{-1}).

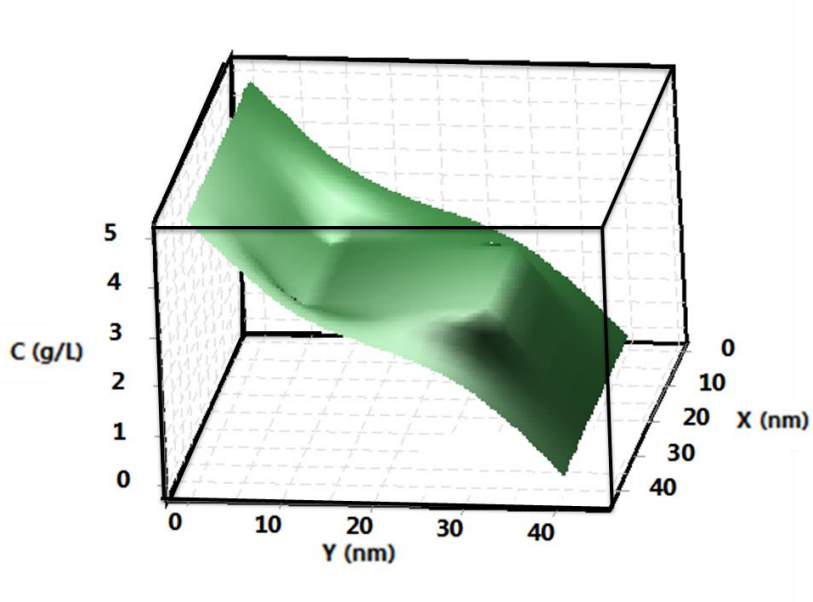

Figure A.3. Surface plot of the concentration profile in the central position of z direction for a permeability ratio $P_d.P_c^{-1}$ = 1000, solubility ratio $S_d.S_c^{-1}$ = 1 and a filler volume fraction of 0.166 for a butanol feed concentration of C_f = 5 g.L^{-1}).